2010-03-04

Time-Resolved Infrared Spectroscopy and Density Functional Theory Study of Weak Interactions of Metal Carbonyls and Organic Solvents

Carolyn Evans Sheffield
Brigham Young University - Provo

Time–Resolved Infrared Spectroscopy and Density Functional Theory Study of Weak Interactions of Metal Carbonyls and Organic Solvents

Carolyn Sheffield

A thesis submitted to the faculty of
Brigham Young University
in partial fulfillment of the requirements for the degree of

Master of Science

Matthew C. Asplund
Eric T. Sevy
James E. Patterson
Roger G. Harrison

Department of Chemistry and Biochemistry

Brigham Young University

April 2010

ABSTRACT

Time–Resolved Infrared Spectroscopy and Density Functional Theory Study of

Weak Interactions of Metal Carbonyls and Organic Solvents

Carolyn Sheffield

Department of Chemistry and Biochemistry

Master of Science

Pulsed laser flash photolysis of $M(CO)_6$ (M = Cr, W) in cyclohexane with a small amount of benzene results in three sequential reactions. The first is the photodissociation of the parent to yield a $M(CO)_5$:C_6H_{12} complex, which takes place faster than the time resolution of our experiments. The second reaction is the replacement of the cyclohexane ligand with benzene to form a $M(CO)_5$:C_6H_6 complex, in which benzene is coordinated to the metal via one side of the ring. This complex then falls apart in solution as $M(CO)_5$ coordinates with a trace impurity in the solution that is likely water. Kinetic studies over a range of temperatures result in the following activation energies: 39 kJ/mol for the dissociation of $W(CO)_5$:C_6H_6; 30 kJ/mol for conversion of $Cr(CO)_5$:C_6H_{12} to $Cr(CO)_5$:C_6H_6; 33 kJ/mol for the dissociation of $Cr(CO)_5$:C_6H_6. DFT calculations of binding energies for each complex suggest that all reactions proceed through a combination of an associative and dissociative mechanism. Further calculations of carbonyl vibrational frequencies for 13 weak metal–solvent complexes using three different density functionals: B3LYP, M06, and M06-L allowed us to calculate scale factors for predicting experimental vibrational frequencies. The scale factors are: 0.952 for B3LYP, 0.943 for M06, and 0.957 for M06-L. Using these scale factors leads to average errors in predicted experimental vibrational frequencies of less than 1% for each functional.

ACKNOWLEDGEMENTS

I would like to thank my advisor, Dr. Matthew Asplund for his support even while I worked away from BYU. I also thank Richard Gates for his assistance in collecting and analyzing data. I thank the Fulton Supercomputing Lab at Brigham Young University for the use of their supercomputers for my many calculations. In addition, I would like to thank Brigham Young University and specifically the Department of Chemistry and Biochemistry for giving me the opportunity to learn.

I also want to thank my family for their support. I am especially thankful for my husband Nathan who always encouraged me and inspired me to keep working.

Table of Contents

List of Figures

List of Tables

Introduction

Reactions of transition-metal complexes and hydrocarbons have been of great interest over the past few decades.[1,2] One reason for this is some transition metal complexes can catalytically break, or activate, C–H bonds. During standard heterogeneous metal catalysis, an organic molecule physisorbs to a metal surface through a metal-hydrogen bond. The C–H bond then breaks and the two fragments chemisorb to the metal surface. We see a similar process in C–H bond activation, however instead of a metal surface, a metal atom is held in molecular scaffolding. After excitation by light, a ligand dissociates and opens a coordination site where an organic molecule can form an agostic interaction (physisorb) with the metal atom through a metal-hydrogen bond. As in standard catalysis, the C–H bond then breaks and the two fragments bond to the metal.

C–H bonds are strong, with bond dissociation energies of 96–105 kcal/mol, and are thus difficult to break. C–H bonds are also non-polar, making activation more difficult. However, some unsaturated transition metal complexes can be used as catalysts to break C–H bonds. One of the first transition metals found to activate C–H bonds was Pt(II).[3] Then complexes containing Ir(III), Ru(II), and Rh(II) were also found to activate C–H bonds. Further research showed certain ligands, such as Tp*(tris-(3,5-dimethylpyrazolyl)borate) or Tp(hydridotris(pyrazolyl)borate), attached to the transition metal center were also useful in activation.[4]

In addition to simply breaking the C–H bond, transition metal complexes can be used as catalysts in addition reactions of hydrocarbons.[5-6] Transition metal-mediated catalysis by C–H bond activation is promising because products are formed from starting materials more readily

available than those used in traditional syntheses. For example, aromatic products with linear alkyl chains are difficult to synthesize by traditional methods. However, these products are easily synthesized by metal-mediated C–H activation. Because of this, transition metal catalysis has potential to be an important synthetic tool in hydrocarbon functionalization reactions.

These potential applications have generated interest in the reaction mechanism involved in C–H activation.[4,7,8,9] It is important to understand how C–H activation occurs in order to design more effective chemical systems. To better understand C–H bond activation, we need to understand the interaction of transition metal complexes with different types of chemical bonds. Because the C–H bond energy is high, reactive intermediates in the bond activation processes must be very high energy. This means their lifetimes tend to be short in solution because frequent collisions with solvent molecules can lead to reaction. Many experiments have been performed on a millisecond time scale. More recently we have seen experiments using nanosecond, picosecond, and even femtosecond time scales.

Though many of the organometallic molecules used in C–H activation are quite complex, we can use simple complexes to understand the basic reactivity of transition metals with organic molecules. Some of the most basic transition metal complexes are $M(CO)_6$ (M = Cr, W, Mo). Many experiments have been performed using these prototype molecules in the gas phase, in solution, at room temperature, and at low temperatures. The carbonyl ligands in these test molecules readily dissociate when the complex is irradiated with UV light. The initial studies of transient organometallic complexes were performed using flash tube excitation and UV-visible absorption spectroscopy. This technique provided a great deal of information about the reactions, but did not provide much structural information about the intermediates. Over time, methods developed to use lasers for excitation and an IR detection system.[10] These were initially

limited to low-temperature experiments and millisecond time resolution, but were eventually improved and now are used over a large temperature range with femtosecond resolution. The carbonyl ligands in these test molecules give us a good target to follow in the IR. In metal–CO bonding, there are two interactions occurring. There is the traditional bond formed by carbon donating electron density to the metal. However, there is a second interaction, called π-back-bonding, formed as the metal donates electron density from a filled d orbital to the empty π* orbital on CO.[11] The amount of electron density back-donated to CO depends on the amount donated to the metal by all the ligands. Thus, changes in solvation of the metal center cause different amounts of π-back-bonding. This in turn changes the strength of the CO bond, causing CO stretching frequencies to be sensitive to changes in electron density around the metal center to which they are bound. These changes are apparent in the IR spectrum.

The first step in any of these reactions is dissociation of one or more of the carbonyl ligands. To understand how this happens in catalytic mechanisms, it is important to know the strengths of the bonds being broken and being formed. Laser pyrolysis studies were used to measure the gas phase organometallic bond dissociation energies for $Fe(CO)_5$, $Cr(CO)_6$, $W(CO)_6$, and $Mo(CO)_6$. Lewis *et al.*[12] measured the first bond dissociation energies to be 41, 37, 46, and 40 kcal/mol (±2), respectively. They also found the rate-determining step in $Cr(CO)_6$ decomposition is not the first bond dissociation, but a later one (probably dissociation from $Cr(CO)_5$)), with a 40 kcal/mol dissociation energy.

In the gas phase, irradiation of $M(CO)_6$ with UV light produces $M(CO)_n$ (n = 1–5), where at least one carbonyl ligand has dissociated from the metal center. However, in solution, only one CO dissociates, giving us a more predictable reaction. The exact nature of these complexes following dissociation is only partly understood. Joly *et al.*[13] studied $Cr(CO)_6$ dissociation and

found that the bare $Cr(CO)_5$ complex is formed in 300 fs, and is in its electronically excited state. Wang *et al.*[14] were able to see the square pyramidal geometry of excited state $Cr(CO)_5$ using picosecond IR transient absorption. They suggest $Cr(CO)_5$ can be found in either a singlet square pyramidal geometry or a triplet trigonal bipyramidal geometry, both of which react with cyclohexane in solution.

These ultrafast experiments show that upon dissociation of a carbonyl, the organometallic complex is in an electronically excited state. It is also a coordinatively unsaturated species that readily reacts with typically inert substances, such as hydrocarbons and noble gases. Many of the experiments are performed in hydrocarbon solvents. Using various solvents and also solvent mixtures can tell us about the reactivity of these solvents with the coordinatively unsaturated metal complex. Church *et al.*[15] performed experiments using cyclohexane as the solvent. After irradiation, they found new CO-stretching vibrations in the IR spectrum that they attributed to $Cr(CO)_5$:CyH (CyH = cyclohexane). The IR spectrum of this complex is consistent with a C_{4v} structure in which the $Cr(CO)_5$ fragment has a square pyramidal geometry. They also found some other important information. The $Cr(CO)_5$:CyH complex did not last forever, but instead quickly dissociated to form a new complex they identified as $Cr(CO)_5 \cdot H_2O$. Thus we can see that these organometallic solvent complexes are not necessarily stable, but will rapidly react with other trace impurities in the main solvent.

Once the basic reaction is established, it is important to study a variety of metals and solvents to try to understand the relative bond strengths between different metals and organic molecules. This information can be very important in catalytic mechanisms to ensure the correct ligand becomes coordinated to the metal center. Experiments using fluorinated hydrocarbons such as perfluoromethylcyclohexane[16] showed that $Cr(CO)_5$ complexes much less with a

fluorinated solvent than with a hydrocarbon. Other experiments using sulfur, oxygen, or nitrogen-containing solvents[17] showed that the order of reactivity with these is N<S<O. Ligands, such as oxygen, that have more electron-donating ability make ΔH for the reaction lower, and thus result in faster reaction times. A study using hydrocarbons of various lengths showed the ΔH for reaction of $Cr(CO)_6$ with heptane or with pentane is indistinguishable.[18] However, this same study showed that it is distinguishable for heptane and cyclohexane; the energy of activation is greater for heptane than for cyclohexane. This result suggests that agostic bonding between the metal and the hydrocarbon prefers secondary C–H to primary, and that the presence of primary vs. secondary vs. tertiary carbons can change the overall reactivity. It is possible this preference is because secondary C–H bonds are more electron rich than primary bonds.

In addition to aliphatic solvents, reactions with aromatic solvents are also of great interest. Benzene is a commonly used aromatic solvent, and is often used to study transition-metal reactions. Solution-phase studies of $Cr(CO)_6$ and $W(CO)_6$ irradiated with 355-nm light show dissociation of one carbonyl ligand. When in a benzene solvent, $M(CO)_5$:C_6H_6 forms as indicated by new CO-stretching frequencies in the IR spectrum.[19]

Another interesting way to study the relative reactivity of various hydrocarbons with coordinatively unsaturated organometallic intermediates is to use solvent mixtures. Organometallic complexes are studied using various aliphatic and aromatic ligands. The exchange between these two types of organic molecules is of great interest. One way to investigate this exchange is to use a large amount of aliphatic solvent mixed with a small amount of aromatic solvent. With these mixtures, the organometallic complex first reacts with the aliphatic hydrocarbon. Following this reaction, the aliphatic hydrocarbon is displaced by the aromatic hydrocarbon.[20,21,22] It seems the thermodynamic product of the reaction is an

interaction with an aromatic molecule, while the kinetic product is an interaction with the more numerous aliphatic solvent molecules. The metal centers form more stable complexes with aromatic hydrocarbons than with aliphatic hydrocarbons. Further similar experiments look at displacement of aliphatic and aromatic hydrocarbons by alkenes[23,24] or other aromatic hydrocarbons.[19]

Our experiments focus on exchange of aliphatic and aromatic hydrocarbon solvents bonded to the metal center. We use $Cr(CO)_6$ and $W(CO)_6$ as test molecules because their reactivity is already fairly well understood. We have tried to better understand the nature of intermediates during reactions with cyclohexane and small amounts of benzene together in solution. Understanding and identifying the intermediates will help us determine the mechanism of these reactions. We used time-resolved IR spectroscopy to follow these reactions. Though using transient IR spectroscopy to probe the reactions rather than UV helps us determine the structure of the intermediates, it does not always give a perfect understanding of what is happening. Additional data is needed to fully understand the reactions, and the intermediates. A few low-temperature solution NMR experiments[25,26] have verified structures for several reactions, but the unstable nature of most intermediates makes this information difficult to acquire. DFT calculations are another tool we can use to better understand intermediates and reaction mechanisms. By calculating energies, geometries, and vibrational frequencies of the suspected intermediates, we can test hypotheses formulated from experimental data.

Density functional theory (DFT) calculations of vibrational frequencies can be helpful when analyzing experimental IR spectra. However, DFT calculated frequencies are almost always higher than experimentally determined frequencies, which can cause difficulty when comparing experimental and calculated frequencies. After realizing that a generic scale factor

does not adequately correct the vibrations in many organometallic complexes, Yu *et al.* came up with scale factors for C≡O frequencies for 31 different organometallic complexes using both HF (Hartree-Fock) and DFT (B3LYP functionals).[27] They found frequencies calculated using B3LYP were more reliable than those calculated using HF. This is expected because B3LYP takes into account exchange potential and electron correlation, while HF does not.

Though B3LYP is better at calculating these C≡O frequencies, there are still several problems with B3LYP. These were addressed by Zhao *et al.*, leading them to develop a new set of density functionals, called M06-class functionals.[28] These functionals overcome some of the shortcomings of B3LYP, such as its inaccuracy when calculating interactions dominated by van der Waals forces. They are also designed to be more accurate for calculations involving transition metals. With these improvements, calculations performed using these M06-class functionals should be more accurate for the organometallic complexes we are studying. With this information, we decided to compare calculations using M06 functionals to those using B3LYP. We hope to use this information to determine accurate scale factors to calculate vibrational frequencies when using M06 functionals for organometallic molecules. We also hope to gain additional insight into the reactions we are studying experimentally.

Time-resolved IR spectroscopy allows us to view changes in the IR during the course of a reaction. During reactions of $W(CO)_6$ and $Cr(CO)_6$ with cyclohexane and benzene, we can use these data to calculate activation energies for the photosubstitution reactions occurring in solution. Using DFT calculations, we can compare experimentally measured activation energies to dissociation energies to better understand the mechanism of reaction. This will also give us information about the bonding between the hydrocarbon and the transitional metal. In addition to comparing energies, we can also compare calculated vibrational frequencies with those seen

experimentally. This comparison can help us verify the hypothesized reaction intermediates. The combination of experimental data and DFT calculations can help us better understand the nature and reactivity of organometallic complexes.

References

(1) Cowan, A. J.; George, M. W. Formation and reactivity of organometallic alkane complexes. *Coord. Chem. Rev.* **2008**, *252*, 2504–2511.

(2) Metz, R. C. Photofragment spectroscopy of covalently bound transition metal complexes: a window into C–H and C–C bond activation by transition metal ions. *Int. Rev. Phys. Chem.* **2004**, *23*, 79–108.

(3) Jensen, M. P.; Wick, D. D.; Reinartz, S.; White, P. S.; Templeton, J. L.; Goldberg, K. I. Reductive Elimination/Oxidative Addition of Carbon–Hydrogen Bonds at Pt(IV)/Pt(II) Centers: Mechanistic Studies of the Solution Thermolyses of $Tp^{Me}{}_2Pt(CH_3)_2H$. *J. Am. Chem. Soc.* **2003**, *125*, 8614–8624.

(4) Bromberg, S. E.; Yang, H.; Asplund, M. C.; Lian, T.; McNamara, B. K.; Kotz, K. T.; Yeston, J. S.; Wilkens, M.; Frei, H.; Bergman, R. G.; Harris, C. B. The Mechanism of a C–H Bond Activation Reaction in Room-Temperature Alkane Solution. *Science* **1997**, *278*, 260–263.

(5) Lail, M.; Arrowood, B. N.; Gunnow, T. B. Addition of Arenes to Ethylene and Propene Catalyzed by Ruthenium. *J. Am. Chem. Soc.* **2003**, *125*, 7506–7507.

(6) Oxgaard, J.; Goddard, W. A. Mechanism of Ru(II)-Catalyzed Olefin Insertion and C–H Activation from Quantum Chemical Studies. *J. Am. Chem. Soc.* **2004**, *126*, 442–443.

(7) Asplund, M. C.; Snee, P. T.; Yeston, J. S.; Wilkens, M. J.; Payne, C. K.; Yang, H.; Kotz, K. T.; Frei, H.; Bergman, R. G.; Harris, C. B. Ultrafast UV Pump/IT Probe Studies of C–H Activation in Linear, Cyclic, and Aryl Hydrocarbons. *J. Am. Chem. Soc.* **2002**, *124*, 10605–10612.

(8) Crabtree, R. H.; Organometallic alkane CH activation. *J. Organomet. Chem.* **2004**, *689*, 4083–4091.

(9) Boutadla, Y.; Davies, D. L.; Macgregor, S. A.; Poblador-Bahamonde, A. I. Mechanisms of C–H bond activation: rich synergy between computation and experiment. *Dalton Trans.* **2009**, *30*, 5820–5831.

(10) Hermann, H.; Grevels, F.; Henne, A.; Schaffner, K. Flash Photolysis with Infrared Detection. The Photochemistry an Secondary Thermal Reactions of $M(CO)_6$ [M = Cr, Mo, and W]. *J. Phys. Chem.* **1982**, *86*, 5151–5154.

(11) Nakashima, K.; Zhang, X.; Xiang, M.; Lin, Y.; Lin, M.; Mo Y. Block-Localized Wavefunction Energy Decomposition (BLW-ED) Analysis of σ/π Interactions in Metal-Carbonyl Bonding. *J. Theor. Comput. Chem.* **2008**, *7*, 639–654.

(12) Lewis, K. E.; Golden, D. M.; Smith, G. P. Organometallic Bond Dissociation Energies: Laser Pyrolysis of $Fe(CO)_5$, $Cr(CO)_6$, $Mo(CO)_6$, and $W(CO)_6$. *J. Am. Chem. Soc.* **1984**, *106*, 3905–3912.

(13) Joly, A. G.; Nelson, K. A. Femtosecond Transient Absorption Spectroscopy of $Cr(CO)_6$ in Methanol: Observation of Initial Excited States and CO Dissociation. *J. Phys. Chem.* **1989**, *93*, 2876–2878.

(14) Wang, L.; Zhu, X.; Spears, K. G. Unsaturated Transition-Metal Complexes in Solution: Naked $Cr(CO)_5$ in Cyclohexane Solution Observed by Picosecond IR Transient Absorption. *J. Am. Chem. Soc.* **1988**, *110*, 8695–8696.

(15) Church, S. P.; Grevels, F.; Hermann, H.; Schaffner, K. Structures and Kinetics of $Cr(CO)_5$ and $Cr(CO)_5 \cdot H_2O$ in Cyclohexane Solution. Flash Photolysis Study of $Cr(CO)_6$ with Infrared and Visible Detection. *Inorg. Chem.* **1985**, *24*, 418–422.

(16) Kelly, J. M.; Long, C. Laser Flash Photolysis of $M(CO)_6$ (M = Cr, Mo, or W) in Perfluoromethylcyclohexane. The Generation of Highly Reactive Coordinatively Unsaturated Species. *J. Phys. Chem.* **1983**, *87*, 3344–3349.

(17) Schultz, R. H. Reactions of the Transient Species $W(CO)_5$(Cyclohexane) with Thiophene and Tetrahydrothiophene Studied by Time-Resolved Infrared Absorption Spectroscopy. *Organometallics* **2004**, *23*, 4349–4356.

(18) Morse, J. M., Jr.; Parker, G. H.; Burkey, T. J. Enthalpy of CO Dissociation from $M(CO)_6$ (M = Cr, Mo, W) in Alkane Solvent: Determination of Intermolecular Agostic Bond Strengths. *Organometallic* **1989**, *8*, 2471–2474.

(19) Zhang, S.; Dobson, G. R.; Zang, V.; Bajaj, H. C.; van Eldik, R. Octahedral Metal Carbonyls. 71. Kinetics and Mechanism of Benzene Displacement from Photogenerated $[(\eta^2$-Benzene)$Cr(CO)_5]$. *Inorg. Chem.* **1990**, *29*, 3477–3482.

(20) Paur-Afshari, R.; Lin, F.; Schultz, R. H. An Unusual Solvent Isotope Effect in the Reaction of $W(CO)_5$(solv) (solv = Cyclohexane or Cyclohexane-d_{12}) with THF. *Organometallics* **2000**, *19*, 1682–1691.

(21) Dobson, G. R.; Zhang, S. Mechanism of Displacement of Alkanes from Photogenerated (Alkane) $Cr(CO)_5$ Complexes. *J. Coord. Chem.* **1999**, *47*, 409–416.

(22) Biber, L; Reuvenov, D.; Revzin, T.; Sinai, T.; Zahavi, A.; Schultz, R. H. Reactions of the transient species $Cr(CO)_5$(cyclohexane) with C_4H_nE (n = 4, 8; E = O, NH, S) studied by time-resolved IR absorption spectroscopy. *Dalton Trans.* **2007**, *1*, 41–51.

(23) Dobson, G. R.; Asali, K. J.; Cate, C. D.; Cate, C. W. Octahedral Metal Carbonyls. 78 Mechanism of Alkane Displacement by 1-Hexene from (Alkane)$W(CO)_5$ Complexes (Alkane = Cyclohexane, *n*-Heptane). Estimates of the Alkane–W Bond Strengths in Condensed Media. *Inorg. Chem.* **1991**, *30*, 44/1–44/4.

(24) Ladogana, S.; Nayak, S. K.; Smit, J. P. Dobson, G. R. Kinetics and Mechanism of Ligand Exchange in Photogenerated (η^2-monoalkylarene)$Cr(CO)_5$ Complexes with Alkenes; Evidence for Involvement of Aliphatic Chains in the Arene and Alkene in the Exchange Process. *Organometallics* **1997**, *16*, 3051–3054.

(25) Geftakis, S.; Ball, G. E. Direct Observation of a Transition Metal Alkane Complex, $CpRe(CO)_2$(cyclopentane), using NMR Spectroscopy. *J. Am. Chem. Soc.* **1998**, *120*, 9953–9954.

(26) Matthews, S. L.; Heinekey, D. M. Photochemical Generation of Dihydrogen Complexes of Chromium and Tungsten. *J. Am. Chem. Soc.* **2006**, *128*, 2615–2620.

(27) Yu, L; Srinivas, G. N.; Schwartz, M. Scale factors for C≡O vibrational frequencies in organometallic complexes. *J. Mol. Struct.* **2003**, *625*, 215–220.

(28) Zhao, Y.; Truhlar, D. G. Density Functionals with Broad Applicability in Chemistry. *Acc. Chem. Res.* **2008**, *41*, 157–167.

Chapter 1: Reactions of $W(CO)_6$

1.1 Introduction

Reactions of transition metals, specifically coordinatively unsaturated intermediates, have been of considerable interest in recent years, mainly due to their ability to activate (break) strong C–H bonds.[1] In order to better understand and use this ability, it is important to understand the reactivity of these transition metals with organic molecules. The class of $M(CO)_6$ (M = transition metal) complexes are often used as test molecules, being some of the simplest transition metal complexes. These test molecules can be used to help understand reactions between the metal center and different organic molecules, and also to understand reactivity of the coordinatively unsaturated complexes.

$W(CO)_6$ was the first transition-metal complex we studied. In a solution of cyclohexane, $W(CO)_6$ dissociates rapidly following irradiation to form $W(CO)_5$:CyH (CyH = cyclohexane).[2,3,4] When in a solution of cyclohexane with a small amount of added benzene, $W(CO)_5$ complexes with benzene following its complexation with cyclohexane.[5] After the initial complexation with benzene, we see an additional reaction occurring, characterized by a shift in the IR spectrum. We focused on this later reaction, which occurred on a millisecond time scale under our experimental conditions.

1.2 Experimental

1.2.1 Reagents

$W(CO)_6$ (Aldrich, 97%) was used as received. C_6H_{12} (Fisher Scientific, HPLC grade), C_6D_6 (Cambridge Isotope Laboratories, 99.5%), and mesitylene (1,3,5-trimethylbenzene) (Acros Organics, 99%) were also used as received. C_6H_6 was dried in a high pressure alumina column in an Ar atmosphere. C_6H_6 and C_6D_6 were used interchangeably because their complexes with $W(CO)_5$ have the same infrared spectra within 4 cm^{-1} resolution.[6] To prepare the solutions, a round bottom flask was charged with $W(CO)_6$. C_6D_6/C_6H_6 was added using a syringe, followed by the addition of C_6H_{12}. All solutions were 1 mM $W(CO)_6$. Benzene concentrations were varied from approximately 0.1% to 4% by volume. Solutions with mesitylene in place of benzene were prepared by the same method. Mesitylene concentrations were 4% by volume.

H_2O and O_2 are known to react with the weak metal:solvent complexes we are generating.[7] Thus, it is important to minimize their presence during sample preparation. To do so, the $W(CO)_6$ solutions went through three freeze-pump-thaw cycles prior to use for analysis. These cycles involved freezing the sample using liquid nitrogen, then pumping down to at least 2 mtorr to remove O_2 from the sample. The sample was then thawed, and the process repeated twice more. Following the third cycle, the flask containing the sample was filled with argon gas and then was removed for analysis while under a positive Ar pressure.

1.2.2 Photochemistry

Transient infrared measurements were made using a Bruker IFS-66 FTIR spectrometer, with the necessary modifications for rapid-scan experiments. All measurements used a liquid

nitrogen cooled, fast Mercury Cadmium Telluride (MCT) detector with a 10 ns rise time, and signals were digitized with a 12-bit, 100 MS/s digitizer. Signals were amplified using a Sonoma 310 instrument amplifier. The recorded signals were the average of the signal following 30 laser pulses. Infrared wavelengths were collected between 700 cm^{-1} and 2400 cm^{-1} and a filter was used to attenuate all wavelengths higher than 2400 cm^{-1}. The IR beam was 8 mm in diameter, and the resolution of our measurements was between 2 cm^{-1} and 8 cm^{-1}.

The basic setup for rapid-scan experiments is represented in Figure 1-1. The delays are set using the DDG (digital delay generator) such that the next FTIR scan begins immediately following a pulse of light from the laser. An oscilloscope is used to monitor this timing. Laser pulses for UV excitation are the frequency tripled (355 nm) output of a Nd:YAG laser (Coherent Infinity). Excitation energy is kept at 2-5 mJ per pulse to minimize sample degradation during the experiment. The pump (UV) and probe (IR) beams are completely overlapped in the sample, with an angle of approximately 20 degrees between the two beams. A 1 mm path length temperature-controllable CaF_2 IR cell is used, and one pulse of UV light is allowed to pass through the sample for each experiment. The sample is kept under a positive pressure of Ar gas, and is maintained at a constant temperature. The time resolution of these experiments is limited by the scanning speed of the detector, which is 160 kHz, resulting in 14 milliseconds per scan.

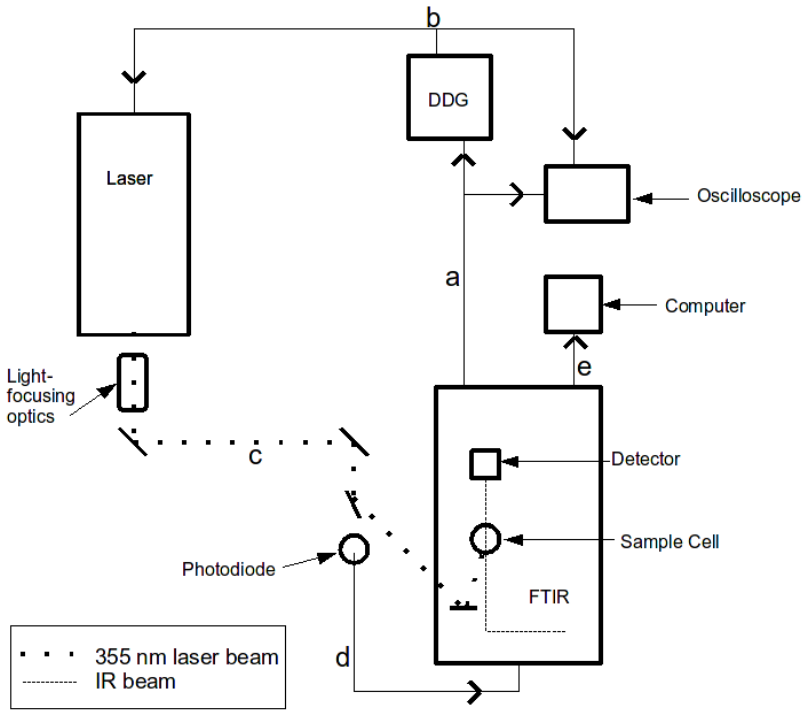

Figure 1-1: Schematic of setup for rapid-scan experiments.

a) The FTIR sends paired signals to the DDG and the oscilloscope when a scan is finished. b) The DDG sends delayed signal to the laser (and to the oscilloscope), which the laser uses as a trigger. c) The laser fires and the light follows the shown path, timed to enter the sample cell right before the next scan begins. d) FTIR collection is triggered off excess laser light hitting the photodiode. e) Data digitized and then collected on a computer.

1.2.3 Data Analysis

Text files from each kinetic trace were extracted from the data using Bruker OPUS Version 3.1. We then used MATLAB 7.0 to analyze the kinetic data. The pseudo-first order

rate constant, k, for each kinetic trace is determined by fitting the absorbance data to an exponential. Both the rate of decay of the intermediate and the rate of growth of the product were measured when possible. At times the S/N was not sufficiently high for both peaks to produce reliable results for k. In these cases, only the decay was used. A single decaying exponential function is used to fit the decay of peaks. However, a more complex equation is required to fit the peak growth. We use a relatively fast growing exponential multiplied by a slow decaying exponential: $y = \left(ae^{-kx} + b\right) * \left(1 - ce^{-dx} + f\right)$. This slower decay is necessary because the time constant of our detector and diffusion of photoexcited sample out of the IR beam cause signal attenuation at very long times. There are also competing reactions as the final complex breaks apart and $W(CO)_5$:C_6H_6 complexes react with trace amounts of O_2, OH^-, or lose additional carbonyl ligands. These all lead to the signal decaying slowly while it is growing in much more rapidly. Using a single exponential growth does not accurately fit the peak profile, so we opted to use a relatively fast growing exponential multiplied by a slow decaying exponential to better capture the true rate of growth of the peak. After calculating k from these fits, Arrhenius plots of ln(k) vs. 1/T are used to calculate the activation energy of the transition.

1.3 Results

1.3.1 Reactions with Benzene and Cyclohexane

To observe the exchange of cyclohexane and benzene ligands, we used a C_6H_{12} solution of $W(CO)_6$ with a low concentration (4%) of C_6D_6. Irradiation of this solution by 355 nm light results in a yellow solution, due to near UV absorption in the $W(CO)_5$:ligand species. The progress of the reaction can be monitored by observing the CO stretches in the infrared spectrum. Within the time resolution of the experiment (milliseconds), we see a bleach of the parent

$W(CO)_6$ as well as two CO stretches at 1948 cm^{-1} and 1921 cm^{-1} that appear and then begin to decay. As they are decaying, new CO stretches at 1933 cm^{-1} and 1908 cm^{-1} grow in with the same time dependence, as shown in Figure 1-2.

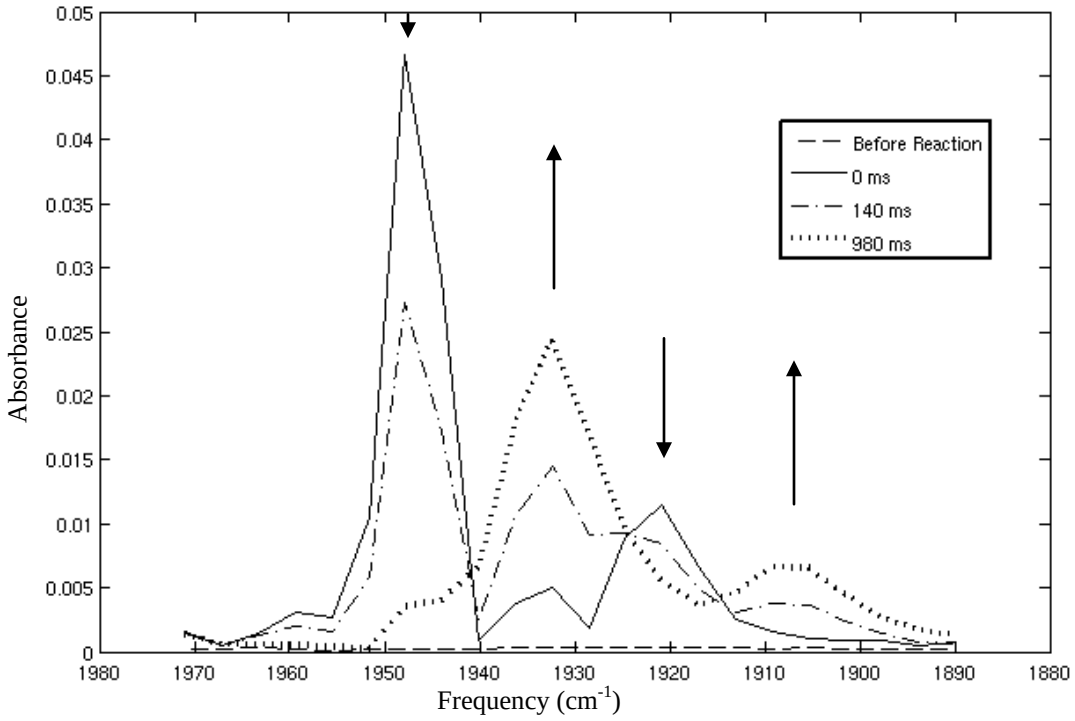

Figure 1-2: IR spectrum after the irradiation of $W(CO)_6$ in C_6H_{12} with C_6D_6.

Peaks at 1933 cm^{-1} and 1908 cm^{-1} grow as peaks at 1948 cm^{-1} and 1921 cm^{-1} decay.

Previous experiments[4] with a solution of $W(CO)_6$ in C_6H_{12} show that upon irradiation, the parent bleach is observed, but within 1 μs two peaks at 1954 and 1928 cm^{-1} appear. These are assigned to the E and A_1 C–O stretches of $W(CO)_5$:CyH formed in the following reaction.

$$W(CO)_6 + C_6H_{12} \rightarrow W(CO)_5{:}C_6H_{12} + CO \qquad (1)$$

In our own step scan experiments (1 microsecond time resolution) with a solution of $W(CO)_6$ in C_6H_{12} without benzene, we see these same peaks at 1954 cm^{-1} and 1928 cm^{-1} grow in as $W(CO)_5$:C_6H_{12} forms. (See Figure 1-3 for structure). However, the peaks do not stay indefinitely, but decay while peaks at 1948 cm^{-1}, 1937 cm^{-1} and 1914 cm^{-1} grow as shown in Figure 1-4. In rapid scan experiments of the same solution (14 millisecond time resolution) we see only the later peaks at 1948 cm^{-1}, 1937 cm^{-1} and 1914 cm^{-1}. Thus, by 14 milliseconds, the cyclohexane complex has fallen apart and been replaced by an impurity complex.

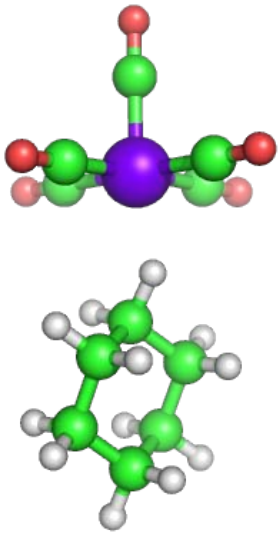

Figure 1-3: Structure of $W(CO)_5$:C_6H_{12}.

The geometry optimization was performed using B3LYP with the LANL2DZ ECP basis set for W, and 6-31G* for all other atoms. A geometry minimum was verified by having no negative vibrational frequencies.

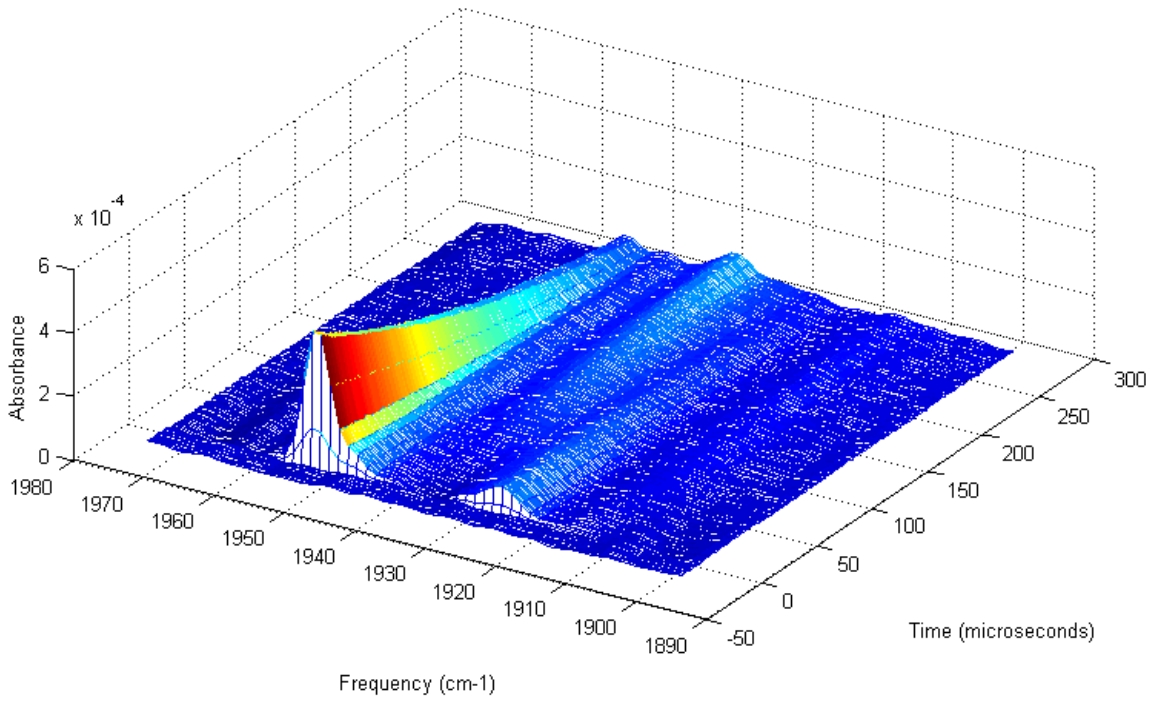

Figure 1-4: $W(CO)_6$ in neat cyclohexane.

Upon irradiation of $W(CO)_6$ in neat cyclohexane, we see two stretches in the IR, one at 1928 cm^{-1} and one much stronger one at 1954 cm^{-1}. These peaks slowly decay, and new peaks appear at 1948 cm^{-1}, 1937 cm^{-1} and 1914 cm^{-1}. The rotation of the 3D plot makes it difficult to make absolute frequency assignments. See Figure 1-2 for frequency spectra at individual times.

Most of our experiments employ a solution of $W(CO)_6$ in cyclohexane, with benzene added at low concentrations. When benzene is present in the solution, the $W(CO)_5$:CyH complex does not last as long as in neat cyclohexane solutions, but dissociates as another complex forms. Further experiments[8,5] with $W(CO)_6$ and C_6H_6 in C_6H_{12} give evidence that the following reaction occurs:

$$W(CO)_5{:}C_6H_{12} + C_6H_6 \rightarrow W(CO)_5{:}C_6H_6 + C_6H_{12} \qquad (2)$$

Stolz *et al.*[8] report IR frequencies of 2083, 1948, and 1921 cm^{-1} for C–O stretches in $W(CO)_5$:C_6H_6, while Tyler *et al.*[5] report frequencies of 1931 and 1908 cm^{-1} and claim that the peaks at 1948 and 1921 cm^{-1} are not from a benzene complex, but are impurities. In our millisecond experiments with benzene and cyclohexane, the first peaks we see are at 1948 and 1921 cm^{-1}. However, we see an additional reaction occur, evident by the disappearance of these two peaks and the simultaneous appearance of two new peaks at 1933 cm^{-1} and 1908 cm^{-1} as shown in Figure 1-5.

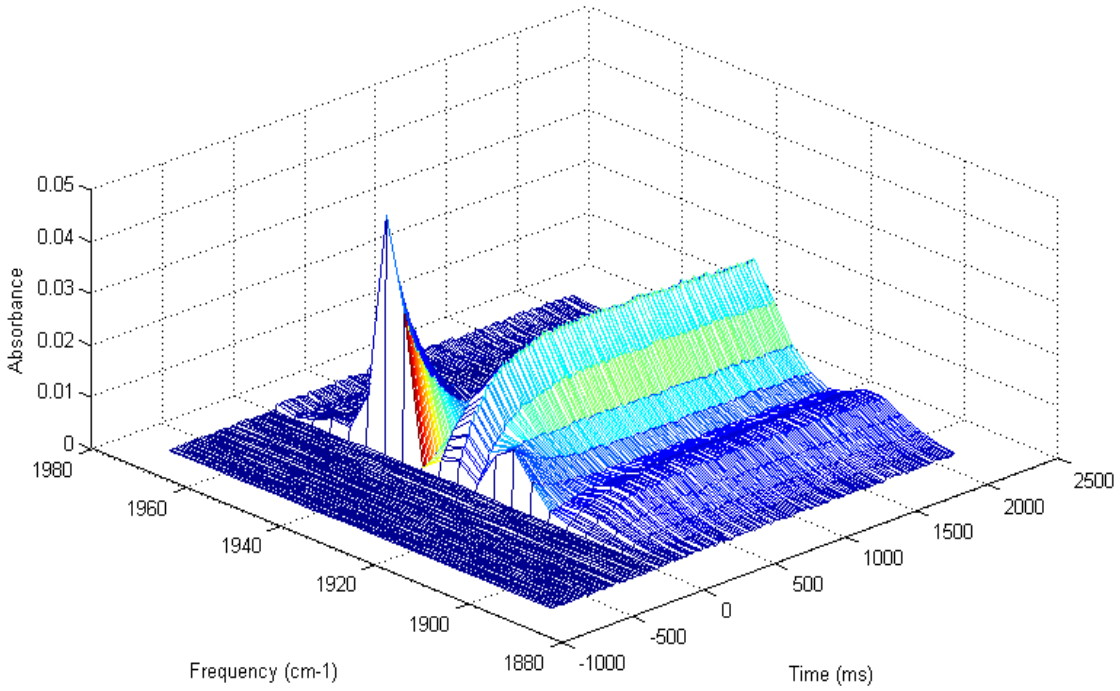

Figure 1-5: Time-resolved IR spectrum of the dissociation of $W(CO)_5$:C_6H_6.

This plot shows the decay of peaks at 1948 cm^{-1} and 1921 cm^{-1}, and growth of peaks at 1933 cm^{-1} and 1908 cm^{-1} over 3 seconds.

We do not see the formation of the initial peaks at 1948 cm^{-1} and 1921 cm^{-1} when there is no benzene in solution. These form at a much faster rate than the second set of peaks seen in our neat cyclohexane experiments. For these reasons, we conclude that this first complex is a $W(CO)_5$ complex with benzene. The second set of peaks are similar to the final peaks we see in our neat cyclohexane experiments. This suggests that the benzene complex is also not indefinitely stable. It too breaks apart and $W(CO)_5$ forms a new complex, likely with trace impurities in solution. However, the benzene complex lasts longer than the cyclohexane complex, which was completely gone by 14 milliseconds. The benzene complex is still present at 1 second, though it is rapidly being replaced (See Figure 1-5). With this information, we propose the following reaction is taking place:

$$W(CO)_5{:}C_6D_6 \rightarrow W(CO)_5{:}\text{impurity} \qquad (3)$$

We assigned the CO stretches at 1948 cm^{-1} and 1921 cm^{-1} to the complex $W(CO)_5{:}\eta^2{-}C_6D_6$, where C_6D_6 is interacting with W through one side of the ring. A DFT calculated structure for this complex is shown in Figure 1-6. The later stretches at 1933 cm^{-1} and 1908 cm^{-1} are assigned to $W(CO)_5$:impurity.

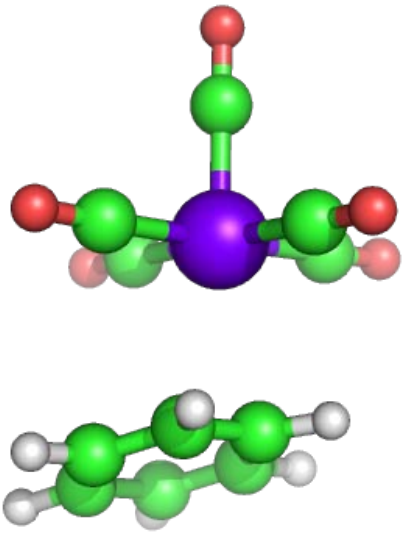

Figure 1-6: Structure of $W(CO)_5$:η^2–C_6H_6.

The geometry optimization was performed using B3LYP with the LANL2DZ ECP basis set for W, and 6-31G* for all other atoms.

To evaluate the temperature dependence on Reaction 3, we irradiated $W(CO)_6$ and a small amount of benzene in cyclohexane over a range of temperatures. However, the exact temperature of the sample during each experiment was not measured. We only measured the temperature of the glycol cooling the cell. We know this was not the temperature of the sample because the glycol temperatures ranged from -5°C to 7.5°C, but cyclohexane freezes at 6.5°C. Even though there is some freezing point depression with the addition of solutes, the solution freezes at temperatures above 0°C. So, there is some error in our measurement of temperature of the sample; however the trend should be the same even if the absolute temperature has some error. As shown in Figures 1-7 and 1-8, decays and rises of the CO stretches (and thus those

complexes) in these experiments are dependent on temperature. This dependence allows us to calculate the activation energy for these reactions, assuming pseudo-first order kinetics.

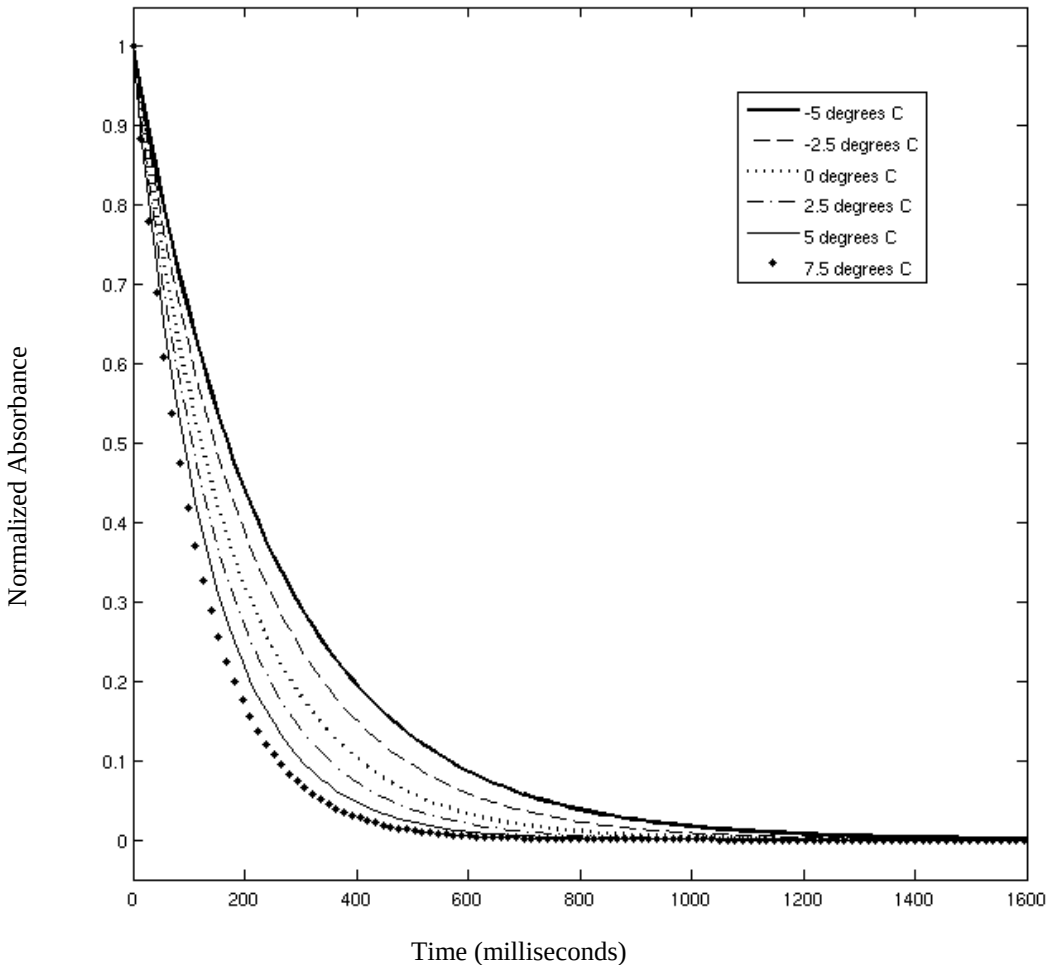

Figure 1-7: Temperature dependence on decay of peak at 1948 cm^{-1}.

A plot of the decay of the peak at 1948 cm^{-1} at several different temperatures. We can see that this peak decays at a faster rate as the temperature is raised.

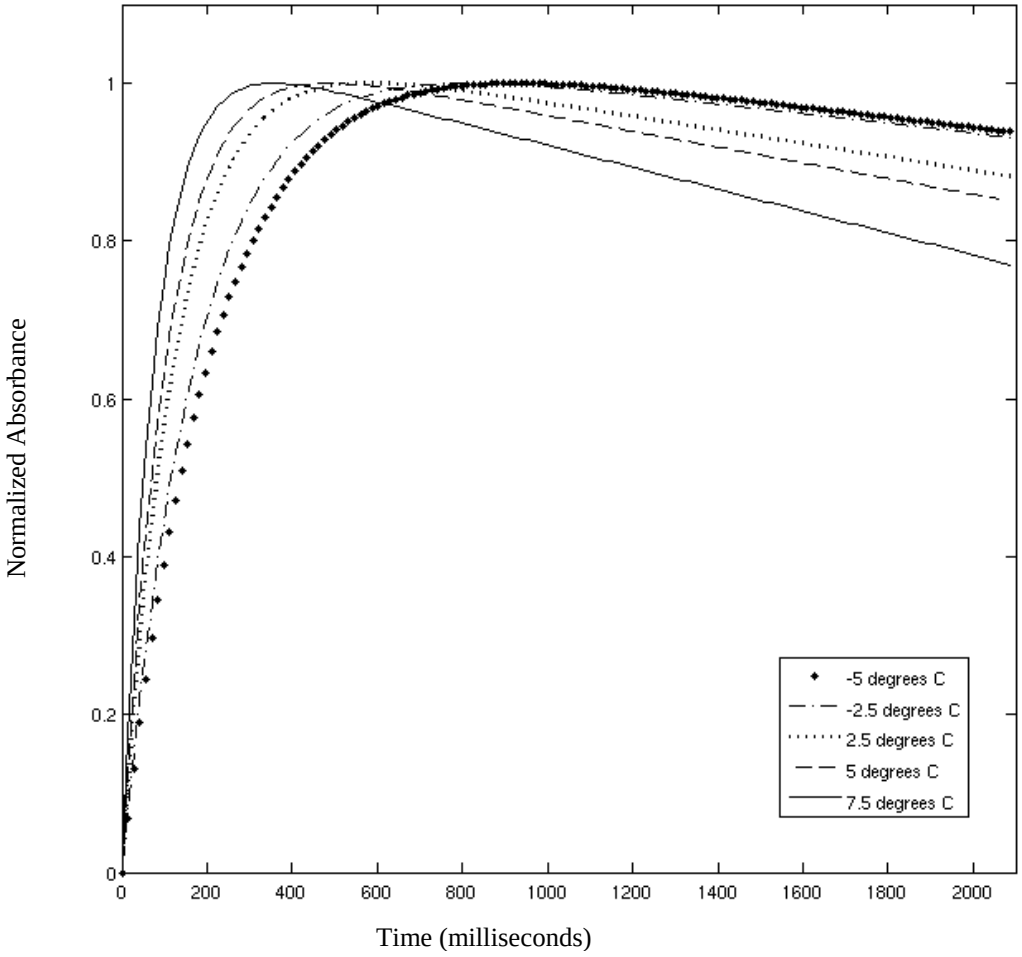

Figure 1-8: Temperature dependence on growth of peak at 1933 cm^{-1}.

A plot of the growth of peak at 1933 cm^{-1} at several temperatures. We see that as the temperature rises, the rate of growth of this peak rises. Thus, at higher temperatures the benzene product falls apart at a faster rate.

We calculated pseudo-first order rate constants by fitting the decays and rises to exponentials, as explained earlier and as shown in Figures 1-7 and 1-8. Table 1-1 shows the results from these fits.

	-5 °C	-2.5 °C	0 °C	2.5 °C	5 °C	7.5 °C
k (s^{-1})	4.08	4.73	5.69	6.55	7.62	8.87

Table 1-1: Rate constants for dissociation of $W(CO)_5$:η^2–C_6D_6.

Values of k (pseudo-first order rate constant) obtained from fitting the decay of the peak at 1948 cm^{-1} to an exponential at six temperatures.

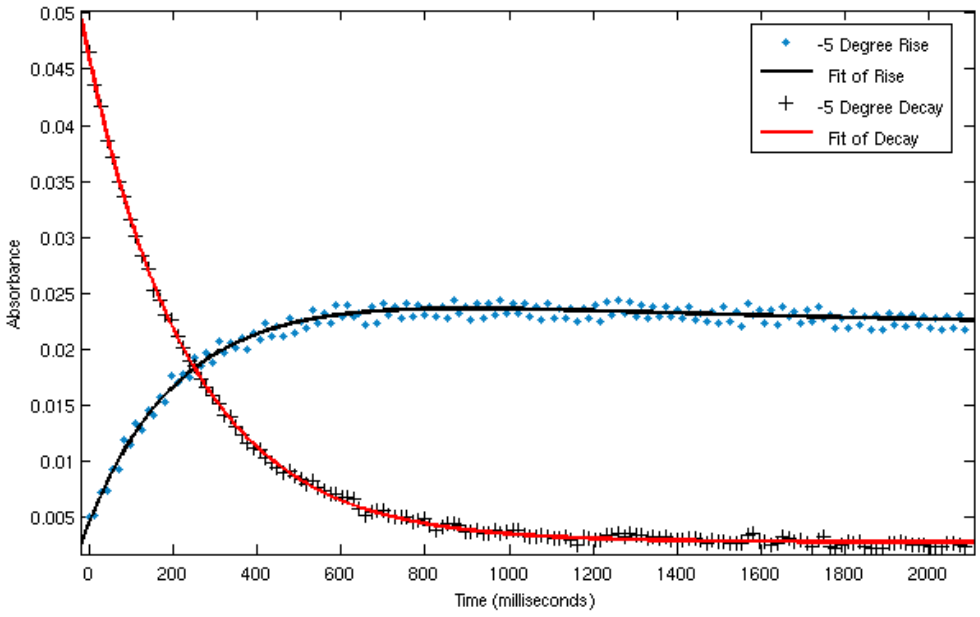

Figure 1-9: Fits of decay of peak at 1948 cm^{-1} and rise of peak at 1933 cm^{-1}.

The decay was fit using the following decaying exponential: $y = 0.04317e^{-0.004082x} + 0.002779$. The rise was fit using the following growing exponential multiplied by a decaying exponential, as discussed earlier: $y = \left(1 - 0.04775e^{-0.004134x} - 0.9426\right) * \left(0.08992e^{-0.0008949x} + 0.3799\right)$. As can be seen from the equation, the values of k (pseudo-first order rate constant) for each fit are approximately the same, 0.0041 ms^{-1}.

Table 1-1 shows only the values of k obtained from fitting the decay of the peak at 1948 cm^{-1}, but we also calculated k values by fitting the rise of the peak at 1933 cm^{-1} and obtained very similar values. An example of fitting both the rise and decay is shown in Figure 1-9. With these k values, we use an Arrhenius plot to calculate the activation energy of this reaction. The activation energy obtained using k values calculated using either the decay of the peak at 1947 cm^{-1} or the rise of the peak at 1933 cm^{-1} yielded the same result, 39 kJ/mol.

We performed these experiments using several different C_6D_6 concentrations: approximately 0.1%, 0.2%, 0.3% and 4%. We found that at the low benzene concentrations, the reaction happened very rapidly; in fact it was too rapid for us to reliably calculate the rate. At concentrations between 0.1% and 0.3% C_6D_6, the peak at 1948 cm^{-1} decays almost instantly, and the peak at 1933 cm^{-1} is already grown in at our initial data point. When we increase the concentration to approximately 4%, we can see the peak at 1933 cm^{-1} grow as the peak at 1948 cm^{-1} disappears. Thus, higher benzene concentrations slow the rate at which $W(CO)_5$:η^2–C_6D_6 falls apart.

The information for most data we collected was averaged over several different experiments to ensure reproducibility. However, we only collected one set of data with 4% C_6D_6. The rate constants and activation energy for this reaction were calculated using this one set of data, but should be repeated to check reproducibility. It would be useful to have data from additional C_6D_6 concentrations to better understand the rate dependence on concentration. Because the decay of the peak at 1948 cm^{-1} was so rapid at low benzene concentrations, exponential fits were poor, so there is error in the calculated rates. We can definitely see a trend in the rate as we increase C_6D_6 concentration, but cannot calculate this dependence with the current data.

1.3.2 Reactions with Mesitylene

After evaluating the reactions of $W(CO)_6$ with benzene in cyclohexane solution, we wanted to compare these to reactions with mesitylene (1,3,5-trimethylbenzene) under the same circumstances. Work by Stolz *et al.*[8] and Tyler *et al.*[5] suggest similar reactions occur, but the CO vibrational frequencies seen in the IR are slightly red shifted from those seen with benzene. This is indeed what we see in our experiments.

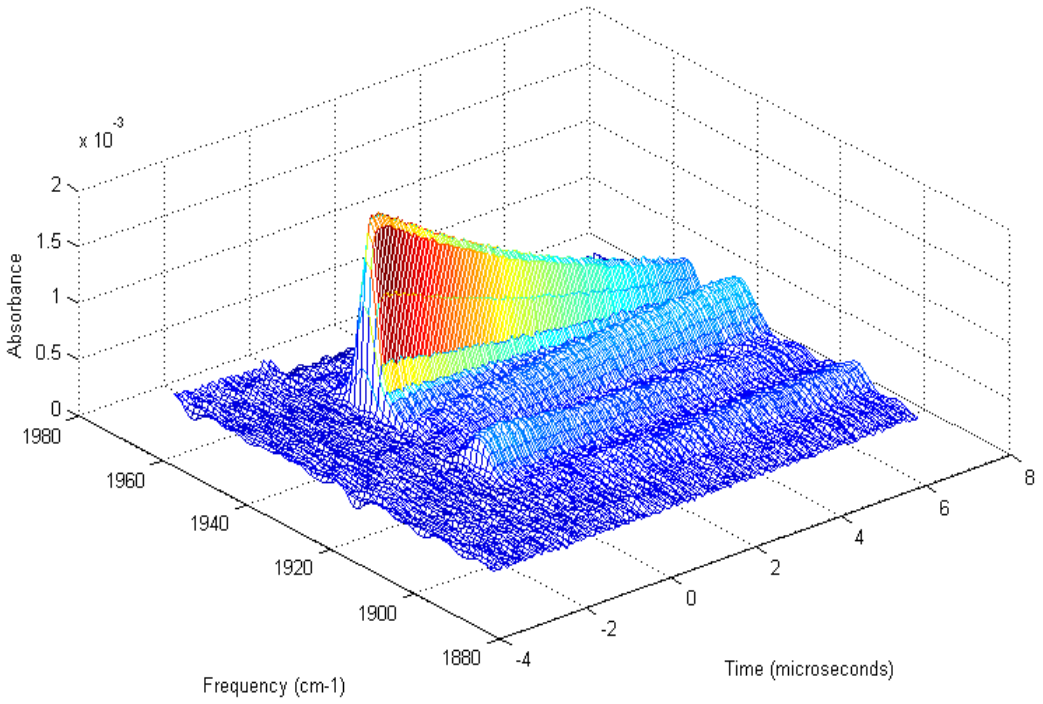

Figure 1-10: Time-resolved step scan IR spectra of $W(CO)_5$:mesitylene.

This plot shows the decay of peaks at 1954 cm^{-1} and 1928 cm^{-1}, and growth of peaks at 1941 cm^{-1} and 1915 cm^{-1} over 10 microseconds.

When a C_6H_{12} solution of $W(CO)_6$ with a low concentration of mesitylene (1,3,5-trimethylbenzene) is irradiated with 355 nm light, we immediately see the appearance of IR peaks at 1954 cm^{-1} and 1928 cm^{-1}. These peaks correspond to $W(CO)_5$:CyH as discussed earlier. On a nanosecond time scale, we see these peaks decay, and see two new peaks grow in at 1941 cm^{-1} and 1915 cm^{-1} as shown in Figure 1-10. These peaks are almost identical to those seen by Stolz *et al.* (1943 cm^{-1} and 1915 cm^{-1}) for $W(CO)_5$:mesitylene.[8] They appear on a time scale similar to the benzene complex, but the mesitylene complex IR peaks are slightly red shifted from the corresponding benzene complex (the benzene complex has peaks at 1948 cm^{-1} and 1921 cm^{-1}).

If we look at this reaction on a longer time scale, we see a difference from the reactions with benzene. On a millisecond time scale, the CO bands for this mesitylene complex decay a little, but not nearly as fast as for the benzene complex. It appears there are two new peaks growing in very slowly, but they appear just as shoulders on the mesitylene peaks, as shown in Figure 1-11. These new peaks are estimated to be at 1930 cm^{-1} and 1906 cm^{-1}.

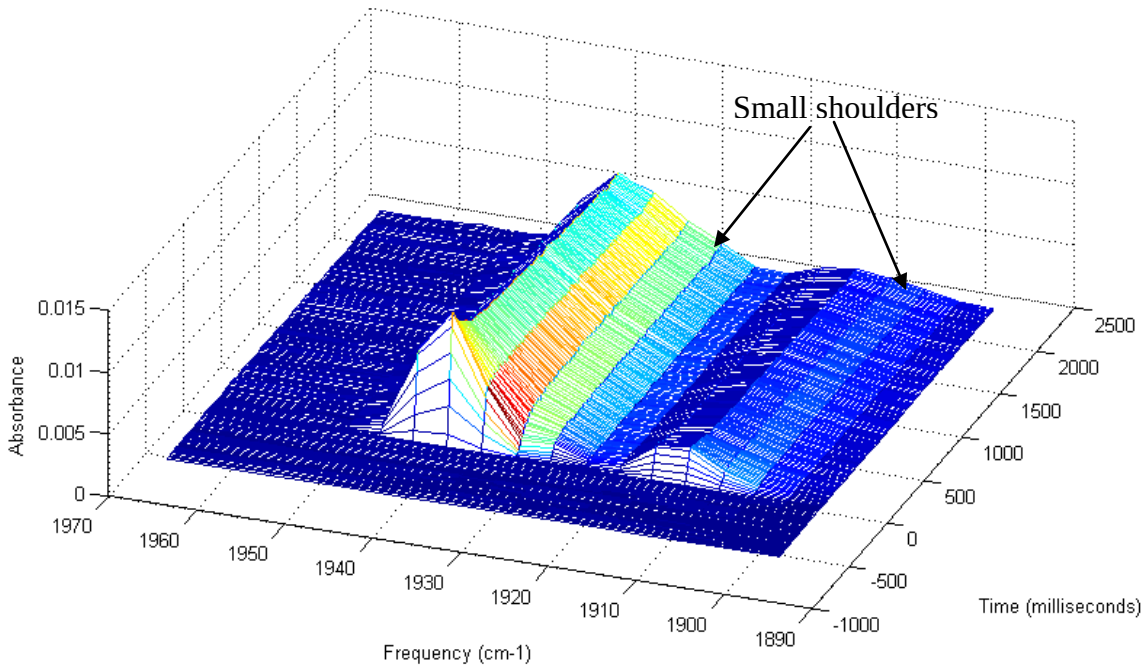

Figure 1-11: Time-resolved rapid can IR spectra of $W(CO)_5$:mesitylene.

This plot shows the very slow decay of peaks at 1941 cm^{-1} and 1915 cm^{-1}. We can also see small shoulders appearing as peaks grow in at approximately 1930 cm^{-1} and 1906 cm^{-1} over 3 seconds.

1.4 Discussion

1.4.1 Nature of the Benzene Complex

Three reactions occur with $W(CO)_6$ in a solution of cyclohexane with a small amount of benzene. The first is a reaction to form $W(CO)_5$:CyH, the second is to form $W(CO)_5$:C_6D_6, and the third is the dissociation of $W(CO)_5$:C_6D_6 as $W(CO)_5$ likely complexes with trace impurities in the solution.

In gas phase experiments, Wang *et al.*[6] report the formation of what they assign to be $W(CO)_5$:η^2-C_6H_6 within 3.2 μs after irradiation with 355-nm light. In the gas phase, this

complex seems to be stable for at least 1 ms. They suggest this complex involves an isolated double bond on benzene, but the transition state involves an agostic W–H–C interaction. Stolz *et al.* report this complex has C–O stretches at 1948 and 1921 cm^{-1}, and propose that the complex involves the entire benzene ring.[8] However, such a structure has never before been seen, and such benzene complexes are usually reported to interact through one side of the ring.[9,10,11] The IR bands seen by Stolz *et al.* are the same as the ones we see forming in Reaction 2, as tungsten complexes with benzene instead of cyclohexane. We believe this complex is $W(CO)_5{:}\eta^2\text{-}C_6H_6$, where the benzene is interacting through one side of the ring rather than the entire ring.

To explore the geometry of this benzene complex, we performed geometry and vibrational DFT calculations for three different types of benzene complexes: the first has benzene complexing through an agostic W–H–C interaction; the second has benzene complexing through one side of the ring; the third has benzene complexing through the entire ring. (Details of these calculations will be included in a later chapter; we will present only the results here.) We cannot calculate a stable complex in which the entire benzene ring is interacting with tungsten. Our attempts result in the benzene ring shifting so it is only interacting through one side of the ring. This result further justifies our proposal that the entire benzene ring is not interacting. It was also difficult to calculate a complex where benzene interacts through an agostic W–H–C interaction. While we were able to calculate a minimum energy structure by DFT methods, a vibrational analysis always showed at least one imaginary frequency. The calculated frequencies for this complex were also not what we see experimentally for $W(CO)_5{:}C_6H_6$. However, we were able to calculate a fully relaxed geometry for a complex in which benzene is interacting through one side of the ring, or a pi interaction. (The structure is shown in Figure 1-6). These computational results seem to support the mechanism suggested by

Wang *et al.*[6] where the benzene interacts with tungsten through only one side of the ring, but the transition state involves an agostic W–H–C interaction.

In solution, we see this benzene complex dissociate in approximately 1 second, and see another complex appear with C–O stretches at 1933 and 1908 cm^{-1}. This is much more stable than similar gas phase measurements, where the complex only lasts for only 1 ms. The difference in stability is primarily because the solvent is able to stabilize the complex in our experiments, while those in the gas phase have no solvent stabilization. But even with solvent stabilization, the benzene complex, while more stable than the corresponding cyclohexane complex, does not last indefinitely. We evaluated the effect of benzene concentration on the rate of dissociation of the benzene complex. We see that the reaction happens faster as we decrease the benzene concentration. This is likely because with more benzene in solution the probability that any $W(CO)_5$ in solution will react with another benzene is higher. Thus, even as the benzene complex falls apart, $W(CO)_5$ could react with another benzene molecule producing more $W(CO)_5$:C_6H_6. On the other hand, it can also react with an impurity in solution, leading to Reaction 3. But, this takes longer if there is more benzene in solution that is competing for reaction with $W(CO)_5$.

1.4.2 Mesitylene Complex

In comparing mesitylene to benzene, we see very similar initial reactivity. When mesitylene is present in small amounts in our solution, we first see $W(CO)_5$:CyH form. Then, just as with benzene, this cyclohexane complex dissociates as mesitylene complexes with $W(CO)_5$ to form $W(CO)_5$:mesitylene. The IR spectrum of the mesitylene complex is slightly red-shifted from the corresponding benzene complex. This is to be expected because the alkyl groups on the benzene in mesitylene are electron releasing. So, they donate more electron

density into the benzene ring, which can then be donated to the metal center. This increased donation to the metal center increases the pi back-bonding from the metal to the anti-bonding orbitals of the COs, and ultimately weakens those bonds.[12] So, the spectral shift is what we expect relative to the corresponding benzene complex.

Though the complexation of mesitylene with $W(CO)_5$ is similar to benzene, the longevity of these complexes is not the same. When benzene is in solution, the CO stretches in the IR spectrum of the $W(CO)_5$:benzene complex decay over approximately 1 second. However, with mesitylene in the same concentration, $W(CO)_5$:mesitylene lasts much longer. As seen in Figure 1-11, the CO stretches for this complex decay very little over 3 seconds. We believe there is a new complex forming, that is seen as shoulders on the red side of the mesitylene complex peaks. However, the rate is much slower than for that of benzene. One possible reason for this difference is steric hindrance. Perhaps it is more difficult for anything else in solution to access the tungsten complex when a larger and bulkier ligand is attached. If the impurity complexes via an associative mechanism, it would be harder to be close enough in proximity for the reaction to occur. Another possibility is that the complex formed with mesitylene is stronger. The alkyl groups on benzene are donating more electron density that can be shared, possibly strengthening the association between the ligand and the metal center. So, it is possible that the strength of the interaction with mesitylene results in a large activation energy for reactions with impurities in the solution, and thus slows down this final reaction.

1.4.3 Impurity Complex

We suspect the final product we see in our reactions is $W(CO)_5$ complexed with an impurity in the solution. There are several possibilities for this impurity. The first is a complex with Ar, which is used as the purge gas. The second possibility is a complex with water or

oxygen. Though we prepare the solutions to minimize the presence of water, it is possible there is still enough water in the solutions to react with the metal. Water could also be introduced by a poor seal by an o-ring or other connection in the experimental apparatus. The third possibility is this final complex is not with an impurity, but is a dimer formed by two $W(CO)_5$ fragments forming a W–W bond.

To investigate these possibilities, we used experiments and DFT calculations. The first experiment was to use He as a purge gas, rather than argon. When a solution of $W(CO)_6$ in neat C_6H_{12} is irradiated under this atmosphere, we see the same peaks in the IR spectrum that we see with Ar. DFT calculations of the vibrational frequencies predict $W(CO)_5$:Ar and $W(CO)_5$:He would have different spectra. In addition to this, the calculations predict IR bands with higher frequencies than those for $W(CO)_5$:C_6H_{12}, which is not consistent with our experimental data. Thus, we conclude that the impurity complex is not with argon. Further calculations of $W(CO)_5$:O_2 also predict higher frequency CO vibrational frequencies, so we do not believe this is the final complex. Calculations of both $W(CO)_5$:H_2O and $W(CO)_5$:$W(CO)_5$ produce vibrational frequencies that are similar to those we see experimentally. However, preliminary experiments with 5 mM $W(CO)_6$ rather than 1 mM $W(CO)_6$ do not show an appreciable change in the rate of formation of this complex. If the complex were indeed a dimer, we would expect it to form more rapidly with a higher concentration of $W(CO)_6$ in solution. We do not see this change, so it seems unlikely this is the case. However, it would be beneficial to do a more rigorous study of the effect of $W(CO)_6$ concentration on the rate of formation of this final complex. With this analysis, it seems likely the final impurity complex is $W(CO)_5$:H_2O, and we will refer to it as such in the following discussion.

1.4.4 Reaction Mechanisms

There has been considerable debate about the mechanism of weak metal:solvent interactions. The consensus seems to be that they are a complex associative interchange mechanism. This means the mechanism is a mixture between an associative reaction and a dissociative reaction, and depends on the specific ligand.[2,13] One study with thiophene and tetrahydrothiophene shows that ΔH and ΔG depend on the nature of the incoming ligand[2]. This suggests the reaction is not purely dissociative because the incoming ligands must play a role in the transition state. Another study using $Cr(CO)_6$ shows a shift from an interchange mechanism to a dissociative mechanism as the size of the incoming ligand increases.[14] Thus, steric hindrance will also play a role in the reaction mechanism. We are interested in investigating the mechanism of the ligand replacement reactions we see in solution. One tool we can use to probe this idea is DFT calculations of the binding energies. If the reactions are dissociative in nature, the activation energy should correspond to the energy required to break the bond with the organic molecule, in this case benzene. If the calculated bond dissociation energies (BDEs) do not correspond to the activation energies for the reactions, either we don't fully understand the kinetics and thus are calculating inaccurate activation energies, or the reactions are more associative in nature.

We will discuss the details of DFT calculations in a later chapter, and will just report relevant results here. Table 1-2 shows results from calculating the binding energies for each $W(CO)_5$ complex.

Complex	Density Functionals	Calculated Binding Energies (kJ/mol)
$W(CO)_5$:CyH	B3LYP	28.1
	M06	54.3
	M06-L	48.7
$W(CO)_5$:η^2-C_6H_6	B3LYP	46.7
	M06	88.0
	M06-L	81.3
$W(CO)_5$:H_2O	B3LYP	84.1
	M06	98.7
	M06-L	94.8

Table 1-2: Calculated binding energies for $W(CO)_5$ complexes.

Binding energies are calculated using three density functionals: B3LYP, M06, and M06-L.

If the reactions are purely dissociative in nature, the experimentally determined activation energy should correspond to the calculated binding energies for these complexes. For the reaction $W(CO)_5$:η^2–$C_6D_6 \rightarrow W(CO)_5$:$H_2O$ we calculated an activation energy of 39 kJ/mol. This is similar to the calculated binding energy for $W(CO)_5$:η^2–C_6D_6 when B3LYP is used, but is much lower than the calculated binding energy using either M06 or M06-L. The results from this are hard to determine because the binding energies calculated using the various density functionals are so varied. If B3LYP is correct, this seems to suggest that the reaction is close to purely dissociative, in which the benzene ring dissociates and then water associates to the free $W(CO)_5$ in solution. However, if the binding energy is indeed much higher than the experimental activation energy the reaction is probably more associative, where the transition state is stabilized by the presence of another ligand or solvent molecules. These calculations alone are not enough to determine the most accurate mechanism. Further experiments will need to be conducted to determine the true mechanism.

1.5 Conclusions

Upon photolysis, the organometallic complex $W(CO)_6$ loses a CO ligand, and coordinates with a solvent molecule. This creates a weak metal:solvent complex that we have measured at short times. Time-resolved infrared spectroscopy is used to observe the changes in frequency of the CO stretches of these short-lived complexes. In a dilute solution of $W(CO)_6$ and C_6H_6 in C_6H_{12}, tungsten first complexes with cyclohexane. However, over time, $W(CO)_5$:C_6H_{12} dissociates as a more stable complex with benzene forms. Calculations and results from similar experiments suggest this complex is $W(CO)_5$:η^2–C_6H_6. This benzene complex is more stable than the cyclohexane complex, but it still falls apart to form an impurity complex that is likely $W(CO)_5$:H_2O. Initial experiments suggest that the activation energy for the dissociation of the benzene complex is 39 kJ/mol. This activation energy is similar to binding energies calculated using B3LYP for $W(CO)_5$:η^2–C_6H_6, but is much smaller than binding energies calculated using M06 and M06-L. This discrepancy leaves us with still no firm conclusion on the mechanism, but suggests it has both dissociative and associative character.

References

(1) Cowan, A. J.; George, M. W. Formation and reactivity of organometallic alkane complexes. *Coord. Chem. Rev.* **2008**, *252*, 2504–2511.

(2) Schultz, R. H. Reactions of the Transient Species $W(CO)_5$(Cyclohexane) with Thiophene and Tetrahydrothiopene Studied by Time-Resolved Infrared Absorption Spectroscopy. *Organometallics* **2004,** *23,* 4349–4356.

(3) Dobson, G. R.; Asali, K. J.; Cate, C. D.; Cate, C. W. Mechanism of Alkane Displacement by 1-Hexene from (Alkane)$W(CO)_5$ Complexes (Alkane = Cyclohexane, *n*-Heptane). Estimates of the Alkane–W Bond Strengths in Condensed Media. *Inorg. Chem.* **1991**, *30*, 44/1–44/4.

(4) Paur-Afshari, R.; Lin, J.; Schultz, R. H. An Unusual Solvent Isotope Effect in the Reaction of $W(CO)_5$(solv) (solv = Cyclohexane or Cyclohexane-d_{12}) with THF. *Organometallics* **2000**, *19*, 1682–1691.

(5) Tyler, D. R.; Petrylak, D. P. Photochemical Studies of $M(CO)_6$ (M = Cr, Mo, W) at Low Temperature in Solution. Infrared Spectra of $M(CO)_5$(Solvent) (Solvent = Methylcyclohexane, methylenechloride) and $W(CO)_5L$ (L = aromatic hydrocarbon). *J. Organomet. Chem.* **1981**, *212*, 389–396.

(6) Wang, W.; Zheng, Y.; Lin, J.; She, Y.; Fu, K. Time-Resolved IR Study of Gas-Phase Reactions of Benzene with Group VIB Metal Pentacarbonyls and Tetracarbonyls. *J. Phys. Chem.* **1993**, *97*, 11921–11928.

(7) Church, S. P.; Grevels, F.; Hermann, H.; Schaffner, K. Structures and Kinetics of $Cr(CO)_5$ and $Cr(CO)_5 \cdot H_2O$ in Cyclohexane Solution. Flash Photolysis Study of $Cr(CO)_6$ with Infrared and Visible Detection. *Inorg. Chem.* **1985**, *24*, 418–422.

(8) Stolz, I. W.; Haas, H.; Sheline, R. K. Infrared Spectroscopic Evidence for New Metal Carbonyl Complexes with Aromatic Ligands. *J. Am. Chem. Soc.* **1965**, *87*, 716–718.

(9) Zhang, S.; Dobson, G. R.; Zang, V.; Bajaj, H. C.; van Eldik, R. Octahedral Metal Carbonyls. 71. Kinetics and Mechanism of Benzene Displacement from Photogenerated [(η^2-benzene)$Cr(CO)_5$]. *Inorg. Chem.* **1990**, *29*, 3477–3482.

(10) Ladogana, S.; Nayak, S. K.; Smit, J. P.; Dobson, G. R. Kinetics and Mechanism of Ligand Exchange in Photogenerated (η^2-monoalkylarene)$Cr(CO)_5$ Complexes with Alkenes; Evidence for Involvement of Aliphatic Chains in the Arene and Alkene in the Exchange Process. *Organometallics* **1997**, *16*, 3051–3054.

(11) Rundle, R. E.; Goring, J. H. Structure of the Silver Perchlorate-Benzene Complex. *J. Am. Chem. Soc.* **1950**, *72*, 5337.

(12) Szilagyi, R. K.; Frenking, G. Structure and Bonding of the Isoelectronic Hexacarbonyls $[Hf(CO)_6]^{2-}$, $[Ta(CO)_6]^{-}$, $W(CO)_6$, $[Re(CO)_6]^{+}$, $[Os(CO)_6]^{2+}$, and $[Ir(CO)_6]^{3+}$: A Theoretical Study. *Organometallics* **1997**, *16*, 4807–4815.

(13) Kelly, J. M.; Long, C. Laser Flash Photolysis of $M(CO)_6$ (M = Cr, Mo, or W) in Perfluoromethylcyclohexane. The Generation of Highly Reactive Coordinatively Unsaturated Species. *J. Phys. Chem.* **1983**, *87*, 3344–3349.

(14) Dobson, G. R.; Zhang, S. Mechanism of Displacement of Alkanes from Photogenerated (Alkane) $Cr(CO)_5$ Complexes. *J. Coord. Chem.* **1999**, *47*, 409–416.

Chapter 2: Reactions of $Cr(CO)_6$

2.1 Introduction

Reactions of organometallic carbonyl complexes are mostly dissociative in nature, and form metal:solvent complexes upon photolysis. Though these reactants can be very complex, we can learn a great deal by studying simplified test molecules. One simple molecule often used for this purpose is $M(CO)_6$, where M is a transition metal. This class of test molecules loses a CO and coordinates to a solvent molecule upon irradiation. $M(CO)_5$:solvent complexes have been studied using infrared spectroscopy, focusing on the stretching modes of the CO ligands. CO stretches are good candidates to study in the IR because their stretching modes have a large absorption cross-section and are very sensitive to the electron density around the metal atom. Weak metal:solvent complexes have short lifetimes, so to study them, these complexes must either be trapped or measured at short times. One way to measure at short times is through time–resolved infrared spectroscopy, which can provide good molecular detail. Limited measurements using NMR have also been made by Ball *et al.*[1]

After looking at $W(CO)_6$ we decided to also look at $Cr(CO)_6$. Cr is a group 6 transition metal like W, so it contains the same number of valence electrons. However, it contains fewer core electrons than W. Thus, we would expect the reactivity to be quite similar, since it is a function of the valence electrons, but expect chromium to be more reactive than tungsten.[2] We were interested to see what differences were caused from the decrease in mass and core electrons in Cr versus W. Similar to W, when in a solution with cyclohexane, $Cr(CO)_6$ reacts rapidly following irradiation to form $Cr(CO)_5$:CyH (CyH = cyclohexane).[3,4] Upon irradiation in solution, one CO dissociates from $Cr(CO)_6$, and $Cr(CO)_5$ is formed initially in an excited state.[5] It then electronically relaxes prior to coordinating a solvent molecule[6], cyclohexane in our case.

Wang *et al.* identified naked $Cr(CO)_5$ in cyclohexane solution that appeared in less than 1 ps following irradiation by 266 nm light, and had all complexed with cyclohexane in 63 ps.[7]

When $Cr(CO)_6$ and benzene are together in a solution, a similar reaction occurs; $Cr(CO)_6$ reacts to ultimately form $Cr(CO)_5$:C_6H_6.[8] Like our studies with tungsten, we are interested in the exchange of ligands when both cyclohexane and small amounts of benzene are present in solution. Similar to tungsten, in this case we see an initial complexation of $Cr(CO)_5$ with cyclohexane. However, over time, this disappears and we see $Cr(CO)_5$ complex with benzene. This complex with benzene then dissociates, as $Cr(CO)_5$ complexes with an impurity in the solution. We are interested in studying both the complexation with benzene, which occurs on a nanosecond time scale, and the dissociation of this complex, which occurs on a microsecond time scale.

2.2 Experimental

2.2.1 Reagents

$Cr(CO)_6$ (Aldrich, 99%) and mesitylene (Acros Organics, 99%) were used as received. C_6H_{12} (Fisher Scientific, HPLC grade) was distilled over Na (Columbus Chemical Industries, ACS grade) with benzophenone (Acros Organics, 99%) under an Ar atmosphere until the solution became blue, indicating that all O_2 and H_2O had been consumed; the solution was then refluxed, and the dried solvent was condensed and collected. C_6H_6 was dried in a high pressure alumina column in an Ar atmosphere to minimize water and O_2.

Water and O_2 are known to react with the weak metal:solvent complexes we are generating.[3] Thus, it is important to minimize their presence during sample preparation. To accomplish this, all preparation and experiments were performed in an Ar environment. All glassware was dried in an oven for at least 12 hours prior to use. A round bottom flask was

charged with $Cr(CO)_6$ and filled with Ar. C_6H_6 was added using a syringe under a positive pressure of Ar, followed by C_6H_{12}. All solutions were 2.5 mM $Cr(CO)_6$. Benzene concentrations were varied from 0.25% to 5% by volume. Solutions using mesitylene rather than benzene were prepared using the same method. Mesitylene concentrations were either 1% or 4% by volume.

2.2.2 Photochemistry

Transient infrared measurements were made using a Bruker IFS-66 FTIR spectrometer, with the necessary modifications for step-scan experiments. Briefly, for a step-scan experiment, the interferometer moving mirror is held in a fixed position, the laser initiates the reaction, and a measurement of the change in signal is taken at that mirror position every 25 ns. The mirror is then stepped to the next position and the process is repeated until enough positions have been measured to generate a spectrum. All measurements used a fast Mercury Cadmium Telluride (MCT) detector with a 10 ns rise time, and signals were digitized with a 12-bit, 100 MS/s digitizer. The IR beam was 8 mm in diameter. The resolution of our measurements is 4 cm^{-1}.

Laser pulses for UV excitation are generated as the frequency tripled (355 nm) output of a Nd:YAG laser (Coherent Infinity). Excitation energy is kept at 2-5 mJ per pulse to minimize sample degradation during the experiment. The pump (UV) and probe (IR) beams are completely overlapped in the sample, with an angle of approximately 20 degrees between the two beams. The solution is flowed through a 1 mm path length temperature-controllable CaF_2 IR cell, and is irradiated with the UV light at 30 Hz. Samples are kept under a positive pressure of Ar, and maintained at a constant temperature.

For experiments on a nanosecond time scale, 200 time slices are collected, each having 25 ns time resolution. The time-dependent part of the signal is amplified 8x to improve signal

detection. For experiments on a microsecond time scale, 300 time slices, each having 1000 ns resolution, are collected. The time-dependent part of the signal is amplified 2x to improve signal detection.

2.2.3 Data Analysis

Text files from each kinetic trace were extracted from the data using OPUS Version 3.1. We then used MATLAB 7.0 to analyze the kinetic data. The pseudo-first order rate constant, k, for each kinetic trace is determined by fitting the absorbance data to an exponential. Both the rate of decay of the intermediate and the rate of growth of the product are measured. For the nanosecond resolution data, a single decaying exponential is sufficient to fit the decay of peaks, as shown in Figure 2-1. However, a more complex equation is required to fit the peak growth. The peak begins to decay over the course of the experiment as this initial complex dissociates to form a new complex. To account for this decay, we use a decaying exponential plus a linear component: $y = ae^{-kx} + bx + c$.

For these same reasons, we use the exponential plus linear component to fit both the rise and the decay of peaks in the microsecond resolution data. In addition to the above reasons, there are also competing reactions when the final complex does actually break apart as $Cr(CO)_5$:solvent complexes react with O_2 or OH^- in solution, or lose additional carbonyl ligands. These all cause the signal to decay slowly while it is growing in much more rapidly. Using just a single exponential growth does not accurately fit the peak profile. So, we opted to use a more complicated fit to better capture the real rate of growth or decay of the peaks. After calculating k from these fits, Arrhenius plots of ln(k) vs. 1/T of the reaction are used to calculate the activation energy of the transition. The pseudo first-order rate constants, as well as the activation energies reported are averaged over several experiments to ensure reproducibility.

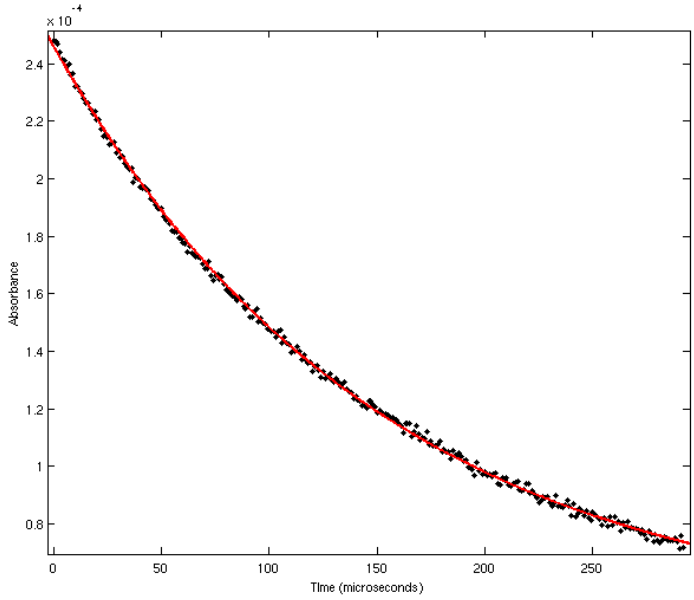

Figure 2-1: Exponential fit of decay of peak at 1957 cm^{-1}.

This is an example of the decay on the nanosecond time scale. It can be fit to a simple decaying exponential, which for this particular decay is: $y = 0.0002e^{-0.00667x} + 4.5\times10^{-5}$.

2.3 Results

2.3.1 Reactions with Cyclohexane and Benzene

Upon irradiation of a C_6H_{12} solution of $Cr(CO)_6$ and a small amount of C_6H_6 by 355 nm light we see three sequential reactions occur, as evidenced by changes in the IR spectrum. The progress of the reactions can be monitored by looking specifically at the CO stretches in the infrared spectrum. The first change we see is a bleach of the parent $Cr(CO)_6$ at 1984 cm^{-1}. Because the absorbance of the parent molecule is so large, there is little to no light reaching the detector at 1984 cm^{-1}. Thus, the calculation of absorbance causes division by zero, which leads to unusable data at 1984 cm^{-1}. For this reason, we cannot show an accurate depiction of the

bleach of $Cr(CO)_6$. As $Cr(CO)_6$ dissociates, CO-stretching vibrations at 1957 cm^{-1} and 1932 cm^{-1} appear. On a nanosecond time scale, these two vibrations begin to decay and new CO stretches at 1950 cm^{-1} and 1925 cm^{-1} grow in on the same time scale (Figure 2-2). Within approximately 4 microseconds, the stretches at 1950 cm^{-1} and 1925 cm^{-1} decay, and new C–O stretches at 1943 cm^{-1}, 1913 cm^{-1}, and 1908 cm^{-1} appear (Figure 2-3).

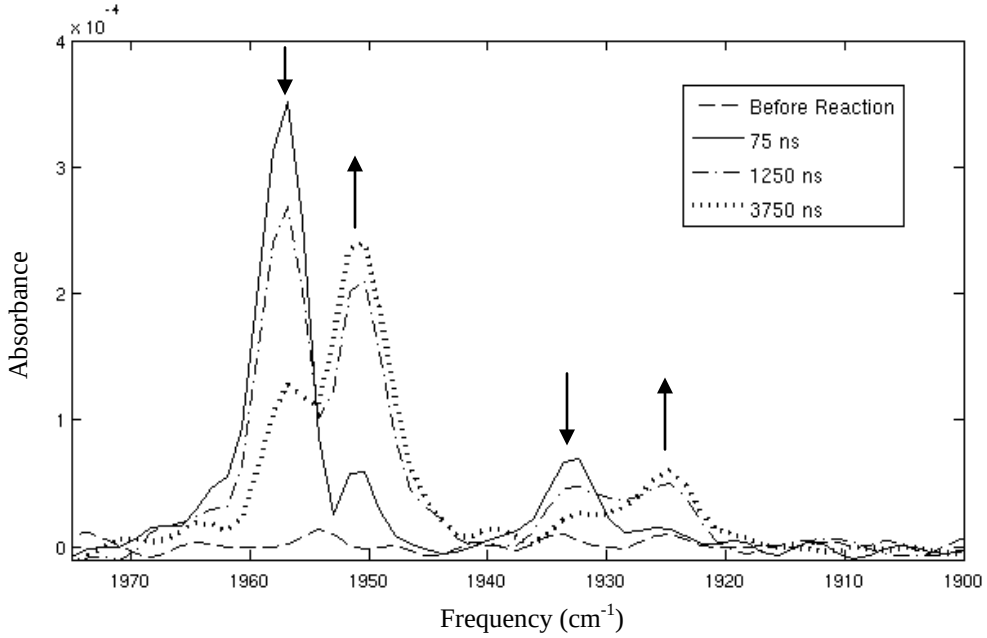

Figure 2-2: Spectrum on a nanosecond time scale, after irradiation of $Cr(CO)_6$ in C_6H_{12} with C_6H_6.

Peaks at 1950 cm^{-1} and 1925 cm^{-1} grow as peaks at 1957 cm^{-1} and 1932 cm^{-1} decay.

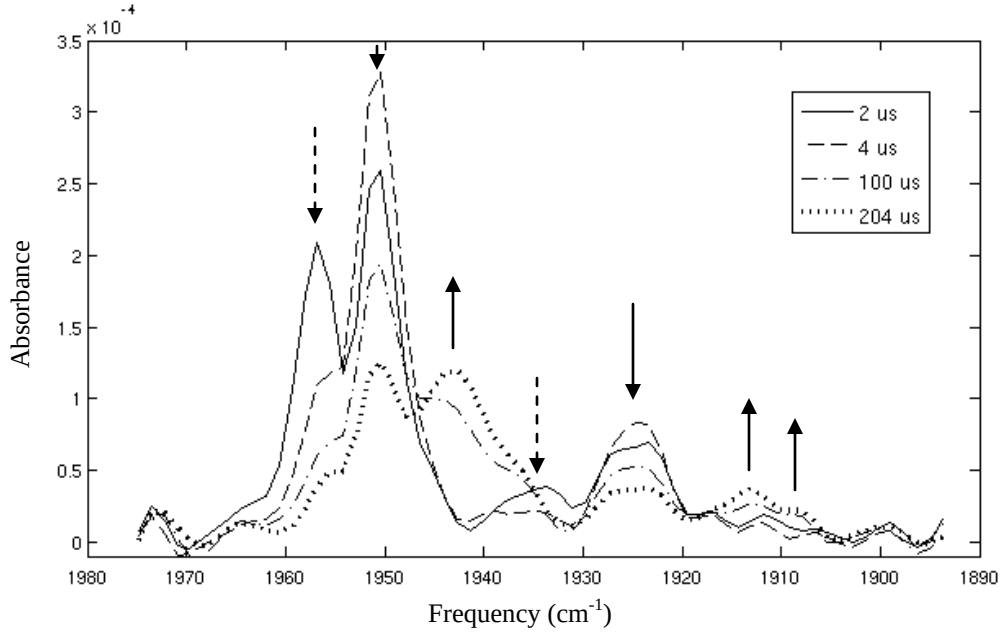

Figure 2-3: Spectrum on a microsecond time scale, after irradiation of $Cr(CO)_6$ in C_6H_{12} with C_6H_6.

Peaks at 1943 cm^{-1}, 1913 cm^{-1}, and 1908 cm^{-1} grow as peaks at 1950 cm^{-1} and 1925 cm^{-1} decay (solid arrows). We can also see peaks at 1957 cm^{-1} and 1932 cm^{-1} decay very rapidly, within the first couple scans (dashed arrows). These are the same peaks we could see decaying on a nanosecond time scale in Figure 2-2.

Experiments with $Cr(CO)_6$ in neat cyclohexane (performed both by us and others[3,4]), result in a bleach at 1984 cm^{-1} and the growth of peaks at 1957 cm^{-1} and 1932 cm^{-1}. These frequencies also match those of the first transient in our reactions containing both C_6H_{12} and C_6H_6. Thus we have assigned this first transient to be $Cr(CO)_5$:C_6H_{12}., formed through the following reaction.

$$Cr(CO)_6 + C_6H_{12} \rightarrow Cr(CO)_5{:}C_6H_{12} \qquad (1)$$

Similar to our experiments with $W(CO)_6$, this cyclohexane complex is not indefinitely stable when no benzene is present in solution. Over time, it dissociates as $Cr(CO)_5$:C_6H_{12} reacts with an impurity in the solution, as can be seen in Figure 2-4. This new impurity complex appears after about 100 microseconds, and increases very slowly. It is evident by new peaks at 1943 cm^{-1} and 1914 cm^{-1} (very weak).

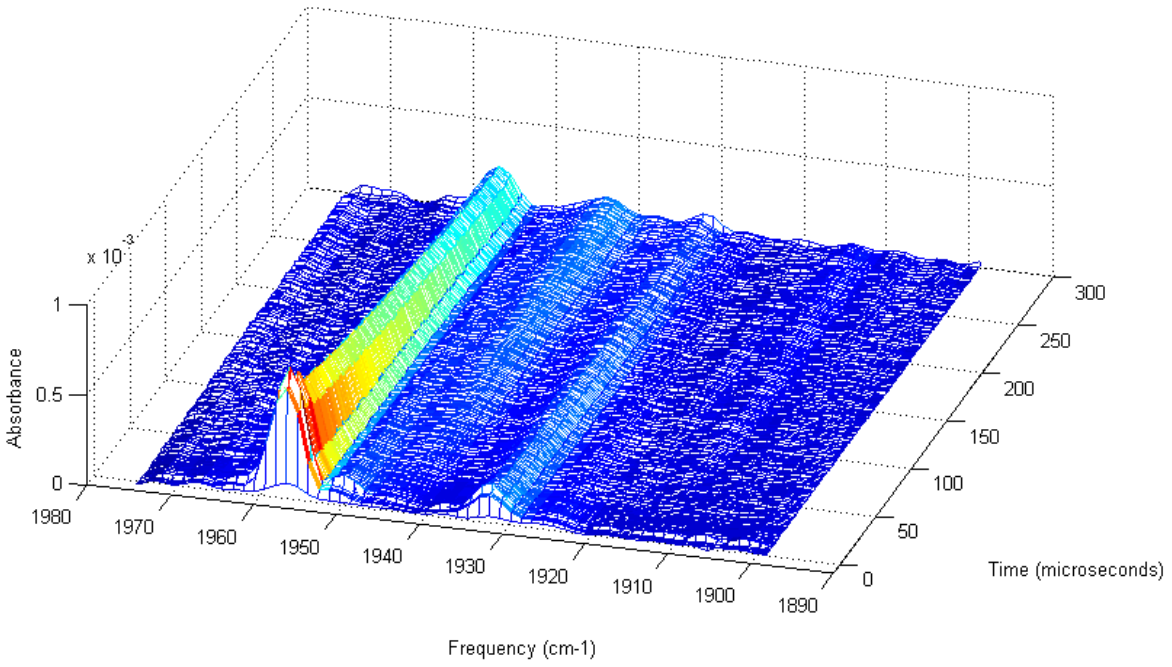

Figure 2-4: $Cr(CO)_6$ in neat cyclohexane.

Upon irradiation of $Cr(CO)_6$ in neat cyclohexane, we see two stretches in the IR, one at 1932 cm^{-1} and one much stronger one at 1957 cm^{-1}. These slowly decay as new peaks at 1943 cm^{-1} and 1914 cm^{-1} grow in.

When $Cr(CO)_6$ is in a solution of cyclohexane with a low concentration of benzene, the first reaction yields $Cr(CO)_5$:CyH (CyH = cyclohexane) as discussed above. Then, the second reaction produces a complex with CO-stretches at 1950 cm^{-1} and 1925 cm^{-1}, as can be seen in

Figure 2-5. The third complex has CO-stretches at 1943 cm^{-1},1913 cm^{-1}, and 1908 cm^{-1} as can be seen in Figure 2-6.

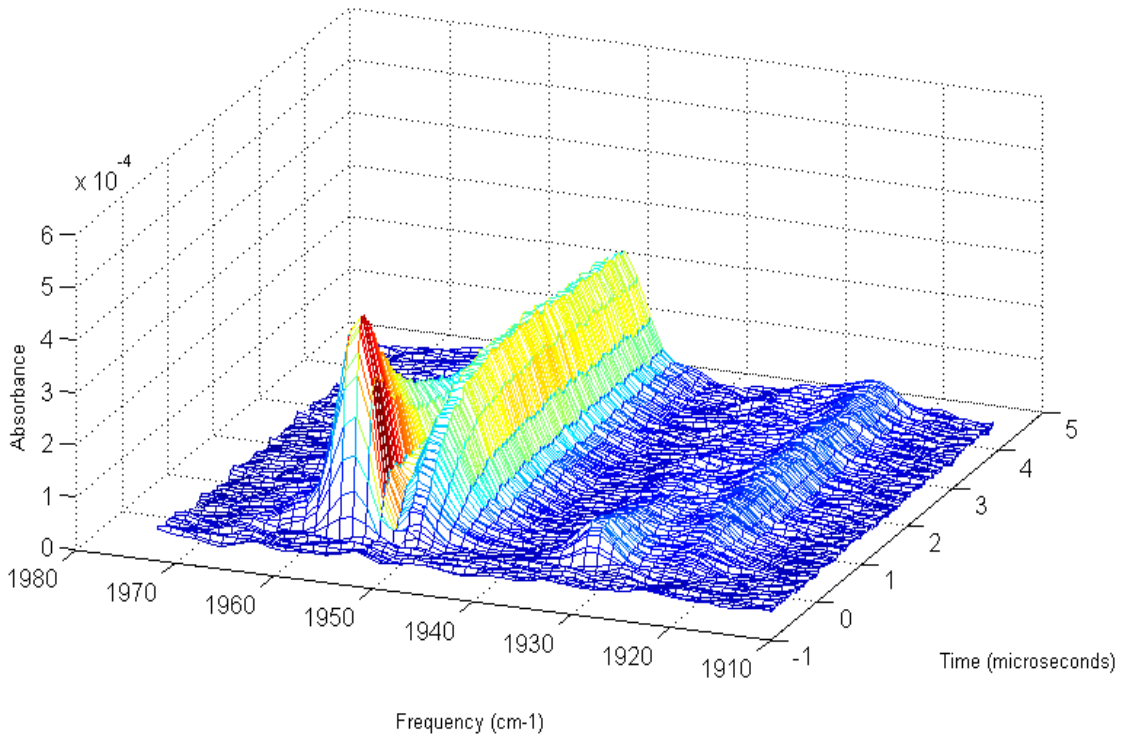

Figure 2-5: Time-resolved IR spectrum of Reaction 2: $Cr(CO)_5$:C_6H_{12} reacting with benzene to form $Cr(CO)_5$:C_6H_6.

This plot shows the decay of peaks at 1957 cm^{-1} and 1932 cm^{-1}, and growth of peaks at 1950 cm^{-1} and 1925 cm^{-1} over 5 microseconds.

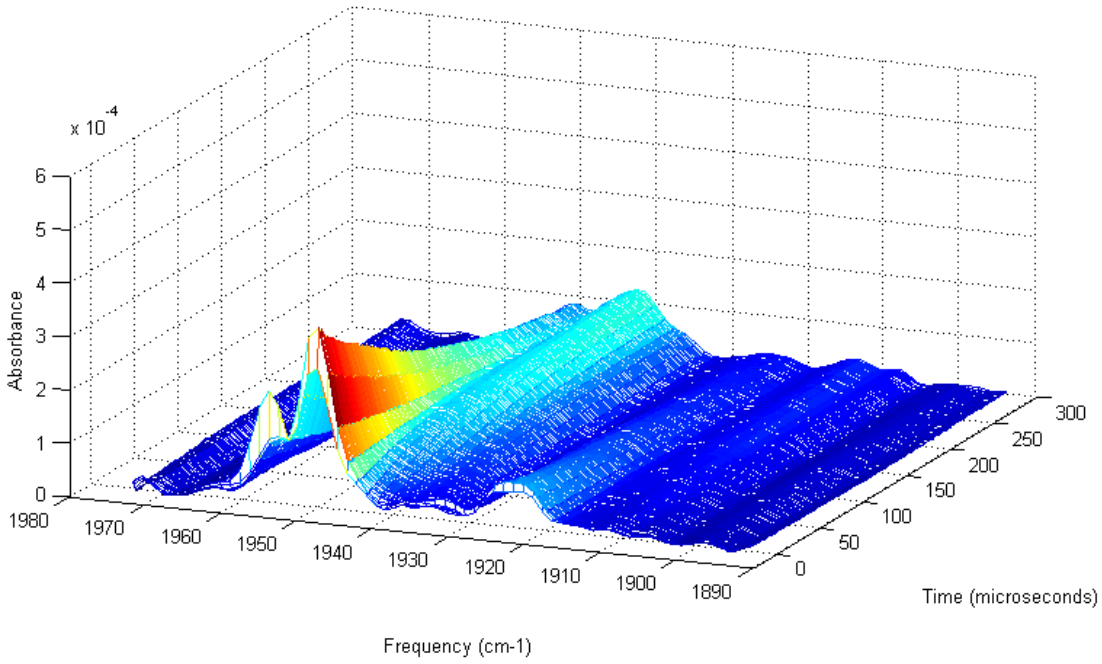

Figure 2-6: Time-resolved IR spectrum of Reaction 3: dissociation of $Cr(CO)_5$:C_6H_6.

This plot shows the decay of peaks at 1950 cm^{-1} and 1925 cm^{-1}, and growth of peaks at 1943 cm^{-1}, 1913 cm^{-1}, and 1908 cm^{-1} over 300 microseconds.

The first set of peaks in Figure 2-5 corresponds to $Cr(CO)_5$:CyH. These peaks decay as a new set of peaks grows in at 1950 cm^{-1} and 1925 cm^{-1}. Hermann *et al.* report IR bands at 1950 cm^{-1} and 1914 cm^{-1} for $Cr(CO)_5$:C_6H_6.[9] The band at 1950 cm^{-1} is consistent with the IR bands we see form as the cyclohexane complex dissociates, but we also see another much weaker band at 1925 cm^{-1}. This reaction parallels what we saw with $W(CO)_6$. As with tungsten, we propose that the benzene ring is interacting with chromium through one side of the ring. (Structure of $(CO)_5$: η^2–C_6H_6 is shown in Figure 2-7.) This benzene complex is formed as follows.

$$Cr(CO)_5{:}C_6H_{12} + C_6H_6 \rightarrow Cr(CO)_5{:}\ \eta^2\text{–}C_6H_6 + C_6H_{12} \qquad (2)$$

Like the complex with cyclohexane, this benzene complex does not last forever. The corresponding CO-stretches decay while new ones appear at 1943 cm^{-1}, 1913 cm^{-1}, and 1908 cm^{-1}. We believe this final product is the interaction with an impurity in the solution, and not with either benzene or cyclohexane. Thus, we propose this complex is formed through the following reaction.

$$Cr(CO)_5{:}\eta^2{-}C_6H_6 \rightarrow Cr(CO)_5{:}\text{impurity} \qquad (3)$$

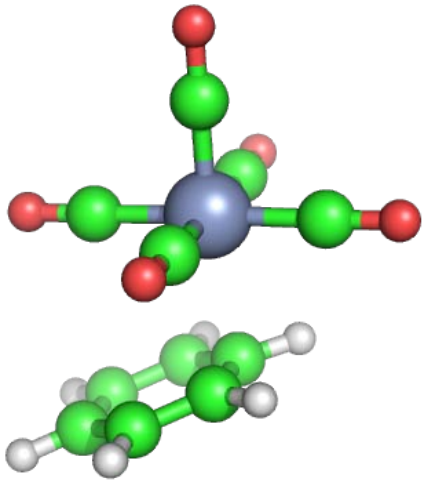

Figure 2-7: Structure of $Cr(CO)_5{:}\eta^2{-}C_6H_6$.

The geometry optimizations were performed using B3LYP with the LANL2DZ basis set for Cr, and 6-31G* for all other atoms.

We performed experiments with $Cr(CO)_6$ and a small amount of benzene in C_6H_{12} over a range of temperatures, from approximately 6°C to 40°C. As can be seen in Figures 2-8 and 2-9,

the decays and rises of the CO-stretches of the various complexes (and thus the complexes themselves) are dependent on temperature. This allows us to calculate the activation energy for these reactions, assuming pseudo-first order kinetics.

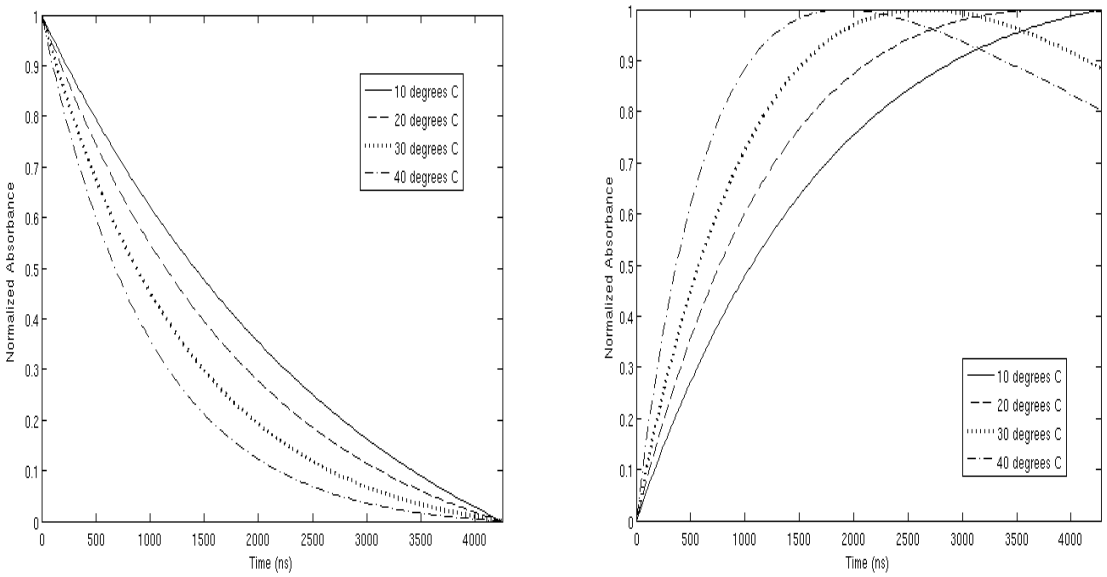

Figure 2-8: Temperature dependence on decay of peak at 1957 cm^{-1} and growth of peak at 1950 cm^{-1} over 4 microseconds.

A plot of the growth of peak at 1950 cm^{-1} and the decay of peak at 1957 cm^{-1} at several temperatures. We see that as the temperature rises, the rate of growth or decay of these peaks increases. Thus, at higher temperatures the reaction to form a complex between $Cr(CO)_5$ and benzene occurs at a faster rate.

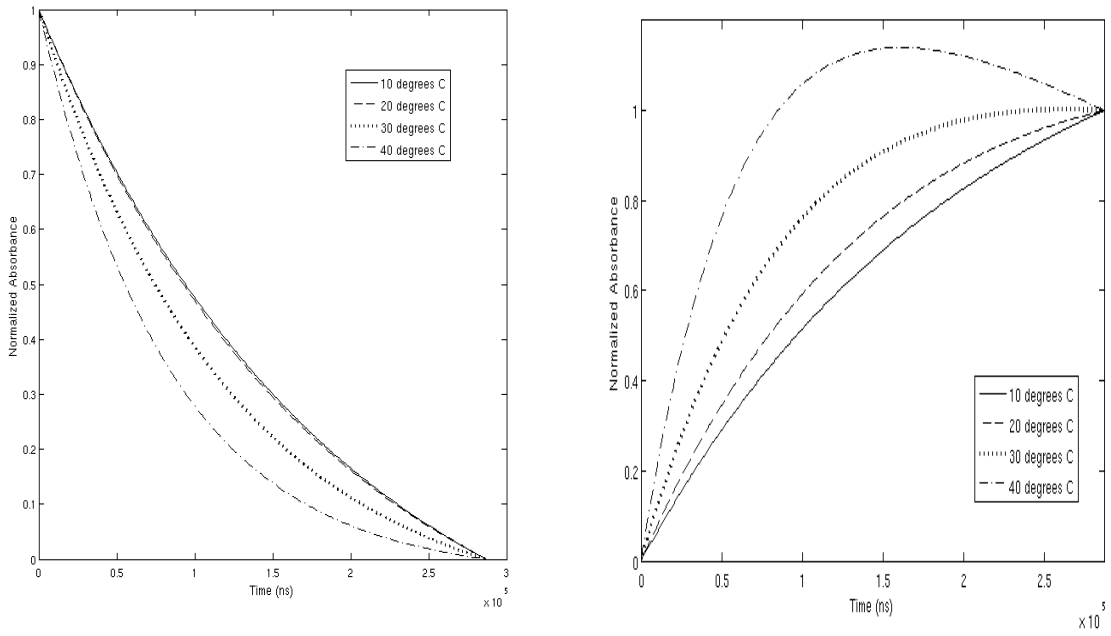

Figure 2-9: Temperature dependence on decay of peak at 1950 cm^{-1} and growth of peak at 1943 cm^{-1} over 300 microseconds.

A plot of the growth of the peak at 1943 cm^{-1} and the decay of the peak at 1950 cm^{-1} at several temperatures. We see that as the temperature rises, the rate of growth or decay of these peaks increases. Thus, the benzene dissociates faster at higher temperatures.

We calculated pseudo-first order rate constants by fitting the decays and rises to exponentials, as explained earlier and as shown in Figures 2-8 and 2-9. We performed these calculations for reactions 2 and 3. Tables 2-1 and 2-2 show the calculated rate constants from these fits.

	10 °C	17 °C	20 °C	26 °C	31 °C	37 °C
k (ns^{-1})	0.00045 (3e-5)	0.00057 (3e-5)	0.00064 (3e-5)	0.00076 (2e-5)	0.00095 (6e-5)	0.0012 (1e-4)

Table 2-1: Rate constants for $Cr(CO)_5$:C_6H_{12} → $Cr(CO)_5$:η^2–C_6H_6.

Values of k (pseudo-first order rate constant) obtained from fitting the decay of the peak at 1957 cm^{-1} to an exponential at six temperatures. These values are from experiments using 1% benzene by volume. Values in parentheses are standard deviations calculated from k values obtained from multiple experiments.

	10 °C	20 °C	30 °C	39 °C
k (ns^{-1})	4e-6 (2e-6)	5e-6 (1e-6)	7.1e-6 (9e-7)	1.1e-5 (2e-6)

Table 2-2: Rate constants for dissociation of $Cr(CO)_5$:η^2–C_6H_6.

Values of k (pseudo-first order rate constant) obtained from fitting the decay of the peak at 1950 cm^{-1} to an exponential at four temperatures. These values are from experiments using 0.5% benzene by volume. Values in parenthesis are standard deviations calculated from k values obtained from multiple experiments.

Table 2-1 shows only the values of k obtained from fitting the decay of the peak at 1957 cm^{-1}, but we also calculated k values by fitting the rise of the peak at 1950 cm^{-1} and obtained similar values (see Figure 2-10). With these k values, we used an Arrhenius plot to calculate the activation energy of this reaction. The activation energy obtained using k values calculated using either the decay of the peak at 1957 cm^{-1} or the rise of the peak at 1950 cm^{-1} yields similar results, with an average activation energy of 30(±8) kJ/mol.

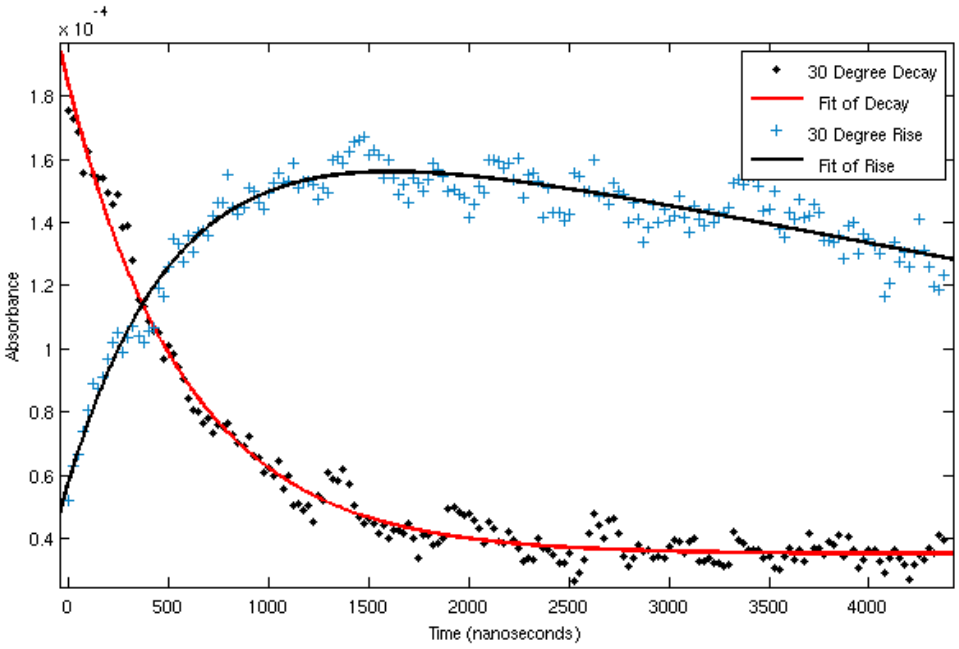

Figure 2-10: Fits of decay of peak at 1957 cm^{-1} and rise of peak at 1950 cm^{-1}.

The decay was fit using the following decaying exponential:

$y = 0.0001488e^{-0.0017x} + 3.501\times10^{-5}$. The rise was fit using the following growing exponential with an added linear portion to account for dissociation of $Cr(CO)_5$:C_6H_6, as discussed earlier:

$y = -0.0001253e^{-0.001802x} - 1.23\times10^{-8}x + 0.0001827$. As can be seen from the equation, the values of k (pseudo-first order rate constant) for each fit are approximately the same, 0.0017 ns^{-1}.

Similar to Table 2-1, Table 2-2 shows only the values of k obtained from fitting the decay of the peak at 1950 cm^{-1}, but we also calculated k values by fitting the rise of the peak at 1943 cm^{-1} and obtained similar values (see Figure 2-11). With these k values, we used an Arrhenius plot to calculate the activation energy of this reaction. The activation energy obtained using k values calculated using either the decay of the peak at 1950 cm^{-1} or the rise of the peak at 1943 cm^{-1} yields similar results, with an average activation energy of 33(±9) kJ/mol.

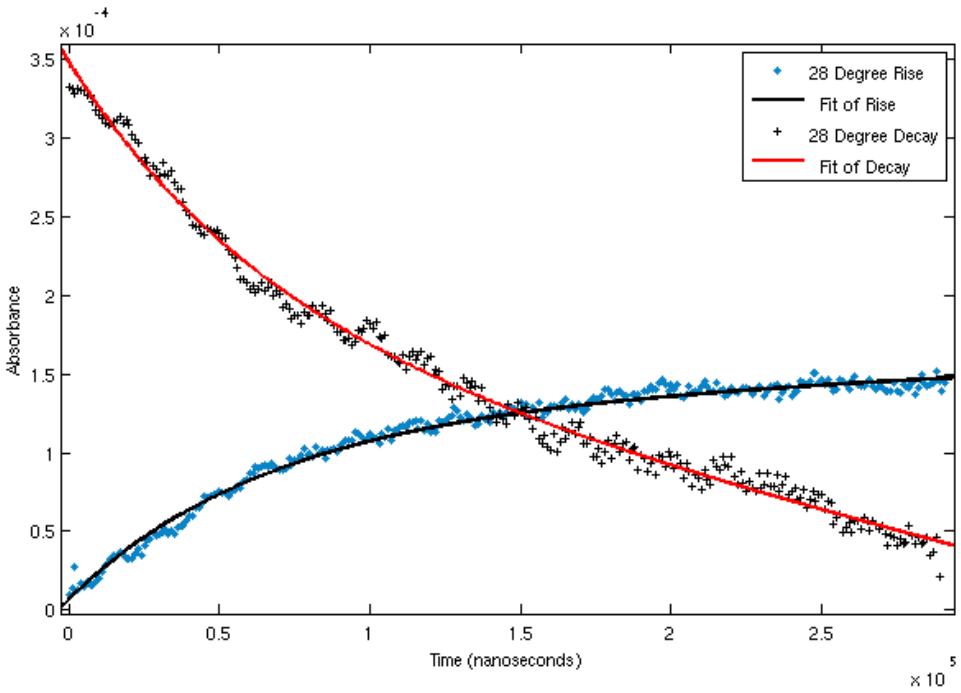

Figure 2-11: Fits of decay of peak at 1950 cm^{-1} and rise of peak at 1943 cm^{-1}.

The decay was fit using the following decaying exponential with an added linear portion: $y = 0.0001683e^{-1.514\times10^{-5}x} - 4.78\times10^{-10x} + 0.0001795$. The rise was fit using the following growing exponential with an added linear portion: $y = -0.0001189e^{-1.509\times10^{-5}x} - 7.962\times10^{-4}x + 0.0001258$. As can be seen from the equations, the values of k (pseudo-first order rate constant) for each fit are approximately the same, 1.51x10^{-5} ns^{-1}.

To evaluate the dependence on benzene concentration, we performed these experiments using several different C_6H_6 concentrations: approximately 0.25%, 0.5%, 1%, 2%, 2.5% and 5%. For Reaction 1, we found the rate increased as the benzene concentration increased, as shown in Figure 2-12. This increase appears to be correlated linearly with the benzene concentration, which agrees with our assumption that the reaction is first order in benzene. For Reaction 2, we

found the opposite: the rate of reaction decreased as the benzene concentration increased (See Figure 2-13). With 5% C_6H_6 the rate of reaction was so slow that we could not fit the decay or rise using an exponential. There was very little decay of the peak at 1950 cm^{-1} and rise of the peak at 1943 cm^{-1}. For this reason, we only have calculated rates for benzene concentrations up to 2.5% instead of 5%. It is not clear from these data if this correlation is also linear; there is too much scatter in the data to determine. Some of this scatter could be caused by poor exponential fits. Even at concentrations lower than 5%, some of the exponential fits were not ideal.

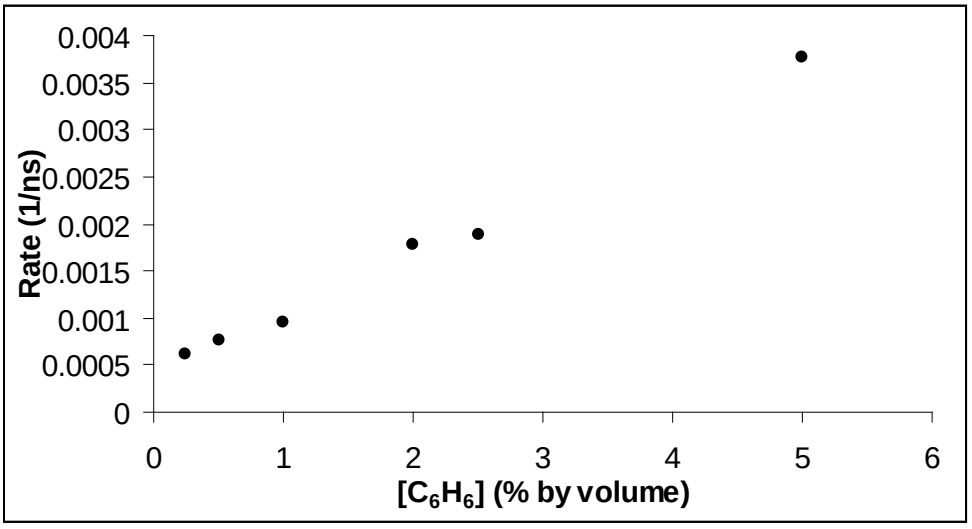

Figure 2-12: Benzene concentration dependence on rate of $Cr(CO)_5$:C_6H_{12} reacting with benzene to form $Cr(CO)_5$:η^2–C_6H_6.

A plot of the rate of decay of the peak at 1957 cm^{-1} ($Cr(CO)_5$:C_6H_{12}) at approximately 30°C. As the benzene concentration increases, the rate of complexation with benzene increases linearly, indicating the reaction is first order in benzene.

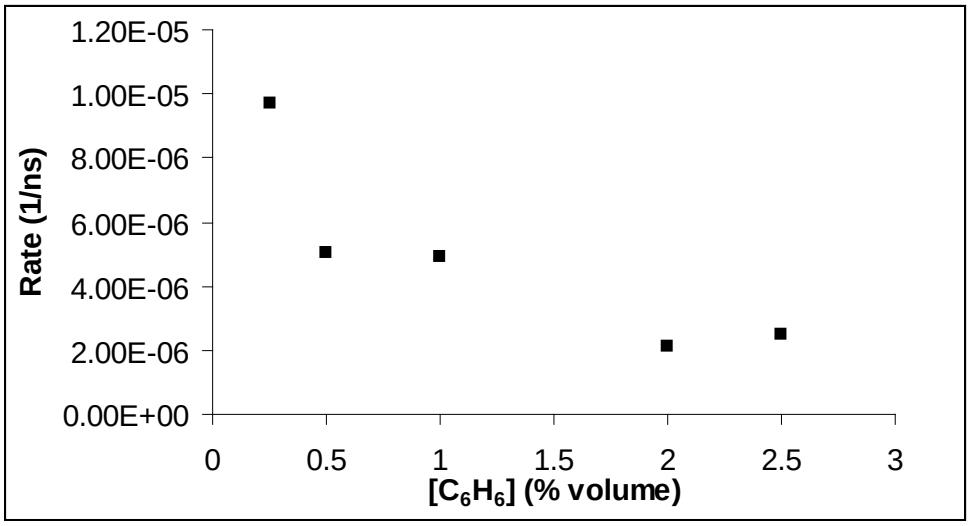

Figure 2-13: Benzene concentration dependence on rate of dissociation of $Cr(CO)_5$:η^2–C_6H_6.

A plot of the rate of decay of the peak at 1950 cm^{-1} ($Cr(CO)_5$: η^2–C_6H_6**)** at approximately 20°C. As the benzene concentration increases, the rate of dissociation of the benzene complex decreases.

2.3.2 Reactions with Mesitylene

We also evaluated the reactivity of $Cr(CO)_6$ in a solution of C_6H_{12} with a small amount of mesitylene (1,3,5-trimethylbenzene) rather than benzene. Because the structures of benzene and mesitylene are similar, we wanted to evaluate what changes occur from the addition of the alkyl groups on the benzene ring in mesitylene. As suggested by experiments done with $W(CO)_6$, we expect to see similar reactivity.[10,11] We also expect to see a red shift in the CO frequencies, as we did with tungsten.

When a C_6H_{12} solution of $Cr(CO)_6$ with a low concentration of mesitylene is irradiated with 355 nm light, we immediately see the appearance of IR peaks at 1957 cm^{-1} and 1932 cm^{-1}. These peaks correspond to $Cr(CO)_5$:CyH and are the same peaks seen in reactions with benzene

in solution. On the nanosecond time scale, we see these peaks decay, and see two new peaks grow in at 1943 cm^{-1} and 1914 cm^{-1}, as shown in Figure 2-14. These appear on a time scale similar to the benzene complex, but the IR peaks are a little red shifted from the corresponding benzene complex (the benzene complex has peaks at 1950 cm^{-1} and 1925 cm^{-1}).

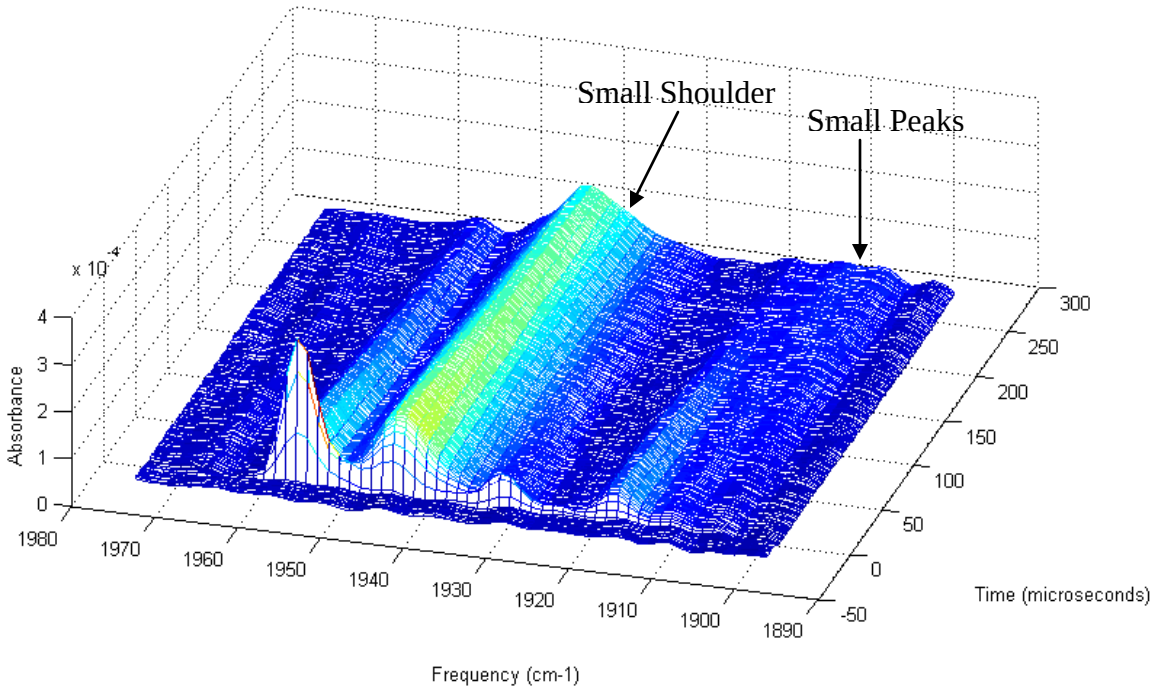

Figure 2-14: Time-resolved IR Spectra of $Cr(CO)_5$:Mesitylene.

This plot shows the rapid decay of $Cr(CO)_5$:CyH peaks at 1957 cm^{-1} and 1932 cm^{-1}, and rapid growth of peaks at 1943 cm^{-1} and 1914 cm^{-1}. These latter peaks then also slowly decay and we can also see a small shoulder and two small peaks appearing as peaks grow in at approximately 1932 cm^{-1}, 1912 cm^{-1} and 1908 cm^{-1} over 300 microseconds.

When using a solution with 4% mesitylene, we see no further reaction on a microsecond time scale. However, when using a solution with only 1% mesitylene, we see a second reaction occur. Similar to the reaction with benzene, we see the peaks corresponding to

$Cr(CO)_5$:mesitylene decay. We can only see this decay with a low concentration of mesitylene, which suggests the reaction with mesitylene has the same concentration dependence as the reaction with benzene. As the mesitylene concentration increases, the rate of dissociation of $Cr(CO)_5$:mesitylene slows. As this complex dissociates, we see several new peaks growing in. As shown in Figure 2-14, the very small peaks at 1912 cm^{-1} and 1908 cm^{-1} are difficult to see after 300 microseconds. Similarly, the shoulder on the mesitylene peak at 1932 cm^{-1} is also much smaller than the mesitylene complex peak after 300 microseconds. So, we see peaks corresponding to a third complex, but only a small amount of this complex is present by 300 microseconds.

2.4 Discussion

2.4.1 Benzene Complex

Upon irradiation with 355 nm light, a CO ligand dissociates from $Cr(CO)_6$.[5] Initially, a C_6H_{12} solvent molecule coordinates to the chromium, forming $Cr(CO)_5$:C_6H_{12}. This can be seen from the CO stretches in the infrared spectrum. The stretch at 1984 cm^{-1} disappears as the $Cr(CO)_6$ loses one CO ligand. Then, two new stretches appear at 1957 cm^{-1} and 1932 cm^{-1} (only 1957 cm^{-1} has adequate signal to noise for quantitative measurements), caused by CO stretches in $Cr(CO)_5$:C_6H_{12}.[4] These appear faster than the time resolution of our experiments, and the rate of appearance has been measured by others to be approximately 200 fs.[7] However, these peaks rapidly decay because $Cr(CO)_5$:C_6H_{12} is not the most stable product of the reaction (Figure 2-2). Benzene coordinates in place of cyclohexane.

There are a few ways in which benzene could complex with $Cr(CO)_5$. One possibility is through a C–H–Cr agostic interaction, where the metal interacts primarily with the hydrogen end of a C–H sigma bond.[8] Such a complex, of the form $Cr(CO)_5$:η^1–C_6H_6 is termed a “sigma

complex". Another possible interaction would be coordination of benzene to Cr through an isolated double bond, termed a "pi complex".[8,12] A final possibility would be coordination of benzene to Cr through the entire ring. Both Zhang *et al*. and *Wang et al*. suggest that bonding in $Cr(CO)_5$:benzene takes place through a pi interaction, with a sigma interaction in the transition state.[8,19] To further investigate this, we performed DFT geometry and vibrational calculations of each possible configuration. According to these calculations (discussed in detail in a later chapter) $Cr(CO)_5$:η^2-C_6H_6 is the most stable. We could not find a minimized geometry for a complex where benzene was interacting through the entire ring. Instead, the geometry would shift so benzene was interacting through one side of the ring. We also had a difficult time calculating a complex where benzene was interacting through a sigma interaction. While we were able to calculate a minimum energy structure by DFT methods, a vibrational analysis always showed at least one imaginary frequency. In addition to this, the vibrational frequencies for the sigma complex did not correlate well with experimentally measured IR spectra. Those for the pi complex were much more similar to our experimental frequencies. So, we conclude that the benzene complex we see is $Cr(CO)_5$:η^2-C_6H_6.

When benzene is coordinated, the CO stretches are shifted to lower frequencies because the benzene ring donates more electron density to chromium than did cyclohexane. This electron density is then back donated from the metal into the π^* orbitals of the COs, weakening the CO bonds and causing the stretches to be less energetic. The $Cr(CO)_5$:η^2–C_6H_6 complex forms, as indicated by the growth of CO stretches at 1950 cm^{-1} and 1925 cm^{-1}. These are slightly lower frequencies than the CO stretches when C_6H_{12} is the ligand coordinated to the metal center, showing that the benzene does indeed donate more electron density to the metal. As the benzene complex dissociates, it is replaced by a complex with frequencies even further red-shifted. We

see this as the peaks at 1950 cm^{-1} and 1925 cm^{-1} decay, and those at 1943 cm^{-1} and 1913 cm^{-1} grow in.

2.4.2 Impurity Complex

We are still unsure of the identity of the final complex formed in the previous reactions, and have the same possibilities with $Cr(CO)_6$ that we had with $W(CO)_6$. These include: an Ar complex, a water or oxygen complex, or a dimer. Because the reactivity of $Cr(CO)_6$ and $W(CO)_6$ is so similar, we assume this final complex is also the same for both metals. So, we accept the results from the experiments with helium as a purge gas and with a higher metal concentration using $W(CO)_6$. The results from these experiments, as discussed for $W(CO)_6$, suggest that the complex is not with argon, and is also not a dimer. It would be beneficial to also perform these experiments using $Cr(CO)_6$ rather than $W(CO)_6$ to be sure both metals behave the same way. To validate our assumption that both metals behave the same way, we compared DFT calculations of $Cr(CO)_5$ complexes with those for $W(CO)_5$ complexes. These calculations of the vibrational frequencies predict $Cr(CO)_5$:Ar would have higher frequency IR bands than we see experimentally. This correlates well with what we saw for tungsten, and supports our conclusion that our final complex is not $Cr(CO)_5$:Ar. Calculations of $Cr(CO)_5$:H_2O produce vibrational frequencies that are similar to those we see experimentally. This was also the result we found with tungsten. So, it seems likely the final impurity complex is $Cr(CO)_5$:H_2O, and we will refer to it as such in the following discussion.

2.4.3 Reaction Mechanism

For both Reactions 2 and 3, the decay and growth of peaks were fit with exponentials with added linear components, as discussed earlier. When the data from experiments at several

temperatures are fit, the rate constants can be used to make a plot of ln(k) vs. 1/T, where k is the pseudo first order rate constant. The slope of this line is $-E_a/R$, where E_a is the activation energy and R is the gas constant (8.3145 J K^{-1} mol^{-1}). So, we can calculate the activation energy for Reactions 2 and 3. The activation energy for the reaction going from $Cr(CO)_5$:C_6H_{12} to $Cr(CO)_5$:η^2–C_6H_6 is calculated to be approximately 30 kJ/mol. The activation energy for the reaction going from $Cr(CO)_5$:η^2–C_6H_6 to $Cr(CO)_5$:H_2O is calculated to be approximately 33 kJ/mol.

Many experiments have suggested the mechanism of ligand exchange reactions on coordinated metal centers are a mixture of associate (interchange) mechanisms, and dissociative mechanisms.[4,8,13] The exact mixture depends on the ligand that is coordinating to the metal center. As would be expected, as the ligand size and thus steric crowding increases, the reaction is more likely to proceed through a dissociative mechanism. Biber *et al.* suggest that substitutions at $Cr(CO)_5$:CyH show both associative and dissociative character.[4] They found that the reaction rate was strongly correlated to properties of the ligand, including electron-donating ability and polarizability. This suggests that the reaction has an associative nature; the incoming ligand must be interacting with $Cr(CO)_5$ in the transition state. However, they also found that ligand polarizability is more important than electron donating ability in reactions with $Cr(CO)_5$:CyH, which suggests the incoming ligand is further from the metal center in the transition state as in a dissociative mechanism.

It is possible to gain further insight about mechanisms using computations. Using DFT calculations, we can calculate the binding energies of the three experimental complexes. For the first reaction, if the activation energy and the binding energy of cyclohexane to $Cr(CO)_5$ are equivalent, this suggests the dissociation of cyclohexane is the limiting step in the reaction to

form a complex with benzene. If they are not similar, it suggests that the reaction is not purely dissociative in nature. Similarly, in the second reaction, if the activation energy is the same as the binding energy for benzene interacting with $Cr(CO)_5$, this suggests benzene must first dissociate before $Cr(CO)_5$ reacts further. We will discuss the details of DFT calculations in a later chapter, and will just report relevant results here. Table 2-3 shows results from calculating the binding energies for each $Cr(CO)_5$ complex.

Complex	Density Functionals	Calculated Binding Energies (kJ/mol)
$Cr(CO)_5(CyH)$	B3LYP	19
	M06	45
	M06-L	41
$Cr(CO)_5{:}\eta^2\text{-}C_6H_6$	B3LYP	26
	M06	65
	M06-L	65
$Cr(CO)_5{:}H_2O$	B3LYP	61
	M06	77
	M06-L	77

Table 2-3: Calculated binding energies for $Cr(CO)_5$ complexes.

Binding energies are calculated using three density functionals: B3LYP, M06, and M06-L.

The experimental activation energy for the reaction going from $Cr(CO)_5{:}C_6H_{12}$ to $Cr(CO)_5{:}\eta^2\text{–}C_6H_6$ is approximately 30 kJ/mol, which is smaller than the calculated binding energy for the cyclohexane complex when using M06 and M06-L, but larger than the calculated binding energy when using B3LYP. Though these calculated values conflict, none are equal to the activation energy. This suggests that the mechanism is not purely dissociative in nature; the activation energy is not equal to the energy required to break the bond between Cr and cyclohexane. The experimental activation energy for the reaction going from $Cr(CO)_5{:}\eta^2\text{–}C_6H_6$ to $Cr(CO)_5{:}H_2O$ is approximately 33 kJ/mol. This activation energy is similar to the binding

energy calculated using B3LYP, but is significantly smaller than the binding energies calculated using M06 and M06-L. This result is similar to what we found for tungsten, and leaves us with conflicting data. If the binding energy calculated using B3LYP is accurate, the reaction mechanism is likely mostly dissociative in nature. However, if the binding energies calculated using M06 and M06-L are correct, the reaction requires much less energy than is required to break the Cr–benzene bond. If this is the case, we would argue that the mechanism is definitely not dissociative. Unfortunately, we do not have experimentally determined binding energies for this complex, and it is difficult to analyze the accuracy of the various DFT functionals. For this reason, we cannot make any firm conclusions about the mechanism.

2.4.4 Mesitylene Complex

Reactions using mesitylene in place of benzene allow us to look at similarities and differences between reactivity of these similar ligands. As we expect, we see very similar reactivity. When mesitylene is present in small amounts in our solution, we still initially see the $Cr(CO)_5$:CyH complex form. Then, just as with benzene, this cyclohexane complex dissociates as mesitylene complexes with $Cr(CO)_5$ to form $Cr(CO)_5$:mesitylene. The IR spectrum we see with the mesitylene complex is slightly red-shifted from the corresponding benzene complex. The benzene complex has peaks at 1950 cm^{-1} and 1925^{-1}, while the mesitylene complex has peaks at 1943 cm^{-1} and 1914 cm^{-1}. This is expected because the alkyl groups on the benzene in mesitylene are electron releasing and donate more electron density into the benzene ring, which can then be donated to the metal center. This increased electron density at the metal center is then back-bonded into the π^* orbitals of the COs, and ultimately weakens those bonds. So, we expect a red shift in the IR spectrum when mesitylene is the ligand, compared to when benzene is the ligand.

The dissociation of the mesitylene complex is also quite similar to that of benzene, though it does happen at a slower rate. When benzene is in solution, we see the $Cr(CO)_5$:benzene complex dissociate over 300 microseconds. By 300 microseconds, the benzene complex is still present, but is diminished by approximately 75%. The new complex ($Cr(CO)_5$:H_2O) has peaks that are larger than those of the decaying benzene complex. When mesitylene is in solution at the same concentration, $Cr(CO)_5$:mesitylene decreases by only approximately 20% over 300 microseconds. The new peaks growing in are very small after that time period, as seen in Figure 2-14. So, it seems that the rate of dissociation of the $Cr(CO)_5$:mesitylene complex is slower than for the corresponding benzene complex. However, even though it is slower, there is not as large of a difference as was seen with $W(CO)_6$. As discussed with tungsten, two possible reasons this reaction proceeds at a lower rate with mesitylene are steric hindrance, or comparative strength of interactions. However, these do not explain the difference between tungsten and chromium. The reaction with tungsten is affected much more by the change in ligand, while that with chromium is not as greatly affected. This suggests that even with steric hindrance of the mesitylene, it must be so much easier to break the chromium-mesitylene bond that the rate of reaction is not as affected for chromium.

2.4.5 Chromium vs. Tungsten

One purpose for evaluating the reactivity of $Cr(CO)_6$ is to compare our results with what we see for $W(CO)_6$. There are many similarities between the two, as we expect for two Group 6 transition metals. However, there are some differences as well. We see the same three basic reactions occurring with both $W(CO)_6$ and $Cr(CO)_6$. Because we did not analyze the rate of formation of the $W(CO)_5$:C_6H_6 complex, we cannot compare this rate with that for $Cr(CO)_5$:C_6H_6. However, from preliminary experiments we know they both take place on a

similar nanosecond time scale. Unlike the formation of the benzene complex, its dissociation is much faster with chromium than with tungsten. With $Cr(CO)_6$ we measure this decay on a microsecond time scale, and see a significant decay by 300 microseconds. With $W(CO)_6$ we measure this on a millisecond time scale, and do not see significant decay until approximately 500 ms. This means the dissociation of $Cr(CO)_5$:C_6H_6 is approximately 1000 times faster than the dissociation of $W(CO)_5$:C_6H_6. We do expect chromium to be more reactive than tungsten, but this is a huge difference.

The calculated binding energy for $W(CO)_5$:C_6H_6 is much larger than that for $Cr(CO)_5$:C_6H_6, which could explain some of the difference in rate. If the tungsten-benzene complex is much more stable, it would be less likely to fall apart in solution. However, it is very interesting to note that the activation energy for the dissociation of $Cr(CO)_5$:C_6H_6 (approximately 33 kJ/mol) is very similar to that for $W(CO)_5$:C_6H_6 (approximately 39 kJ/mol). On first thought we would expect the activation energy to be much lower for the faster reaction with chromium, but this is not the case. The concentrations used for the two different metals were not identical, which could cause some difference in rate. $W(CO)_6$ is present at 1 mM, while $Cr(CO)_6$ is present at 2.5 mM. We have not fully evaluated the effect of metal concentration on the rate of reaction, but it likely has some effect, though probably not as large as the discrepancy we see here.

If the two reactions have very different rates but similar activation energies, this means the Arrhenius A factor must be causing the difference. In transition state theory, the A factor is related to the entropy of activation. In a similar comparison between reactions of tungsten and chromium complexes, Biber *et al.*[4] concluded that the rate difference between the two metals is indeed an entropic effect. One possible explanation is the smaller Cr center causes more steric

interference for ligands entering and leaving the metal atom. For this reason, reactions with chromium complexes are likely more dissociative in nature than those with tungsten complexes. In the transition states for the chromium reactions, the ligands will be further from the metal center, meaning there is a smaller loss in entropy compared to the corresponding tungsten reactions. This more favorable entropy of activation causes the chromium reactions to proceed at a higher rate.

$W(CO)_6$ and $Cr(CO)_6$ show similar reactivity with mesitylene and benzene. The $Cr(CO)_5$:mesitylene complex dissociates much more rapidly than the $W(CO)_5$:mesitylene complex, which is also true for the corresponding benzene complexes. For both metals, the mesitylene complex is more long-lasting than the corresponding benzene complex. However, the rate of dissociation of $W(CO)_5$:mesitylene is much slower than the rate of dissociation of $W(CO)_5$:benzene, while they are more similar for chromium. A possible explanation is that the bulky mesitylene ligand causes more steric hindrance in the more associative tungsten reaction than in the more dissociative chromium reaction. This increased steric hindrance when reacting with tungsten causes the rate to decrease. It would be interesting to evaluate additional substituted benzene complexes to compare with benzene and mesitylene to better understand these rate differences.

A comparison between the IR spectra of chromium complexes and tungsten complexes shows the CO stretches in the chromium complexes are slightly higher frequencies, but only by a few wavenumbers. Because chromium is smaller and has fewer electrons, it donates less into the π^* orbitals of the COs. This leads to slightly stronger CO bonds in the $Cr(CO)_6$ complexes. The relative shift in CO frequency when going from $M(CO)_5$:C_6H_{12} and $M(CO)_5$:C_6H_6 is the same for M = Cr and W, approximately 7 cm^{-1}. However, the shift when the benzene complex dissociates

is much greater for tungsten than for chromium. For the tungsten complex we see a shift of approximately 14 cm^{-1}, while we see a shift of only another 7 cm^{-1} for chromium.

2.5 Conclusion

Upon photolysis, the organometallic complex $Cr(CO)_6$ loses a CO ligand, and coordinates with a solvent molecule. This creates a weak metal:solvent complex that must be measured at short times. Time-resolved infrared spectroscopy is used to observe the changes in frequency of the CO stretches of these short-lived complexes. In a dilute solution of $Cr(CO)_6$ and C_6H_6 in C_6H_{12}, the weak $Cr(CO)_5$:C_6H_{12} complex forms and dissociates as the more stable $Cr(CO)_5$:η^2–C_6H_6 complex forms. Experimental results suggest that the activation energy for this reaction is 30 kJ/mol. This complex also dissociates to yield a new complex that is likely $Cr(CO)_5$:H_2O, due to sample impurities. We calculated the activation energy of this reaction to be 33 kJ/mol. Though there are some differences between the reactions of $Cr(CO)_6$ and $W(CO)_6$, they are very similar as would be expected for two Group 6 metals.

References

(1) Ball, G. E.; Darwish, T. A.; Geftakis, S.; George, M. W.; Lawes, D. J.; Portius, P.; Rourke, J. P. Characterization of an organometallic xenon complex using NMR and IR spectroscopy. *Proc. Natl. Acad. Sci. U.S.A.*, **2005**, 102, 1853–1858.

(2) Cowan, A. J.; George, M. W. Formation and reactivity of organometallic alkane complexes. *Coord. Chem. Rev.*, **2008**, *252*, 2504–2511.

(3) Church, S. P.; Grevels, F.; Hermann, H.; Schaffner, K. Structures and Kinetics of $Cr(CO)_5$ and $Cr(CO)_5 \cdot H_2O$ in Cyclohexane Solution. Flash Photolysis Study of $Cr(CO)_6$ with Infrared and Visible Detection. *Inorg. Chem.*, **1985**, *24*, 418–422.

(4) Biber, L.; Reuvenov, D.; Revzin, T.; Sinai, T.; Zahavi, A.; Schultz, R. H. Reactions of the transient species $Cr(CO)_5$(cyclohexane) with C_4H_nE (n = 4,8; E = O, NH, S) studied by time-resolved IR absorption spectroscopy. *Dalton Trans.*, **2007**, *1*, 41–51.

(5) Joly, A. G.; Nelson, K. A. Femtosecond Transient Absorption Spectroscopy of $Cr(CO)_6$ in Methanol: Observation of Initial Excited States and CO Dissociation. *J. Phys. Chem. Soc.*, **1989**, *93*, 2876–2878.

(6) Simon, J. D.; Xie, Xiaoliang. Photodissociation of $Cr(CO)_6$ in Solution: Direct Observation of the Formation of $Cr(CO)_5$(MeOH). *J. Phys. Chem. Soc.*, **1986**, *90*, 6751–6753.

(7) Wang, L.; Zhu, X.; Spears, K. G. Unsaturated Transition-Metal Complexes in Solution: Naked $Cr(CO)_5$ in Cyclohexane Solution Observed by Picosecond IR Transient Absorption. *J. Am. Chem. Soc.*, **1988**, *110*, 8695–8696.

(8) Wang, W.; Zheng, Y.; Lin, J.; She, Y.; Fu, K. Time-Resolved IR Study of Gas-Phase Reactions of Benzene with Group VIB Metal Pentacarbonyls and Tetracarbonyls. *J. Phys. Chem.*, **1993**, *97*, 11921–11928.

(9) Hermann, H.; Grevels, F.; Henne, A.; Shaffner, K. Flash Photolysis with Infrared Detection. The Photochemistry and Secondary Thermal Reaction of $M(CO)_6$ [M = Cr, Mo, and W]. *J. Phys. Chem.*, **1982**, *86*, 5151–5154.

(10) Stolz, I. W.; Haas, H.; Sheline, R. K. Infrared Spectroscopic Evidence for New Metal Carbonyl Complexes with Aromatic Ligands. *J. Am. Chem. Soc.*, **1965**, *87*, 716–718.

(11) Tyler, D. R.; Petrylak, D. P. Photochemical Studies of $M(CO)_6$ (M = Cr, Mo, W) at Low Temperature in Solution. Infrared Spectra of $M(CO)_5$(Solvent) (Solvent = methylcyclohexane, methylene chloride) and $W(CO)_5L$ (L = aromatic hydrocarbon). *J. Organomet. Chem.*, **1981**, *212*, 389–396.

(12) Zhang, S.; Dobson, G. R.; Zang, V.; Bajaj, H. C.; van Eldik, R. Octahedral Metal Carbonyls. 71. Kinetics and Mechanism of Benzene Displacement from Photogenerated [(η^2-Benzene)$Cr(CO)_5$]. *Inorg. Chem.*, **1990**, *29*, 3477–3482.

(13) Morse, J. M., Jr.; Parker, G. H.; Burkey, T. J. Enthalpy of CO Dissociation from $M(CO)_6$ (M = Cr, Mo, W) in Alkane Solvent: Determination of Intermolecular Agostic Bond Strengths. *Organomet.*, **1989**, *8*, 2471–2474.

Chapter 3: Density Functional Theory Calculations

3.1 Introduction

Computational chemistry is a very valuable tool when studying chemical reactions. When paired with experimental data, it can help us identify intermediates as well as help determine reaction mechanisms. Density functional theory has become a preferred method of theoretical calculations for many molecular properties.[1] The development of more accurate functionals has expanded this use to include transition metal complexes. There are several difficulties to overcome when calculating properties of transition metal complexes.[2,3] However, with improvements in functionals, DFT is becoming more widely used as a method to probe molecular properties of transition metal complexes. Calculated molecular and binding energies of various complexes allow us to model chemical pathways that we can compare to measured activation energies. Calculated vibrational frequencies can also aid in identification of intermediates seen during reactions.

One of the most commonly used density functionals is B3LYP. It is a hybrid functional, taking into account electron correlation as well as exchange potential. However, it has some shortcomings that are important to consider when performing calculations on complexes containing weak metal-solvent interactions.[4] One serious shortcoming for our purposes is that B3LYP is not as accurate for transitional metals as it is for main-group chemistry. Another shortcoming is it does not accurately account for van der Waals forces, or other medium-range correlation energy. Since the complexes we are interested in contain both transitional metals and medium-range correlation energy, this is a concern. A new class of functionals, called M06-

class functionals, developed by Zhao *et al.* take these into account, hopefully resulting in more accurate calculations for organometallic interactions.[4]

Our goals for this computational work are two-fold. The first is to better understand what we see experimentally when $Cr(CO)_6$ and $W(CO)_6$ react with both cyclohexane and benzene. To do this, we used B3LYP functionals as well as M06-class functionals for calculations on chromium and tungsten complexes. By comparing vibrational frequencies and calculated binding energies, we hope to augment our understanding of the experimental reactions. Our second goal is to evaluate metal-carbonyl complexes with known experimental CO vibrational frequencies, and compare these to calculated vibrational frequencies. By using three different density functionals, we hope to evaluate the precision and accuracy of the three functionals, and develop scale factors for assignment of experimental vibrational frequencies based on calculated frequencies.

3.2 Methods

All calculations were performed using density functional methods, with the NWChem computational chemistry program. The Extensible Computational Chemistry Environment (ECCE) developed by Pacific Northwest National Laboratories was used to set up, manage, and analyze all calculations. We used a mixed basis set for all calculations, in which we employed the Los Alamos effective core potential LANL2DZ (Los Alamos National Laboratory 2 double-ζ) for the transition metal atoms and a Pople-type split valence double-ζ polarized basis set, 6-31G*, for all other atoms.

DFT calculations were performed using three different functionals. The first is the hybrid GGA with Becke's three parameter exchange functional in conjunction with the LYP correlation functionals (B3LYP). The second is a hybrid meta-GGA, M06 (Minnesota 2006).[4] The third is

a local functional, M06-L (Minnesota 2006 local functional).[5] Geometry calculations were minimized using the standard tight convergence criteria, and correct minimization was tracked by vibrational analysis to eliminate negative frequencies. In many cases, it was difficult to find a stable geometry; we were required to use fine or extra fine grids, and tight geometry convergence criteria. Even with these techniques, for some complexes we were not able to find minimum geometries with no imaginary frequencies. These will be noted when these results are discussed. Vibrational frequencies were computed using numerical differentiation of the energy gradients.

In addition to geometry and vibrational frequency calculations, we did single-point energy calculations to calculate the binding energy of ligands to the transition metal complexes, using the counterpoise method. This means we calculated the binding energy as the difference between the total energy of the complex and the energies of its constituent parts,[6] as demonstrated in Figure 3-1.

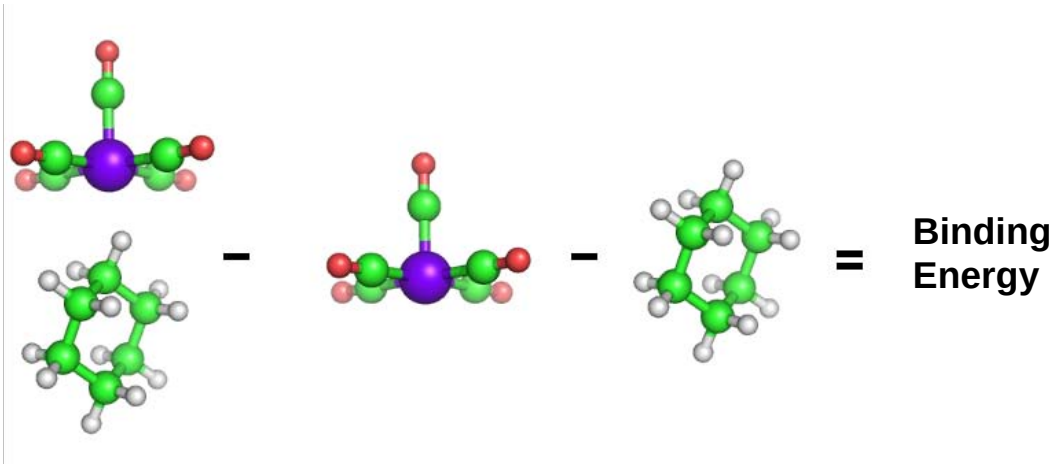

Figure 3-1: Method of calculating binding energy.

This is an representation of the method used to calculate the binding energy for $W(CO)_5$:C_6H_{12}. The energy of each part of the complex is subtracted from the energy of the entire complex using the counterpoise method.

To calculate binding energies, we calculate the energy of the entire complex (following geometry minimization). After doing this, we create two new calculations with the minimized geometry so we can determine the energy of each constituent part. Variational theory tells us that more basis functions cause the energy of the complex to go down, so we do not want to delete any basis functions that were present in the entire complex or we will get higher energies. So, in one calculation we set all the atoms in the ligand to be ghost atoms, and in the other we set all of the atoms in the transition metal complex to be ghost atoms. This means we will still consider the wavefunctions of all atoms that were in the complete complex, but will not consider the nuclei or electrons of the atoms that are ghost atoms. We then use single-point energy calculations to find the energy of each part.

3.2.1 Functionals

Though density functional theory is widely used for calculations of molecular properties, this does not mean the results are always correct. We know the ground state density defines the system, but we do not know the exact form of the functionals that describe this density. Thus, all DFT methods are approximations, and their accuracy is dependent upon the treatment of the exchange-correlation functional.[3] As DFT has been applied to more transition-metal chemistry, it has become apparent that methods need to be evaluated for this specific subset of chemistry. DFT has a tendency to overestimate metal–ligand bond dissociation energies, and does not accurately describe atomic multiplets which are relatively common among transition-metal complexes.[7] Even with this inaccuracy, Jonas *et al.* concluded that for a set of transition-metal carbonyl hydrides, DFT provided more accurate geometries than either RHF or MP2

calculations.[8] In addition to this, DFT calculated vibrational frequencies are accurate enough to aid in assignment of vibrational spectra.

B3LYP is one of the most commonly used density functionals and has proven very accurate for main group chemistry, but it does have some shortcomings, specifically when applied to transition-metal compounds. Some of these shortcomings include: it is inaccurate for van der Waals interactions and other medium-range correlations, it is less accurate for transition metals than main group chemistry,[4] and it does not effectively deal with systems with substantial changes in either self-interaction error or the balance between static and dynamic correlation.[3] To try to combat some of these shortcomings, Zhao *et al.* developed four new functionals included in their M06-class functionals. These use spin densities, spin density gradients, spin kinetic energy densities, as well as Hartree–Fock exchange (this is not used for local functionals). In addition to this, all of these functionals are one-electron self-correlation free, and are also constrained to give the correct uniform electron gas limit.[4]

We used only two of these four functionals: M06 and M06-L. The first functional, M06, is a hybrid functional useful for transition metals as well as main-group chemistry. It is also accurate for complexes containing medium-range correlation energy. The second one, M06-L, is a local functional (does not use Hartree–Fock exchange). It is the most accurate of the four functionals for transition metals, and can also be used for main group chemistry.[5] Zhao *et al.* tested their local functional M06-L against several different local functionals and hybrid functionals. They found its overall performance is better than the others tested for a combination of thermochemistry, thermochemical kinetics, metallochemical and noncovalent interactions, bond lengths, and vibrational frequencies. In addition to this, they tested both M06 and M06-L for 496 data in 32 databases and recommend both for transition-metal thermochemistry and for

noncovalent interactions. They recommend M06 for rearrangements of transition metal bonds.[4] We were interested to see differences between B3LYP, M06, and M06-L in our transition metal calculations. The complexes we are considering all contain transition metals, as well as weak interactions. Our hope was that these M06-class functionals would give improved results relative to B3LYP.

3.3 Results and Discussion

3.3.1 Geometries

We calculated minimized geometries for the following complexes containing tungsten using B3LYP, M06 and M06-L functionals: $W(CO)_5$:C_6H_{12}, $W(CO)_5$:η^1-C_6H_6, and $W(CO)_5$:η^2-C_6H_6. The calculated geometries are shown in Figure 3-2. From our experimental results, we know benzene complexes with tungsten, but were unsure of the geometry of such an interaction. For this reason, we wanted to explore several possibilities computationally. Of these complexes, the $W(CO)_5$:η^1-C_6H_6 complex was the most difficult to calculate for all three functionals. In the end, after using an extra fine grid and tight geometry tolerance we still could not find a minimum geometry with no imaginary frequencies when using any of the three functionals. Thus, all results presented are from the calculations with the smallest imaginary frequencies.

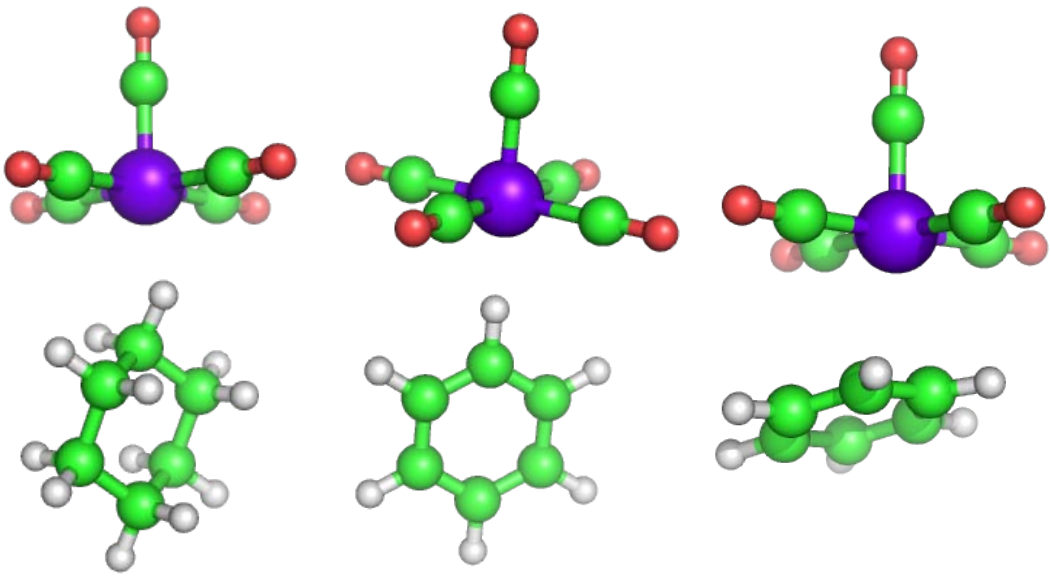

Figure 3-2: DFT calculated structures of $W(CO)_5$:solvent complexes.

From left to right: $W(CO)_5$:C_6H_{12}, $W(CO)_5$:η^1-C_6H_6, and $W(CO)_5$:η^2-C_6H_6.

We also calculated minimized geometries for the following chromium complexes: $Cr(CO)_5$:C_6H_{12}, $Cr(CO)_5$:η^1-C_6H_6, $Cr(CO)_5$:η^2-C_6H_6, and $Cr(CO)_5$:η^6-C_6H_6. Similar to the tungsten complexes, we had the same difficulty with the $Cr(CO)_5$:η^1-C_6H_6 complex with all three functionals. We were never able to find a minimum geometry with no imaginary frequencies using any of the three functionals. So, the results that are given are of the calculations with the smallest imaginary frequencies. In most cases we had only one small imaginary frequency, suggesting a relatively stable geometry. We had even more difficulty with the $Cr(CO)_5$:η^6-C_6H_6 complex because all geometry calculations result in the benzene ring shifting to $Cr(CO)_5$:η^2-C_6H_6. For this reason, we conclude that this complex is not stable and would not be present experimentally. The calculated geometries of these complexes are shown in Figure 3-3. $Cr(CO)_5$:η^6-C_6H_6 is not included because it relaxed to $Cr(CO)_5$:η^2-C_6H_6.

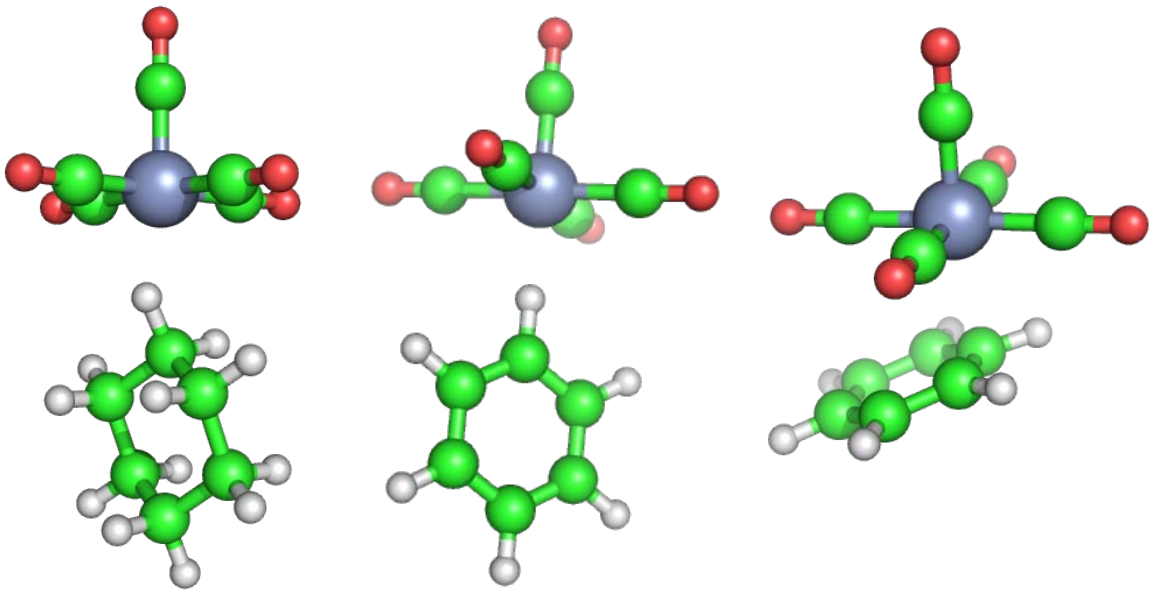

Figure 3-3: DFT calculated structures of $Cr(CO)_5$:solvent complexes.

From left to right: $Cr(CO)_5$:C_6H_{12}, $Cr(CO)_5$:η^1-C_6H_6, and $Cr(CO)_5$:η^2-C_6H_6.

Because we had such difficulty in calculating minimum geometries for the sigma complexes, we conclude that our experimental benzene complex is probably not a sigma complex, but a pi complex. However, it is possible if the sigma complex is present experimentally, it is being stabilized by other benzene molecules in the solution. To evaluate this possibility we attempted to add additional solvent molecules around the coordinated benzene to see if this stabilizes the complexes. By adding just one additional benzene molecule, we quickly find a stable geometry when using some density functionals. We expect the benzene molecules to be arranged as in benzene pi-stacking, but the benzene rings pucker, as shown in Figure 3-4. This is true for all three functionals, and for both chromium and tungsten complexes.

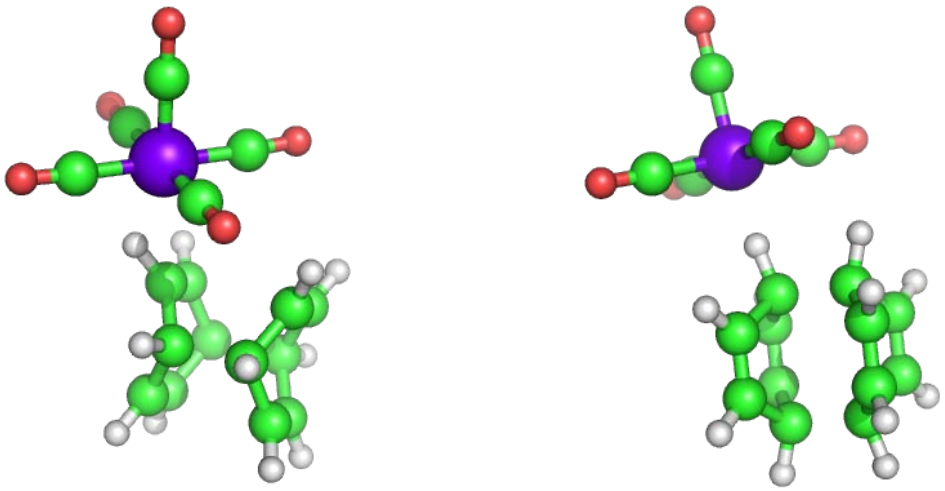

Figure 3-4: Structures of $Cr(CO)_5$:C_6H_6 with an additional benzene molecule.

These are two examples of the puckered geometry resulting from the addition of a second benzene ring. Structures of $W(CO)_5$:C_6H_6 with an additional benzene ring look similar. The geometry optimizations were performed using B3LYP for the first structure and M06 for the second structure.

Though we do find stable geometries when an additional benzene ring is added, we still do not believe this is the geometry of our experimental benzene complex. In addition to the geometry, we looked at the calculated vibrational frequencies for each complex (shown in Table 3-3). The CO frequencies for the complexes with an added benzene ring do not correspond well with those we see experimentally. The calculated frequencies are generally very similar to those seen in the cyclohexane complex; they are not as far red-shifted from $M(CO)_5$:C_6H_{12} as we expect from our experimental data. The frequencies corresponding to the pi complex are much more similar to what we see experimentally. From these computational results, we still believe the experimental benzene complex is $M(CO)_5$:η^2-C_6H_6.

3.3.2 Binding Energies

We calculated binding energies as described above using the counterpoise method to account for basis set superposition error. As with geometries, we calculated these using all three density functionals: B3LYP, M06, and M06-L. When we do not have a minimum geometry with no imaginary frequencies, we use the energy of the complex that seems closest to the minimum geometry (has the fewest number and smallest imaginary frequencies). Table 3-1 shows the calculated binding energies.

Complex	Density Functionals	Calculated Binding Energy (kJ/mol)
$W(CO)_5$:CyH	B3LYP	28.1
	M06	54.3
	M06-L	48.7
$W(CO)_5$:η^1-C_6H_6	B3LYP	9.0*
	M06	28.3*
	M06-L	25.2*
$W(CO)_5$:η^2-C_6H_6	B3LYP	46.7
	M06	88.0
	M06-L	81.3
$W(CO)_5$: η^1-C_6H_6 + added benzene	B3LYP	20.7*
	M06	45.3
	M06-L	80.8
$Cr(CO)_5$:CyH	B3LYP	18.8
	M06	44.8
	M06-L	41.2
$Cr(CO)_5$:η^1-C_6H_6	B3LYP	4.5*
	M06	23.2*
	M06-L	21.7*
$Cr(CO)_5$:η^2-C_6H_6	B3LYP	25.2
	M06	64.6
	M06-L	65.4
$Cr(CO)_5$: η^1-C_6H_6 + added benzene	B3LYP	21.6
	M06	41.7*
	M06-L	40.1*

* Vibrational analysis of this compound with the corresponding density functional results in imaginary vibrational frequencies

Table 3-1: Calculated binding energies for $Cr(CO)_5$ and $W(CO)_5$ complexes.

The binding energies calculated using M06 and M06-L are generally very similar, but the binding energies calculated using B3LYP are always significantly smaller. B3LYP has a tendency to underbind complexes,[3] so we expect those calculated using B3LYP to be lower than the true binding energies. Schultz *et al.* report a mean signed error of −2.7 kcal/mol (−11.3 kJ/mol) for B3LYP when using a double-zeta quality basis set, for a database with metal–ligand bond energies for 21 compounds. They also report a mean signed error of −11.6 kcal/mol (−48.5 kJ/mol) for a combined database with the above 21 compounds and an additional 8 metal dimers.[1] Since our calculations are metal−ligand bond energies, we would expect an error closer to −11.3 kJ/mol than to −48.5 kJ/mol for B3LYP. Zhao *et al.* report a mean signed error of 4.7 kcal/mol (19.7 kJ/mol) for M06-L for a database of 21 metal-ligand bond energies when using a triple-zeta quality basis set.[5] They also report mean unsigned errors of approximately 11.5 kcal/mol (48.1 kJ/mol) for B3LYP, 5.6 kcal/mol (23.4 kJ/mol) for M06, and 5.8 kcal/mol (24.3 kJ/mol) for M06-L for a database containing 9 transition metal atomization energies, 21 metal-ligand bond energies, and 18 3d transition metal reaction energies.[4] These evaluations suggest binding energies calculated using M06 and M06-L are closer to the true binding energies than those calculated using B3LYP. However, it seems that M06 and M06-L overbind complexes, so the true activation energy is probably somewhere between that calculated using B3LYP and that calculated using the M06-class functionals. Unfortunately, we cannot calculate the true error in our calculations since we do not know the true binding energies of these complexes.

Despite the inaccuracies of the calculated binding energies, we can still gather important information by comparing the binding energies of the various complexes. The $M(CO)_5$:η^1-C_6H_6 has a much smaller binding energy than any other complex, indicating that it is not as stable.

This is just what we expect from our geometry calculations. When the additional benzene solvent is added, this stabilizes the complex and increases the activation energy. However, it is still less stable than the pi complex. These data show that $M(CO)_5{:}\eta^2\text{-}C_6H_6$ has a larger binding energy than the cyclohexane complex, indicating the benzene complex is more stable than the cyclohexane complex. This is in agreement with our experimental data. One final observation is the binding energies for $W(CO)_5$ complexes are larger than the corresponding binding energies for $Cr(CO)_5$ complexes. The binding energy for $W(CO)_5{:}\eta^2\text{-}C_6H_6$ in particular is much larger than that for $Cr(CO)_5{:}\eta^2\text{-}C_6H_6$. This is also in agreement with our experimental data, where we see the less stable $Cr(CO)_5{:}\eta^2\text{-}C_6H_6$ complex dissociate much faster than the more stable $W(CO)_5{:}\eta^2\text{-}C_6H_6$ complex.

In addition to simply evaluating the calculated binding energies, we are interested in comparing them to experimentally determined activation energies. By comparing the activation energy in going from one $M(CO)_5$ complex to another, and the binding energy of the first complex, we hope to gain some insight about the mechanism of the reaction. Table 3-2 shows the comparison between the calculated binding energies and the corresponding activation energies. The final complex, $M(CO)_5{:}H_2O$ is included only as a comparison of calculated binding energies. The binding energies of these two complexes do not correspond to anything we have done experimentally. However, we can see from comparing the binding energies that $M(CO)_5{:}H_2O$ is a stronger complex than $M(CO)_5{:}C_6H_6$ because the binding energy for the water complex is significantly larger than for the benzene complex. Since this is the final complex we form, we expect it to be more stable than the previous complexes, and this is indeed what we see.

Complex	Density Functionals	Calculated Binding Energy (kJ/mol)	Experimental Activation Energy (kJ/mol)
$W(CO)_5$:CyH	B3LYP	28.1	
	M06	54.3	
	M06-L	48.7	
$W(CO)_5$:η^2-C_6H_6	B3LYP	46.7	39
	M06	88.0	
	M06-L	81.3	
$W(CO)_5$:H_2O	B3LYP	84.1	
	M06	98.7	
	M06-L	94.8	
$Cr(CO)_5$:CyH	B3LYP	18.8	30
	M06	44.8	
	M06-L	41.2	
$Cr(CO)_5$:η^2-C_6H_6	B3LYP	25.2	33
	M06	64.6	
	M06-L	65.4	
Cr(CO)5:H_2O	B3LYP	61.2	
	M06	77.1*	
	M06-L	76.8*	

* Vibrational analysis of this compound with the corresponding density functional results in imaginary vibrational frequencies

Table 3-2: Calculated binding energies vs. experimental activation energies.

Experimental activation energies are those corresponding to the dissociation of the complex with which they are associated in the table.

The experimental activation energies are generally more similar to the binding energies calculated using B3LYP than to those calculated using M06 or M06-L. However, with the large possible errors for B3LYP and presumably for M06 and M06-L as well, this does not guarantee anything. Also, the activation energy is not necessarily the same as the dissociation energy; in fact, the binding energy and activation are equal only if the reaction is purely dissociative. This would mean the limiting step in the reaction is the dissociation of the ligand, and the energy required to do so is the dissociation energy. However, if the reaction has associative character, this is not the case.

As we discussed earlier, the likely true activation energies are somewhere between those calculated using B3LYP, and those calculated using the M06-class functionals. If this is the case, the experimental activation energy for the dissociation of $W(CO)_5$:η^2-C_6H_6 is lower than the binding energy. This suggests that the mechanism is not purely dissociative, but that something is stabilizing the transition state to lead to an activation energy that is lower than the energy required to break the metal–ligand bond. For both chromium reactions, the experimental activation energy is between the energy calculated using B3LYP and the energy calculated using M06 or M06-L, and is likely similar to the true binding energy. This corresponds well with the explanation by Biber *et al.*[9] that the tungsten reactions are more associative, while the chromium reactions are more dissociative.

3.3.3 Vibrational Frequencies

Each $M(CO)_5$ compound has five CO vibrational frequencies, though two are close to degenerate. The degenerate modes are predicted to have the strongest IR intensity. The lower frequency mode is predicted to have medium intensity. Of the two highest frequency modes, one is predicted to have weak IR intensity, and the other very weak IR intensity. The calculated CO frequencies for the $M(CO)_5$ complexes are shown in Table 3-3. Unlike the bond dissociation energies, there is definitely a difference between the vibrational frequencies calculated using M06, M06-L, and B3LYP. M06 gives the largest frequencies, followed by B3LYP, and finally M06-L. All the calculated frequencies are higher than experimental frequencies, which is a well-known fault for DFT calculations.

Complex	Functionals	Calculated C≡O Frequencies				
$W(CO)_5$:CyH	B3LYP	2042	2052	2054	2086	2164
	M06	2063	2072	2074	2108	2190
	M06-L	2034	2035	2036	2067	2152
$W(CO)_5$:η^1-C_6H_6	B3LYP	2039*	2054*	2056*	2091*	2167*
	M06	2058*	2076*	2076*	2115*	2194*
	M06-L	2034*	2043*	2043*	2075*	2158*
$W(CO)_5$:η^2-C_6H_6	B3LYP	2033	2041	2042	2081	2156
	M06	2052	2060	2061	2098	2177
	M06-L	2030	2030	2040	2069	2148
$W(CO)_5$:η^1-C_6H_6 + added benzene	B3LYP	2006*	2010*	2016*	2053*	2136*
	M06	2059	2073	2074	2114	2193
	M06-L	2024	2030	2033	2065	2148
$W(CO)_5$:H_2O	B3LYP	2034	2037	2043	2078	2159
	M06	2053	2059	2064	2099	2183
	M06-L	2031	2037	2039	2061	2151
$Cr(CO)_5$:CyH	B3LYP	2054	2063	2064	2088	2163
	M06	2068	2079	2079	2111	2188
	M06-L	2039	2047	2048	2071	2151
$Cr(CO)_5$:η^1-C_6H_6	B3LYP	2054*	2067*	2068*	2091*	2168*
	M06	2067*	2081*	2081*	2113*	2190*
	M06-L	2037*	2050*	2050*	2075*	2152*
$Cr(CO)_5$:η^2-C_6H_6	B3LYP	2045	2054	2058	2082	2157
	M06	2064	2069	2072	2105	2178
	M06-L	2032	2039	2044	2069	2144
$Cr(CO)_5$:η^1-C_6H_6 + added benzene	B3LYP	2052	2057	2063	2085	2158
	M06	2069*	2074*	2076*	2109*	2186*
	M06-L	2040*	2049*	2049*	2078*	2155*
$Cr(CO)_5$:H_2O	B3LYP	2044	2051	2054	2081	2159
	M06	2059*	2066*	2070*	2107*	2182*
	M06-L	2030*	2038*	2041*	2067*	2149*

* Vibrational analysis of this compound with the corresponding density functional results in imaginary vibrational frequencies

Table 3-3: Calculated C≡O vibrational frequencies for $M(CO)_5$ complexes.

Looking at Table 3-3, we can compare the frequency changes between the complexes for each functional. Though the frequencies are not the same as those we see experimentally, we can compare the relative shifts between complexes when using the same DFT functionals. For example, the frequency shift for the second lowest energy (and most intense) vibration going

from $W(CO)_5$:CyH to $W(CO)_5$:C_6H_6 is: -11 cm^{-1} for B3LYP, -12 cm^{-1} for M06, and -5 cm^{-1} for M06-L, and -6 cm^{-1} experimentally. Similarly, the frequency shift for the second lowest energy (and most intense) vibration going from $Cr(CO)_5$:CyH to $Cr(CO)_5$:C_6H_6 is: -9 cm^{-1} for B3LYP, -10 cm^{-1} for M06, and -8 cm^{-1} for M06-L, and -7 cm^{-1} experimentally. In both cases, the frequency shift calculated using M06-L is closest to the experimental shift.

In our experiments we see a red shift when benzene binds to the metal atom, so we expect the calculated frequencies of the benzene complex to be lower than those for the cyclohexane complex. We can see that this is the case when going to the pi benzene complex. However, this is not true when going from the cyclohexane complex to the sigma benzene complex. In fact, many of the vibrational frequencies are higher energy in the calculated sigma complex than in the cyclohexane complex. When an additional benzene ring is added to the sigma complex, the frequencies decrease a little, but they are still similar to the cyclohexane complex. We do not see enough of the expected red shift, further validating this is not the benzene complex we see experimentally.

In addition to simply comparing these frequencies to each other, we can also compare them to the frequencies we see experimentally, as shown in Table 3-4. In our experiments there is one very prominent band in the IR, one moderately strong band of lower frequency, and sometimes a third much weaker band at higher frequency. The most prominent band seems to correspond to the two calculated frequencies that are degenerate. They both are expected to be strong in the IR. The second band seems to correspond to the lowest frequency calculated IR band, which is predicted to have medium intensity. Our experimental frequency is always further red-shifted from the strong IR band than is predicted in these calculations. The third seems to correspond to the highest calculated frequency, which is predicted to be weak in the IR.

The second highest calculated frequency is predicted to be very weak, so it is unlikely to ever see this frequency experimentally. The $M(CO)_5$:H_2O complexes are a little different from the others reported. Here we believe there is another experimental band at 1948 cm^{-1} for tungsten, and at 1950 cm^{-1} for chromium that is overlapped by the benzene complex. We see these additional frequencies in experiments with neat cyclohexane and no benzene. So, it seems the lowest frequency, very weak experimental bands are not well-correlated with those calculated. However, we believe the 1933 cm^{-1} for tungsten, and 1943 cm^{-1} for chromium correspond to the second lowest calculated IR modes. The middle calculated IR mode then correlates with the two additional bands that are only seen when benzene is not present in solution because they overlap with stronger bands from the benzene complexes.

		C≡O Vibrational Frequencies							
Complex	**Functionals**	**Calculated**					**Experimental**		
$W(CO)_5$: CyH	B3LYP	2042	2052	2054	2086	2164	1928	1954	2086
	M06	2063	2072	2074	2108	2190			
	M06-L	2034	2035	2036	2067	2152			
$W(CO)_5$: η^2-C_6H_6	B3LYP	2033	2041	2042	2081	2156	1921	1948	2079
	M06	2052	2060	2061	2098	2177			
	M06-L	2030	2030	2040	2069	2148			
$W(CO)_5$: H_2O	B3LYP	2034	2037	2043	2078	2159	1908	1933	
	M06	2053	2059	2064	2099	2183			
	M06-L	2031	2037	2039	2061	2151			
$Cr(CO)_5$: CyH	B3LYP	2054	2063	2064	2088	2163	1932	1957	
	M06	2068	2079	2079	2111	2188			
	M06-L	2039	2047	2048	2071	2151			
$Cr(CO)_5$: η^2-C_6H_6	B3LYP	2045	2054	2058	2082	2157	1925	1950	2075
	M06	2064	2069	2072	2105	2178			
	M06-L	2032	2039	2044	2069	2144			
$Cr(CO)_5$: H_2O	B3LYP	2044	2051	2054	2081	2159	1908	1913	1943
	M06	2059*	2066*	2070*	2107*	2182*			
	M06-L	2030*	2038*	2041*	2067*	2149*			

* Vibrational analysis of this compound with the corresponding density functional results in imaginary vibrational frequencies

Table 3-4: Calculated vs. experimental C≡O vibrational frequencies.

From this limited set of data, we can calculate the difference between the experimental and calculated CO frequencies to get a better idea of the accuracy of each functional in calculating vibrational frequencies. For these calculated frequencies to be useful in identifying experimental complexes, they must be scaled to correspond better to the true frequencies, since they are always calculated too high. Thus, in addition to a difference, we can also calculate a scale factor. This will be done to a greater degree, with many additional weak metal–solvent complexes in the following section. Here we will just report in Table 3-5 the limited statistics for our experimental complexes from Table 3-4.

Functional	Average Difference (cm^{-1})	Scale Factor
B3LYP	105 ± 16	0.949 ± 0.008
M06	123 ± 14	0.941 ± 0.008
M06-L	94 ± 17	0.954 ±0.009

Table 3-5: Scale factors for calculating C≡O vibrational frequencies.

The difference is calculated as Calculated – Experimental. The scale factor is calculated as Experimental/Calculated.

This table shows that for our experimental $M(CO)_5$ complexes, the most accurate vibrational frequencies are calculated using M06-L. However, they are still quite far from the true experimental frequencies. For this reason it is probably more important to note that M06 has the highest precision in calculating vibrational frequencies, though all scale factors have average errors less than 1%. Thus, for this limited data set, the most accurate way to predict experimental frequencies would be to calculate them using M06, and then multiply by the scale

factor of 0.941. It is interesting to note that all three scale factors are slightly smaller than the general scale factor 0.9614 used for B3LYP.[10]

3.3.4 Weak Metal–Solvent Complexes

Now that we have evaluated the complexes we studied experimentally, the second part of the computational study is to evaluate additional similar weak metal–solvent complexes. We are specifically interested in the calculated CO vibrational frequencies, and how these compare with experimentally determined frequencies. We know that computed frequencies are almost always greater than experimental frequencies for several reasons. One reason is that we assume harmonic potentials, a second is the imperfections of basis sets used in the calculations, and the final is that the electron correlation is not treated completely.[10] Since many vibrational calculations have been completed, there is a general scale factor used to convert between calculated and experimental frequencies. However, we wanted to evaluate a scale factor specifically for COs in weak metal–solvent complexes. In addition to this, we wanted to evaluate the differences between frequencies calculated using B3LYP, M06, and M06-L. We did this to a small degree using only our experimental complexes, but would like to broaden the data set to include additional complexes.

We calculated vibrational frequencies using B3LYP, M06, and M06-L for the following complexes: $Cr(CO)_5$:THF, $Mo(CO)_5$:THF, $W(CO)_5$:THF, $W(CO)_5$:CH_3CN, $W(CO)_5$:CS, $Cr(CO)_5$:N_2, $Fe(CO)_4$:N_2, $Mo(CO)_5$:N_2, and $W(CO)_5$:N_2 in addition to those calculated earlier for comparison with our experimental work. All these complexes have known experimental vibrational frequencies, which are shown in Table 3-6 along with the calculated frequencies.

		C≡O Vibrational Frequencies								
Complex	**Functionals**	**Calculated**					**Experimental**			**Ref**
$Cr(CO)_5$: THF	B3LYP	2038	2044	2054	2074	2154	1877	1933	2059	11
	M06	2055	2060	2067	2099	2178	1895	1937	2073	12
	M06-L	2026	2034	2036	2061	2143				
$Mo(CO)_5$: THF	B3LYP	2030	2046	2049	2070	2154	1959	1982	2080	11
	M06	2053	2064	2068	2096	2181				
	M06-L	2023*	2028*	2029*	2064*	2146*				
$W(CO)_5$: THF	B3LYP	2030	2033	2036	2070	2154	1912	1933		13
	M06	2047	2052	2054	2092	2177	1941	1972	2069	11
	M06-L	2022*	2025*	2026*	2057*	2145*				
$W(CO)_5$: CH_3CN	B3LYP	2041	2045	2045	2079	2155	1926	1944	2077	14
	M06	2063	2066	2066	2101	2179				
	M06-L	2036*	2037*	2037*	2067*	2148*				
$Cr(CO)_5$: N_2	B3LYP	2079	2081	2081	2103	2167	1966	1976		15
	M06	2093	2096	2097	2126	2189	1960	1972	2084	16
	M06-L	2061	2067	2068	2092	2153				
$Mo(CO)_5$: N_2	B3LYP	2070	2075	2075	2098	2169	1959	1974	2089	16
	M06	2091	2098	2098	2125	2194	1964	1978	2092	
	M06-L	2059	2066	2066	2088	2157				
$W(CO)_5$: N_2	B3LYP	2071	2071	2072	2100	2167	1974	1985		17
	M06	2093	2093	2095	2125	2194	1959	1967	2086	16
	M06-L	2063	2066	2067	2085	2158				
$Fe(CO)_4$: N_2	B3LYP	2090	2091	2111	2163		1984	1992		17
	M06	2116	2116	2130	2185					
	M06-L	2071	2072	2089	2146					
$W(CO)_5$: CS	B3LYP	2084	2084	2099	2109	2178	1988	2006	2096	14
	M06	2104	2105	2121	2130	2201	1985	2005	2096	16
	M06-L	2179	2080	2086	2094	2172				
$W(CO)_5$: C_6H_{12}	B3LYP	2042	2052	2054	2086	2164	1928	1954	2086	This work
	M06	2063	2072	2074	2108	2190				
	M06-L	2034	2035	2036	2067	2152				
$W(CO)_5$: η^2-C_6H_6	B3LYP	2033	2041	2042	2081	2156	1921	1948	2079	This work
	M06	2052	2060	2061	2098	2177				
	M06-L	2030	2030	2040	2069	2148				
$W(CO)_5$: H_2O	B3LYP	2034	2037	2043	2078	2159	1908	1933	1948	This work
	M06	2053	2059	2064	2099	2183				
	M06-L	2031	2037	2039	2061	2151				
$Cr(CO)_5$: C_6H_{12}	B3LYP	2054	2063	2064	2088	2163	1932	1957		This work
	M06	2068	2079	2079	2111	2188				
	M06-L	2039	2047	2048	2071	2151				
$Cr(CO)_5$: η^2-C_6H_6	B3LYP	2045	2054	2058	2082	2157	1925	1950	2075	This work
	M06	2064	2069	2072	2105	2178				
	M06-L	2032	2039	2044	2069	2144				
$Cr(CO)_5$: H_2O	B3LYP	2044	2051	2054	2081	2159	1913	1943	1950	This work
	M06	2059*	2066*	2070*	2107*	2182*				
	M06-L	2030*	2038*	2041*	2067*	2149*				

* Vibrational analysis of this compound with the corresponding density functional results in imaginary vibrational frequencies

Table 3-6: Calculated vs. experimental frequencies for weak metal–solvent complexes.

All calculated frequencies were performed in this work. The references are for the experimental frequencies. For some complexes, there are multiple sets of frequencies and references.

DFT calculated frequencies for the additional metal–solvent complexes are similar to those from the experimental complexes in this work. In all cases, the frequencies calculated using M06-L are the lowest energy, followed by B3LYP, and finally those calculated using M06. In addition to this, most complexes have very similar geometries so there are five vibrational frequencies for all complexes other than $Fe(CO)_4$:N_2 because it has one fewer CO group. The predicted strength in the IR generally follows the same pattern as for our experimental complexes: the lowest energy frequency has medium intensity, the second two have strong intensity, the fourth highest is very weak, and the highest frequency is weak. Two of the complexes are slightly different than this. For $Fe(CO)_4$:N_2 and $W(CO)_5$:CS, the two lowest vibrational frequencies are predicted to be the most intense in the IR, followed by the third frequency, which has medium intensity. The highest two frequencies follow the same trend as the rest of the complexes.

Using this larger set of data, we can calculate the difference between the experimental and calculated CO frequencies to get a better idea of the accuracy of each functional in calculating vibrational frequencies. We can also calculate scale factors for each functional, and compare the scale factor here to the one earlier in Table 3-5 when using only a few complexes. To calculate differences we need to assign which calculated frequency goes with which experimental frequency. In most cases, this is pretty straight forward. When a third higher energy experimental frequency is present, this always corresponds to the highest frequency mode calculated. The other experimental frequencies correspond to the three lowest frequency calculated modes. We never see the second highest frequency mode experimentally, which is expected from its extremely weak predicted IR intensity. Though there is possibly some error in

our correlation of experimental frequencies and calculated modes, in most cases it seems pretty straightforward because of the few frequencies available, and the degeneracy in calculated modes. The calculated scale factors are reported in Table 3-7.

Functional	Average Difference (cm^{-1})	Scale Factor
B3LYP	100 ± 19	0.95 ± 0.01
M06	120 ± 17	0.943 ± 0.009
M06-L	90 ± 19	0.96 ±0.01

Table 3-7: Scale factors for calculating C≡O vibrational frequencies.

These are reported using all complexes in Table 3-6. The difference is calculated as Calculated – Experimental. The scale factor is calculated as Experimental/Calculated.

The scale factors and average differences calculated using all complexes in Table 3-6 are very similar to those using only the four complexes in Table 3-4. Again we see that the vibrational frequencies calculated using M06-L are the most accurate. However, we also see that M06 has the greatest precision, as represented by the lowest standard deviation. Still, all three are quite similar to each other and very similar to those presented before. In fact, the scale factor for M06, 0.943, is almost identical to the scale factor calculated earlier. The great similarity between the two data sets gives additional confidence to our assignment of experimental complexes. If these assignments were incorrect, we might expect larger frequency differences for just our experimental complexes than when using this entire set of known complexes. To further evaluate this claim, we also calculated these statistics for the data included in Table 3-6 without the complexes from this work. The calculated differences and scale factors were the same. So, including our data in the calculations does not manipulate them to be more similar to calculations in which only our data are present.

The experimental frequencies included in Table 3-6 come from a variety of sources, and also from a variety of methods. Though most experiments were performed in organic solutions, similar to our measurements, there were three gas phase measurements and also three using KBr. To evaluate these differences, we calculated the average difference and scale factors for the data including only experiments that were done in solution. We found the standard deviation was slightly smaller, but the calculated scale factors were the same. We also calculated these values for the KBr experiments, and the gas phase experiments. We found that there was higher error in the KBr measurements, closer to 1.5%. Also, the scale factors were all slightly larger than for the experiments done in solution. For the gas phase experiments, the errors were all lower than those in Table 3-7, but the calculated scale factors were the same. We cannot calculate reliable statistics from only three measurements, so these gas phase and KBr values should not be used. The comparison was done to be sure the different experimental methods were not skewing the overall statistics. From these results, we find that the scale factors are accurate for solution and gas phase measurements.

From these comparisons, it seems all three density functionals, B3LYP, M06, and M06-L can be useful in calculating vibrational frequencies. All three give frequencies that are quite a bit higher than the true vibrational frequencies. But, if the calculated scale factors are used to predict experimental frequencies, this analysis shows average errors of one percent or less. We used the scale factors in Table 3-7 to scale the calculated frequencies for each complex used in the analysis. When these scaled frequencies were compared to the true experimental frequencies, most had errors of 1% or less. For B3LYP: 35 had errors from 0-1%, 21 had errors from 1-2, and 2 had errors greater than 2%. For M06: 38 had errors from 0-1%, 18 had errors from 1-2%, and 2 had errors greater than 2%. For M06-L: 35 had errors from 0-1%, 19 had

errors from 1-2%, and 4 had errors greater than 2%. Although a 1% error is low, that still means errors of approximately 20 cm^{-1} for CO vibrational frequencies. With this large of an error, it would be hard to predict experimental frequencies. However, these computed frequencies can still be useful when trying to identify or verify experimental structures.

3.4 Conclusions

Density functional theory calculations have been applied to the complexes we studied experimentally, to verify and help interpret our findings. Through these calculations we found that the three experimental reactions proposed are consistent with calculated vibrational frequencies. The $M(CO)_5$:benzene complex is oriented so benzene interacts with the metal through one side of the ring. We also conclude that the final complex formed is most likely $M(CO)_5$:H_2O. By calculating the binding energies of each structure we found that none compared perfectly to the experimental activation energies, suggesting mechanisms with both associative and dissociative character.

We calculated scale factors of 0.952 for B3LYP, 0.943 for M06, and 0.957 for M06-L for converting calculated CO vibrational frequencies to experimental frequencies for weak metal–solvent complexes. These resulted in scaled frequencies that were on average different than the true experimental values by 1% or less.

References

(1) Schultz, N. E.; Zhao, Y.; Truhlar, D. G. Density Functionals for Inorganometallic and Organometallic Chemistry. *J. Phys. Chem. A*, **2005**, *109*, 11127–11143.

(2) Yang, Y.; Weaver, M. N.; Merz, K. M., Jr. Assessment of the "6-31+G** + LANL2DZ" Mixed Basis Set Coupled with Density Functional Theory Methods and the Effective Core Potential: Prediction of the Heat of Formation and Ionization Potentials for First-Row-Transition-Metal Complexes. *J. Phys. Chem. A*, **2009**, *113*, 9843–9851.

(3) Harvey, J. N. On the accuracy of density functional theory in transitional metal chemistry. *Annu. Rep. Prog. Chem., Sect. C: Phys. Chem.*, **2006**, *102*, 203–226.

(4) Zhao, Y.; Truhlar, D. G. Density Functionals with Broad Applicability in Chemistry. *Acc. Chem. Res.*, **2008**, *41*, 157–167.

(5) Zhao, Y.; Truhlar, D. G. A new local density functional for main-group thermochemistry, transitional metal bonding, thermochemical kinetics, and noncovalent interactions. *J. Chem. Phys.*, **2006**, *125*, 194101-1–194101-18.

(6) van Duijneveldt, F. B.; van de Rijdt, J. G. C. M.; van Lenthe, J. H. State of the Art in Counterpoise Theory. *Chem. Rev.*, **1994**, *94*, 1873–1885.

(7) Gonzalez-Blanco, O.; Branchadell, V. Density functional study of the Fe–CO bond dissociation energies of $Fe(CO)_5$. *J. Chem. Phys.*, **1999**, *110*, 778–783.

(8) Jonas, V.; Thiel, W. Theoretical study of the vibrational spectra of the transition metal carbonyl hydrides $HM(CO)_5$ (M=Mn, Re), $H_2M(CO)_4$ (M=Fe, Ru, Os), and $HM(CO)_4$ (M=Co, Rh, Ir). *J. Chem. Phys.*, **1996**, *105*, 3636–3648.

(9) Biber, L.; Reuvenov, D.; Revzin, T.; Sinai, T.; Zahavi, A.; Schultz, R. H. Reactions of the transient species $Cr(CO)_5$(cyclohexane) with C_4H_nE (*n* = 4,8; E = O, NH, S) studied by time-resolved IR absorption spectroscopy. *Dalton Trans.*, **2007**, *1*, 41–51.

(10) Yu, L.; Srinivas, G. N.; Schwartz, M. Scale factors for C≡O vibrational frequencies in organometallic complexes. *J. Mo. Struct.*, **2003**, *625*, 215–220.

(11) Karahan, S.; Kose, P.; Subasi, E.; Alp, H.; Temel, H. Photochemical reactions of $M(CO)_5$THF (M = Cr, Mo, W) with thio Schiff bases. *Transition Met. Chem.*, **2008**, *33*, 849–854.

(12) Barre, C.; Boudot, P.; Kubicki, M. M; Moise, C. Synthesis, Spectroscopy, Bonding and Structure in Phosphido Bridged Bimetallics Derived from Bent Metallocenes of Molybdenum and Tungsten and from Group 6 Metal Carbonyls. *Inorg. Chem.*, **1995**, *34*, 284–291.

(13) Paur-Afshari, R.; Lin, J.; Schultz, R. H. An Unusual Solvent Isotope Effect in the Reaction of $W(CO)_5$(solv) (solv = Cyclohexane or Cyclohexane-d_{12}) with THF. *Organometallics*, **2000**, *19*, 1682–1691.

(14) Banno, M.; Iwata, K.; Hamaguchi, H. Intra- and intermolecular vibrational energy transfer in tungsten carbonyl complexes $W(CO)_5(X)$ (X = CO, CS, CH_3CN, and CD_3CN). *J. Chem. Phys.*, **2007**, *126*, 204501-1–204501-9.

(15) Church, S. P.; Grevels, F.; Hermann, H.; Schaffner, K. Fast Infrared Detection of $Cr(CO)_5N_2$ in Room-Temperature Solution. *Inorg. Chem.*, **1984**, *23*, 3830–3833.

(16) Goff, S. E.; Nolan, T. F.; George, M. W.; Poliakiff, M. Chemistry of Reactive Organometallic Compounds at Low Temperatures and High Pressures: Reactions of $M(CO)_6$ (M = Cr, Mo, W), (η^6-$C_6H_3Me_3$)$M(CO)_3$ (M = Cr and Mo), and $W(CO)_5CS$ with H_2 and N_2 in Polyethylene Matrices. *Organometallics*, **1998**, *17*, 2730–2737.

(17) Grills, D. C.; Huang, K.; Muckerman, J. T.; Jujita, E. Kinetic studies of the photoinduced formation of transition metal–dinitrogen complexes using time-resolved infrared and UV–vis spectroscopy. *Coord. Chem. Rev.*, **2006**, *250*, 1681–1695.

Appendix 1: Step Scan Data Extraction and Analysis

Steps for Extracting Step Scan Data in OPUS

- Load AC and DC files into OPUS.
- Double click on each file to open in 3D mode and see the scan
- Select the DC scan and go to the “Measure” menu and click on “Data Extraction”
- Type the path where you will save the file,
- Select the following settings: extract from beginning of file to end of file, coadd all to one block, and load the extracted file
- Click “extract”
- The extracted file will load. Highlight the extracted file and then go to the “File” menu and click “Save As..”
- Save as a .asc file with the Mode output a “Data point table”
- Click “Save”
- Select the AC scan and go to the “Macro” menu and click “Run macro”
- Select “AC extract xxx slices.mtx” (the xxx is the number of time slices you collected)
- Type the path where you want the data saved
- Click “continue” several times
- The data files will then be extracted

Macro Used for Extracting AC Step Scan Data in OPUS

The macros used to extract AC step scan data in OPUS are titled “AC Extract xxx Slices.mtx”, where xxx is the number of time slices that were collected during the data collection. These are located in the mcalab research directory under “OPUS Macros”. We will include a representative macro “AC Extract 200 Slices” below. This macro can be adjusted to be used for different numbers of time slices.

```
VARIABLES SECTION

FILE <Ffilename> = ScSm/Multiple;
NUMERIC <filenumber> = 1;
STRING <filename> = '1';
FILE <Sfilename> = ScSm;
*STRING <outfile> = '200.asc';
FILE <$ResultFile 1> = Spec;
*STRING <finaldir> = 'S:\mcalab\cevans\110707\forty_4';
FILE <$ResultFile 2> = Spec;
*STRING <tmpdir> = 'c:\data\TEMP';
BUTTON <IncorrectDirectory> = Goto (FinalDirectory);
*STRING <finalDirBase> = 'S:\mcalab\cevans\110707\forty_4';
NUMERIC <scanno> = 1;

PROGRAM SECTION
```

```
UserDialog ('Enter destination directory', STANDARD, EDIT:'<finalDirBase>',
BLANK, BLANK, BLANK, BLANK, BLANK, BLANK, BLANK, BLANK, BLANK,
BLANK, BLANK, BLANK, BLANK);

<scanno>=0;

<scanno>=<scanno>+1;

PostrunExtract ([<Ffilename>:ScSm/Multiple], {EXS=0, EXE=1, ENT=0, ENE=10,
ECO=0, XTP='<tmpdir>', XTN='0.ext', XTI=1});

<finaldir>='<finalDirBase>';

Label (FinalDirectory);

UserDialog ('Files will be written to', STANDARD, TEXT:'<finaldir>',
BUTTON:'<IncorrectDirectory>', BLANK, BLANK, BLANK, BLANK, BLANK,
BLANK, BLANK, BLANK, BLANK, BLANK, BLANK, BLANK);

<filenumber>=1;

StartLoop (200, 1);

<outfile> = '<filenumber>.asc';

<filename> = '<filenumber>.ext';

[<Sfilename>:ScSm] = LoadFile ('<tmpdir>\<filename>', WARNING | ABORT);

If (MACROERROR, .EQ., TRUE);

Goto (end);

Endif ();

SaveAs ([<Sfilename>:ScSm], {DAP='<finaldir>', OEX='1', SAN='<outfile>', COF=64,
INP='C:\OPUS_NT\METHODS', IFP='C:\OPUS_NT\METHODS', INM='DEFAULT',
IFN='DEFAULT', DPA=5, DPO=5, SEP=', ', YON=, YON='0', ADP='1'});

Unload([<Sfilename>] , {});

Delete ('<tmpdir>\<filename>');

<filenumber> = <filenumber> + 1;
```

```
EndLoop (1);

Label(end);


PARAMETER SECTION


ELF=0;

EAB=0;

ECO=0;

ENE=1;

ENT=0;

XTI=1;

XTN=1.ext;

XTP=F:\TEMP;

EXE=0;

EXS=0;
```

MATLAB Script Used to Import AC Step Scan Data

The following script, called “nsread”, is used to import AC step scan data into MATLAB following extraction in OPUS. The current directory must be set to the folder in which the extracted files are located. The script is included below.

```
function [freq,data]=nsread(nfiles)
for ii=1:nfiles
   fname=[num2str(ii),'.asc'];
```

```
    fid=fopen(fname);
    dd=fscanf(fid,'%f,%f',[2,Inf]);
    data(ii,:)=dd(2,:)';
    fclose(fid);
end
freq=dd(1,:);
```

Appendix 2: Rapid Scan Data Extraction and Analysis

Steps for Extracting Rapid Scan Data in OPUS

- Load data files into OPUS
- Select all the single channel files for one set of data (for example, all the replicate measurements at a particular temperature)
- Go to the “Macro” menu and click “Run macro”
- Select “MSEXTRT.mtx”
- Type the path where you want the data saved
- Set totalscans to 204
- Click “continue” several times
- The data files will then be extracted
- At the end a window will pop up; click “Cancel”

Macro Used for Extracting Rapid Scan Data in OPUS

The macro used to extract rapid scan data in OPUS is titled “MSEXTRT.mtx”. It located in the mcalab research directory under “OPUS Macros”. This macro will take each selected run and extract it to its own folder. All selected runs will have the same directory base but will have “_#” at the end, where # is a numeral counting up from 1. The macro is included below.

VARIABLES SECTION

FILE <Ffilename> = ScSm/Multiple;

```
NUMERIC <filenumber> = 1;

STRING <filename> = '1';

FILE <Sfilename> = ScSm;

*STRING <outfile> = '204.asc';

FILE <$ResultFile 1> = Spec;

*STRING <finaldir> = 'g:\data\extract\fifteendegree_7';

FILE <$ResultFile 2> = Spec;

*STRING <tmpdir> = 'c:\data\TEMP';

BUTTON <IncorrectDirectory> = Goto (FinalDirectory);

*STRING <finalDirBase> = 'g:\data\extract\fifteendegree';

NUMERIC <scanno> = 1;

NUMERIC <totalscans>=204;


PROGRAM SECTION


UserDialog ('Enter destination directory', STANDARD, EDIT:'<finalDirBase>', BLANK,
BLANK, BLANK, BLANK, BLANK, BLANK, BLANK, BLANK, BLANK, BLANK, BLANK,
BLANK, BLANK, BLANK);

UserDialog ('Total number of scans', STANDARD, EDIT:'<totalscans>', BLANK,
BLANK, BLANK, BLANK, BLANK, BLANK, BLANK, BLANK, BLANK, BLANK, BLANK,
BLANK, BLANK, BLANK);

<scanno>=0;

StartLoop ([<Ffilename>:ScSm/Multiple], 0);

<scanno>=<scanno>+1;
```

```
PostrunExtract ([<Ffilename>:ScSm/Multiple], {EXS=0, EXE=1, ENT=0, ENE=10,
ECO=0, XTP='<tmpdir>', XTN='0.ext', XTI=1});

Timer (WAITTIME, 5);

<finaldir>='<finalDirBase>_<scanno>';

Label (FinalDirectory);

<filenumber>=1;

StartLoop (<totalscans>, 1);

<outfile> = '<filenumber>.asc';

<filename> = '<filenumber>.ext';

[<Sfilename>:ScSm] = LoadFile ('<tmpdir>\<filename>', WARNING | ABORT);

UnDisplaySpectrum ([<Sfilename>:ScSm]);

If (MACROERROR, .EQ., TRUE);

Goto (openerror);

Endif ();

SaveAs ([<Sfilename>:ScSm], {DAP='<finaldir>', OEX='1', SAN='<outfile>', COF=64,
INP='C:\OPUS_NT\METHODS', IFP='C:\OPUS_NT\METHODS', INM='DEFAULT',
IFN='DEFAULT', DPA=5, DPO=5, SEP=', ', YON=, YON='0', ADP='1'});

Unload([<Sfilename>] , {});

Delete ('<tmpdir>\<filename>');

<filenumber> = <filenumber> + 1;

EndLoop (1);

Label(end);

EndLoop(0);

Label(openerror);
```

UserDialog ('Open failed', STANDARD, TEXT:'<filenumber>', BLANK, BLANK, BLANK, BLANK, BLANK, BLANK, BLANK, BLANK, BLANK, BLANK, BLANK, BLANK, BLANK);

Goto (end);

PARAMETER SECTION

ELF=0;

EAB=0;

ECO=0;

ENE=1;

ENT=0;

XTI=1;

XTN=1.ext;

XTP=F:\TEMP;

EXE=0;

EXS=0;

MATLAB Script Used to Import Rapid Scan Data

The following script, called “msread4” is used to import rapid scan data into MATLAB following extraction in OPUS. The current directory must be set to the folder in which the individual rapid scan folders with the same directory base and “_#” on the end are located. This script will import each data set within the range of numbers specified. The script is included below.

```
function [absorb,freq]=msread4
 first = 1;
 directoryBase = input('Enter directory base containing data > ', 's');
 firstRun = input('Enter first run number > ');
 lastRun = input('Enter last run number > ');
 numScans = input('Enter the number of full scans > ');
 TotalScans=numScans*4;
 backNum = 1;
 figure;
 upper = input('High frequency limit > ');
 lower = input('Low frequency limit > ');

 for runno = firstRun:lastRun,
   directory = [directoryBase '_' num2str(runno)];
   disp(directory)
   disp(runno)
   disp(firstRun)
   %create four background vectors
   back1 = load(['./' directory '/1.asc']);
   lowIndex = min(find(back1(:,1)<upper));
   upIndex = min(find(back1(:,1)<lower));
   freq=back1(lowIndex:upIndex);
   numfreq=length(freq);

   for i = 1:TotalScans,
      filename = ['./' directory '/' num2str(i) '.asc'];
      indata = load(filename);
%       disp(i)
%       disp(lowIndex)
%       disp(upIndex)
      data=indata(lowIndex:upIndex,2);
      fullstack(:,i,runno)=data;
   end %TotalScans

   for j=1:4,
      stback(:,j:4:TotalScans)=mean(fullstack(:,j:4:32,runno),2)*ones(1,TotalScans/4);
   end

   absorb(:,:,runno)=abs(-log10(fullstack(:,:,runno)./stback));
   if runno==firstRun,
      disp('Hi')
      plot(freq,absorb(:,200,runno))
      [x,y]=ginput(1);
      peak=min(find(freq<x));
```

```
        pause(1)
        [val,tzero]=max(diff(absorb(peak,:,runno)))
        tzero=tzero+1;
    end
    tzeroCorr=1;
    while tzeroCorr~=0
        plot(1:TotalScans,absorb(peak,:,runno),'+',2:TotalScans,diff(absorb(peak,:,runno)))

        plotaxis=axis;
        plotaxis(1)=tzero-20;
        plotaxis(2)=tzero+20;
        axis(plotaxis);
        hold on
        plot([tzero tzero],[plotaxis(3) plotaxis(4)],'r')
        hold off
        tzeroCorr=input('Input t zero correction:  ');
        if tzeroCorr>0,
            absorb(:,1:(TotalScans-
tzeroCorr),runno)=absorb(:,(tzeroCorr+1):TotalScans,runno);
        end
        if tzeroCorr<0
            tzeroCorr=-tzeroCorr;
            absorb(:,(tzeroCorr+1):TotalScans,runno)=absorb(:,1:(TotalScans-
tzeroCorr),runno);
        end
    end
    pause(1)


    pause(5)
 end %major loop
```